Fall 12-21-2017

Microstructure and Mechanical Properties of Additive Manufacturing Titanium Alloys After Thermal Processing

Ahmet Alptug Tanrikulu
Portland State University

Microstructure and Mechanical Properties of Additive Manufacturing Titanium Alloys After Thermal Processing

by

Ahmet Alptug Tanrikulu

A thesis submitted in partial fulfillment of the
requirements for the degree of

Master of Science
in
Materials Science Engineering

Thesis Committee:
Tae-Kyu Lee, Chair
Jun Jiao
Lemmy Meekisho

Portland State University
2017

Abstract

Titanium alloys are widely used for aerospace and biomaterial applications since their high specific strength, and high corrosion resistivity. Besides these properties, titanium is an excellent biocompatible material widely used for internal body implants. Because the products have complex geometries in both applications, Additive Manufacturing (AM) methods have been recently applied for production. AM methods can process a direct 3-D shape of the final product, decrease total production time and cost. However, high residual stress of the final product limits the application of AM components, especially the ones that are exposed to cyclic loading. In the present study, the initial microstructures and impact toughness of Ti6Al4V processed by EBM and CMT, and CP:Ti processed by SLM were experimented. In addition to initial microstructure and impact toughness, their response to different heat treatments were examined. Gleeble® 3500 was used for rapid heat treatment process. The change of mechanical properties due to different heat treatments were monitored with impact tests. Phase transformation kinetics of CP:Ti and Ti6Al4V were investigated with a Differential Scanning Calorimeter at slow heating and cooling rates. Microstructure examination was done with a scanning electron microscope. EBSD data was used to analyze the microstructure behavior. It is observed that toughness of the samples that are produced by powder-based AM methods were improved. Overall, residual stress, strain values, and grain orientation are the key elements that affected impact toughness AM produced components.

Dedication

‘Until you start believing in yourself, you ain’t gonna have a life.’

Rocky Balboa

I dedicated my humble effort to my lovely family; Hulya Tanrikulu, Ahmet Kenan Tanrikulu, Osman Goktug Tanrikulu and Ayca Soygut who have always encouraged me and helped me to believe in myself. I will always be grateful to their devoted supports for my dreams become true.

Acknowledgement

I am grateful to people who have walked alongside me during my masters' degree. The support and supervision of my thesis committee members helped me complete my work. Firstly, I would like to thank Dr. Tae-Kyu Lee for his guidance; his limitless support and kindness. I also would like to thank Dr. Jun Jiao for her invaluable insights and assistance. Moreover, I am grateful to Dr. Lemmy Meekisho who supported my research significantly, and whom I learned greatly during his class.

Furthermore, I would like to thank Dr. Graham Tewksbury and Benjamin Adam who were always friendly and helpful to me with their deep metallurgy knowledge and engineering skills.

Finally, special thanks to my real friend Thomas Langston who has always been by my side, from the beginning to the end.

Table of Contents

List of Tables

List of Figures

Chapter 1. Introduction and Background

The element, titanium was first discovered in rutile ores by William Gregor in 1791, in Cornwall, Great Britain. It was then confirmed as a new element in 1975, and named by a German chemist Martin Heinrich Klaproth for the Titans of Greek mythology, also named for the Latin word for Earth. Titanium is present in the earth's crust at a level of about 0.6% and is therefore the fourth most abundant structural metal after aluminum, iron, and magnesium. [1]

Corrosion resistance and the strength-to-density ratio of titanium are the highest of any metallic element. In addition to these, good creep resistance up to 550 °C, and low modulus of elasticity properties of titanium and its alloys allows widespread applications in many industries especially in aerospace and biomedical industries in which strength-to-weight ratio is crucial. Pure titanium (unalloyed condition) has strength values as some of the steels. Having same strength with lower density makes titanium more preferable than some steels. Commercially pure titanium (CP:Ti) has ultimate tensile strength (UTS) around 434 MPa which is close to most low-grade steel alloys. It is softer when we compare it with heat threated (hardened) steels, has low conductivity and is non-magnetic.

Titanium is a dimorphic allotrope of hexagonal close pack (HCP) α-Ti and body centered cubic (BCC) β-Ti. α phase is stable at room temperature and the β phase is stable at above transition temperature, β-transus temperature. Theoretical transition temperature for pure titanium is 882 °C. Phase transformation temperature depends on heating/cooling rate and also chemical composition of titanium alloys. Some elements act as α-Ti stabilizer when the others act as β-Ti stabilizer. For instance, iron (Fe) is a β stabilizer element on

the contrary of oxygen (O_2) and nitrogen (N_2) which are α stabilizer elements. There are many studies available on transition temperature of titanium, Kim and Park mentioned in their studies that β-transus temperature is almost independent of Fe and that the oxygen and nitrogen are the major influencing elements. After examination of the binary phase diagrams. [2] Bieler, Trevino and Zeng also mentioned oxygen and nitrogen are α-stabilizers and addition to that they showed the effects of each alloying element in titanium. [3]

Titanium alloys can be classified in three groups; alpha alloys, alpha + beta alloys, and beta alloys. Single alpha alloys are extensively used in applications that are not particularly demanding in terms of strength but focus more on the attractive corrosion resistance of titanium. [4] CP:Ti is the most common single alpha phase titanium and it has better elevated temperature creep resistance, and is less expensive than the other titanium alloys. [3] Alpha + beta alloys offer a range of combinations of strength, toughness and high temperature properties that make them attractive in wide ranging aerospace applications and other products demanding high specific properties up to temperature of ~873 K (~600°C). [4] Beta alloys enable the development of compositions and processing routes that can satisfy diverse requirements of very high strength with adequate toughness and fatigue resistance required in airframe applications. They also meet requirements of low modulus and biocompatibility with shape memory response and fatigue strength for use in biomedical applications. [4]

Mechanical properties of titanium and its alloys like; tensile strength, toughness, fracture toughness, ductility depend on microstructure which is determined by

compositions and process. Distribution of alpha and beta phases, grain size, texture, orientations in between phases and grains are results of thermomechanical history of the component. Microstructure of Ti and Ti alloys can be manipulated by post heat treatments to improve mechanical properties. Heat treatment of titanium alloys classified in 4 main groups according to ASM International which are: Stress-relief, Annealing, Solution treating, Aging. [5]

Production of titanium and titanium alloys depends on countries and the regions. For instance, in North America and Europe the major industry demanding titanium is the aerospace industry in contrast to Japan. CP:Ti accounts 26% of USA total titanium market and Ti6Al4V has 74% market share. The rest of the breakdown is 4% of β alloys and 14% other α+β alloys, Fig. 1.1

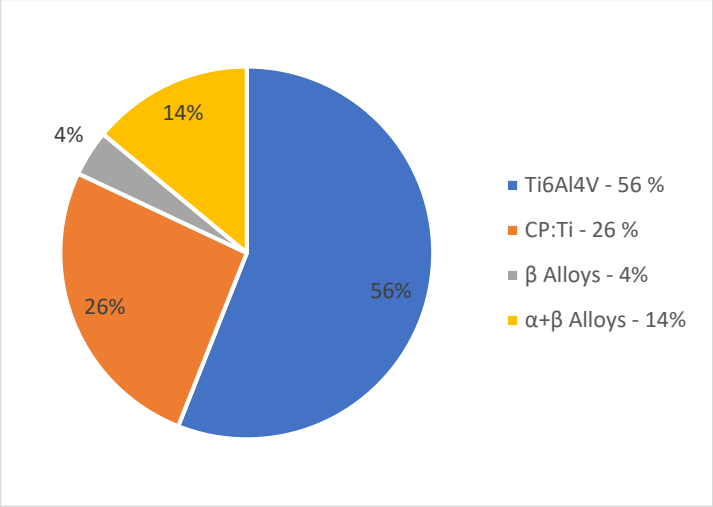

Fig. 1.1 Approximate breakdown of the USA market by titanium alloy type, 1998 [1]

In the present study two types of titanium were evaluated, CP:Ti, and Ti6Al4V. The alloy Ti6Al4V and CP:Ti were chosen for investigation since they have a wide variety applications and have the biggest market share of titanium alloys. In addition these two titanium alloys are commonly subjected to the new production method of Additive Manufacturing.

Production methods that build 3-D objects by adding material layer-on-layer, whether it is powder based or wire based material, either metals or plastics, are named as Additive Manufacturing (AM) which is the industry standard term, ASTM F2792, for all applications of Rapid Prototyping (RP) technology. [6] These technologies are also known as 3D Printing, Additive Techniques. Layer Manufacturing, Freedom Fabrication, Direct Digital Manufacturing, Additive Fabrication. [6-7]

AM technologies became alternatives to conventional production methods in high value-added industries and applications including those involved aerospace, and biomedical products which require highly complex and customized designs at low volumes. AM makes it possible to manufacture these required complex shapes in short lead time with Non-recurring cost (NRC). [6-8]

Direct fabrication with AM will increase rapidly as it is employed this technique in new markets; it is now just beginning of this technology. Currently, just one in a thousand products is fabricated using AM technologies. Global manufacturing was worth $ 10.5 trillion in 2011 and is predicted to be worth $ 15.9 trillion in 2025. The U.S. is currently a major user of additive manufacturing technology and primary producer of additive manufacturing systems. U.S. accounting approx. 38.3% of globally revenue collected from

additive manufactured goods. [6-9] According to 2013 Wohlers report in 2025 estimated worth of AM economy will be $10+ billion which was worth $1.7 billion in 2011, the estimated growth shown in Fig. 1.2 [10]

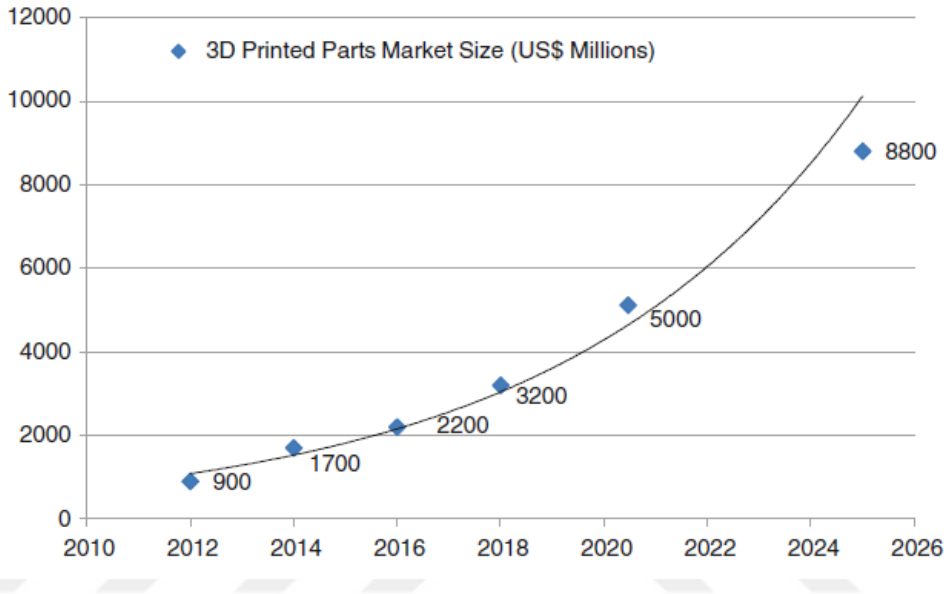

Fig. 1.2 'Estimated growth of additive manufacturing components market size' [6-10]

Comparison of traditional manufacturing and AM shows the benefits of the new technology. There is no assembly process required which has additional and it is possible to produce components with shorter lead time. For instance, the average shipment of manufactured transportation equipment travels 801 miles. This amounts to 45.3 billion ton-miles of transportation in U.S. annually. Building an entire assembly in one reduces the need for some of the transportation and inventory costs, resulting in impacts throughout the supply chain. [11]

Companies should maximize their profit to compete at the market and in order to allocation of resources become an important issue. The major element in the production and services is time. In addition to that companies consider land, labor, human capital, entrepreneurship as basic inputs for production and services. Thomas and Gilbert mentioned there is a tradeoff between time and labor. For instance, it takes one hundred people less time to build a house than it takes for one person. There is also a tradeoff between time/labor and natural resources, a machine can reduce both time and the number of the people needed for production, but utilizes more energy. In the triangular plane in Fig 1.3 (b) AM reduces resources needed for production and will move the plan toward the origin. [11]

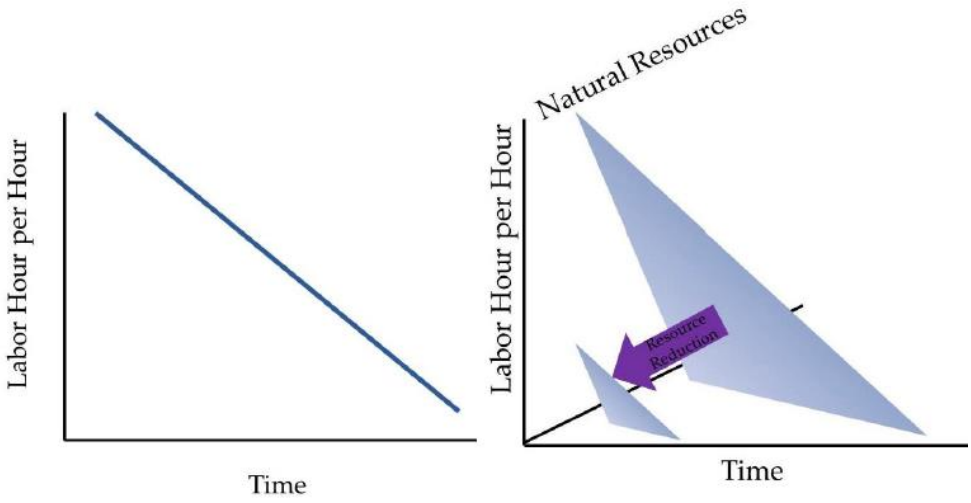

(a) (b)

Fig. 1.3 'Time and Labor needed to produce a product (a), Time, Labor and Natural Resources needed to produce a product' [11]

In the current study three different AM methods were, evaluated; Electron Beam Melting (EBM), Selective Laser Melting (SLM), and Cold Metal Transfer (CMT) Each process is elaborated in Section 3. CP:Ti and Ti6Al4V components produced by different methods and their initial microstructures depending on process parameters and their response to thermal treatments are investigated and results associated with mechanical properties of the materials.

Chapter 2. Additive Manufacturing

AM technology was born in 1980's with the development of stereolithography which links chains of of polymers by laser curing. [11] AM has significance due to its cost-effective method that provides the ability to produce previously unachievable geometries in both prototyping and end user industrial applications. [12] Besides these, 3D scanning technologies enabled the replication of real components without using expensive molds. [11]On the other hand due to high porosity, and residual stresses it is hard to meet the quality requirements of the specifications for aerospace and biomedical components. In addition to these slow print speed limits application for mass production. [11-12]

In the present study, titanium alloys that we evaluated are produced by two different AM techniques: powder based, and wire based. EBM and SLM build 3D components using a powder bed of titanium components on the other side CMT uses titanium wire feeding process. When we compared the two processes, the most significant difference is the deposition rate. CMT built geometries are not as precise as others but deposition rate is significantly higher which decrease total production time. Monitoring superiorities of these three techniques is not a subject of the present study still for any comparison, energy consumption values of these three techniques should be consider.

Fig. 2.1 'Gas turbine blades produced using Additive Manufacturing technology' (Siemens AG®)

2.1 Electron Beam Melting (EBM)

EBM uses an electron beam as a heating source which is applied to metal powder to build up dense metal components. Metal powder is melted by a powerful electron beam layer-by-layer to make the exact geometry defined by the CAD model. After melting and solidifying one layer the buildup process continuous with next layer upon solidified layer this process repeats until the geometry of the component finished.

When the high-speed electrons strike the metal powder, the kinetic energy is instantly converted into thermal energy in a very small confined region. The incident beam rapidly liquefies the metal in that region.

Schematic below, Fig. 2.2 shows the features of the EBM machine. Incident beam electrons emitted from the electron beam gun. Electron emission occurs with thermal energy which excites the electrons to overcome the work function. A tungsten filament, triggers electron jumps from valance band to conduction band at very high temperatures. Electrons stream through the filament has at approximately half speed of light velocity. [13] Moving electrons can be directionally manipulated by magnetic fields. There are two electro-magnetic fields to govern the fast electrons. The first one magnetic lens is used to focus the incident beam to correct diameter. The second one is used to focus the incident beam to the target point on the powder bed. The gun is stationary and there is no need to move mechanical parts to deflect the beam. This delivers very high scanning speeds, up to 1000 m/sec and fast build rates, up to 60 cm^3/hour. The process three is to five times faster than other additive technologies. [13]

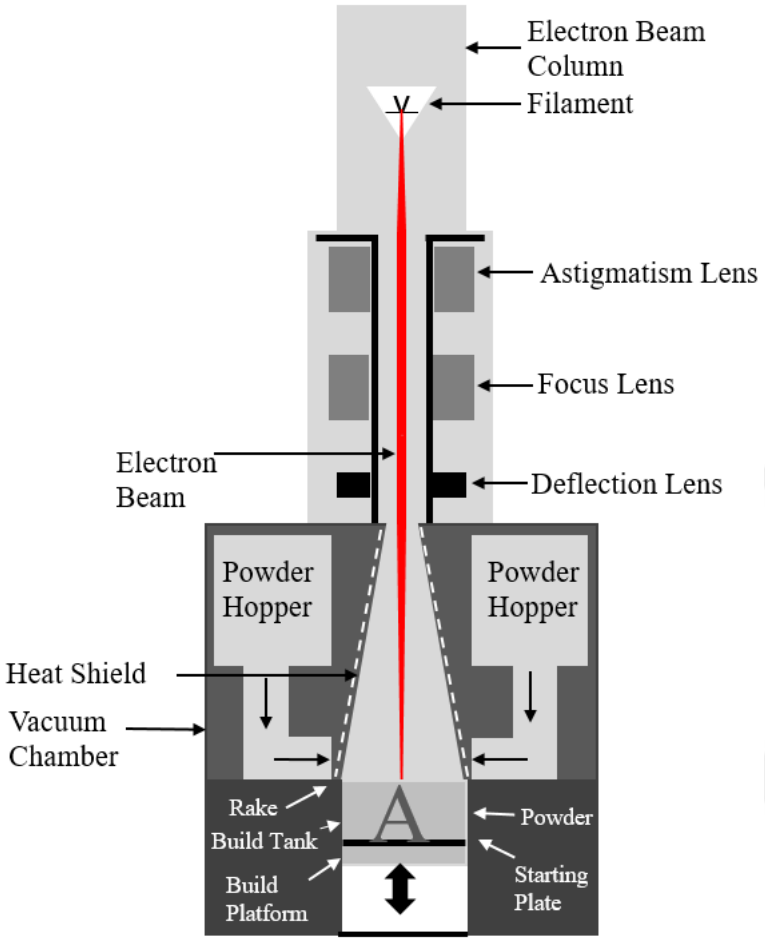

Fig. 2.2 'Schematic of the features of EBM machine' (Arcam EBM® Systems)

EBM technology requires controlled vacuum atmosphere inside the building chamber both to protect the filament and the molten material from any contaminations. Vacuum systems provide a base pressure of $1x10^{-5}$ mbar or better throughout the entire build cycle. During the melting process, partial pressure of Helium (He) is introduced to $2x10^{-3}$ mbar which cleans and controls the build environment. [Arcam EBM®]

Ti6Al4V parts that are manufactured with EBM technology exhibit properties that match those of wrought materials and exceed those of investment castings, Hiemenz [13].

Directly from the EBM machine, the parts are 100% dense, and there is no need for a secondary infiltration process. [13]

Components produced via EBM are near-net shape, like casting process. Since the incident beam fully melts the metal the liquefied metal conforms to surrounding metal powder, which yields a surface finish similar to a precision sand casting. As result, some light secondary machining or grinding of the surface maybe required. [13] EBM allows aerospace companies to produce titanium prototypes and production parts without the inherent cost and challenges of machining, casting, and welding. The ease and speed of producing titanium parts with the EBM machine makes functional prototypes readily accessible to the design and manufacturing team which means that the functional evaluations can be completed earlier and more frequently in the design cycle. [13]

In addition to its fast scanning, high build up rates, and near-net shape production, EBM has more superiorities, Hiemenz [13]. Multi-piece assembles: AM can make a multi-piece assembly as one component. In those cases where the limits of machining and casting force a designer to create an assembly, EBM can reduce production costs. By combining multiple individual components into a single piece, assembly is eliminated, and the cost of manufacturing may be reduced. Buy-to-fly ratios: EBM creates an opportunity to design and manufacture aircraft components with unprecedented strength-to-weight and buy-to-fly ratios. Hollow parts: EBM process can also produce hollow parts with an internal strengthening scaffold. Impossible with any other method, EBM can provide the required mechanical strength with much less mass. This reduces the cost of raw materials and the weight of the component.

2.2 Selective Laser Meting (SLM)

SLM is the other powder bed fusion process in the current study, which is most widely used in the AM industry. In this technology laser used as the source of melting on the contrary to EBM. A thin layer of powder is deposited over a substrate plate or on the previously deposited layer and the laser beam melts and fuses the powder particles selectively, as dictated by the CAD data. [14]

Schematic view of SLM process shown in Fig. 2.3 below. The powder feed is contained in a hopper or dispenser bed. Metal powder supplier feeds prescribed dose of powder upon the build plate that spread in a thin layer over the build surface by a re-coater arm. The re-coater mechanism may consist of a hard scraper, soft squeegee, or roller. [15] Powder layer thickness depends on the metal powders, but usually in between 10 to 100μm. Selective portions of the powder layer corresponding with a slice of the part to be manufactured are melted by a focused laser scanning across the surface. Lasers in the metal powder bed system are typically fiber lasers with wavelengths in the 1.06- 1.08μm. The magnitude of lasers depends the machine ability and in order of 100s of Watts. [15]

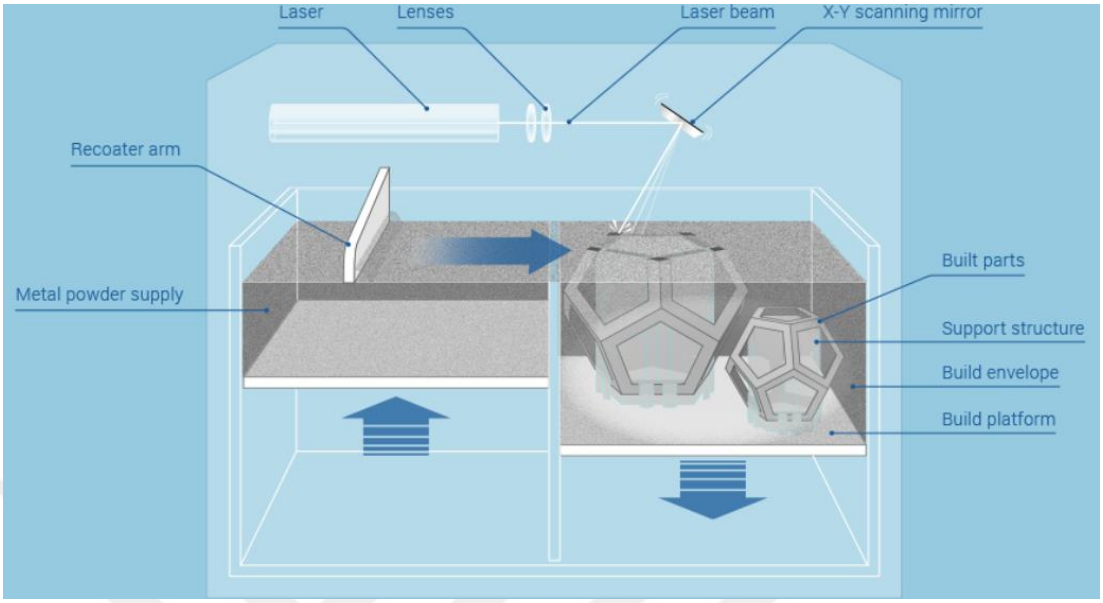

Fig. 2.3 'Schematic view of SLM process' (© additively.com)

In SLM process several parameters have to be tuned carefully to have a defect free component which are laser power, laser scan speed, hatch distance, hatch overlaps, hatch style. Besides their effect on production, defects these parameters have significant effect on mechanical properties of the materials. [14]

The process takes place inside a purge chamber similar to EBM process to avoid any contamination of either laser source or the molten metal. Nitrogen (N_2) and Argon (Ar) usually used as a back-fill gas depending on the reactivity of the metal powder that used for buildup. [14]

Wide spectrum of metals can be process by SLM likewise; aluminum alloys, titanium alloys, iron-steel alloys, nickel alloys, cobalt alloys, copper alloys, and their combinations. Furthermore; since the SLM process has high cooling rates so amorphous materials can be processed. Mechanical properties of materials can be tuned with process

parameters. Process parameters have significant effect on microstructure which determines the mechanical properties of the component. [14] For the SLM process there are over 50 different process parameters [15] that effect the final quality of product. These parameters can be classified in 4 groups; 1) laser and scanning parameters, 2) powder material properties, 3) powder bed properties and recoat parameters, 4) build environment parameters. [15]

Slow deposition rate and slow scanning speed of the laser are drawbacks of the technique similar to EBM process however, multiple laser sources can be introduced to improve the building rate. Different lasers can be employed to improve the final product quality as well. Continuous lasers are standard in industrial machines however, pulsed lasers have been demonstrated to provide some advantages in preventing cracking or controlling the microstructure of the component. [15]

Similar to EBM final surface finish of the product of SLM is limited and need to be improved by post-processing. Slow process drawback can be overcome with additional laser source however, it is an expensive way to improve the deposition rate.

SLM and EBM are both beam-based and powder bed AM techniques however, model by Vastola, G. Zhang, Pei and W. Zhang showed there is significantly different microstructures observed in two processes using the same material, Ti6Al4V. [16] Authors mentioned in the model that given processing temperature conditions, it was shown that EBM manufacturing allows for complete decomposition of martensite after build, while SLM mostly retains the martensite. Difference in between two microstructure governs the

phase transformation mechanism and kinetics during heat treatment in the current study and explained in later sections.

2.3 Cold Metal Transfer

Cold metal transfer (CMT) process was invented by M. Schorghuber and patented in 2009. [17] As the patent of the process is named, this is a kind of welding process (Cold-Metal-Transfer Welding Process and Welding Installation), which can be classified as a subset of gas metal arc welding. The cold term in the name of the process has to be understood in terms of a welding process. Fronius^{TM} who offers this technology to the market, innovates the MIG/MAG robot welding with digitally controlled wire motion. The motion of the wire is directly incorporated into the process. When the digital process-control detects a short circuit, it retracts the wire so as to help detach the molten droplet. This is the most significant difference from the conventional dip-transfer welding. [18] Second difference with the conventional dip-transfer methods is current-free metal transfer in other words off-circuit transfer. Wire moves until the short circuit happens as soon as the short circuit happens, wire pulled back this means the arc itself only inputs heat very briefly in the arching period, after which the thermal input is immediately reduce. This makes possible welding processes of very thin sheet metals and in addition to that welding of thin sheet metals this technology also explored as a cladding process for thin aluminum plates, as an alternative of traditional pulsed mode of operation which is associated higher heat inputs. [19]

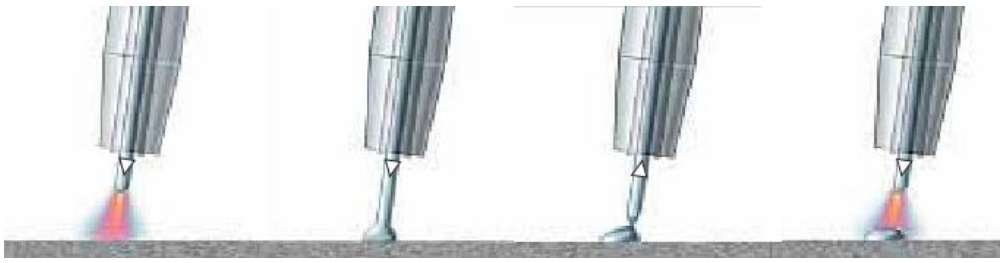

Fig 2.4 'Schematic view of the wire move (electrode) in CMT process' (Fronius^{TM})

The welding process and cyclic alternations between arcing and short-circuiting phases by wire moving are shown in Fig. 2.4. Wire moved towards the weld-pool during the arcing. When wire dips into the weld-pool the welding current is lowered since arc is extinguished. The pulling back of the wire, showed by the arrow in the Fig 2.4, provides detachment of the droplet during the short circuit period. This wire motion repeats, and the process begins again.

In addition to its low heat input the CMT process also provides spatter-free material transfer. [18-20] Fokens presents that precisely defined retraction of the wire facilitates controlled droplet detachment to give a clean, virtually spatter-free material transfer making CMT suitable for mechanized pipeline girth welding. He applied CMT with a conventional bug and band system for both horizontal and vertical joining applications. Results showed CMT is an up and coming mechanized root pass welding technology and has the potential to increase quality, productivity and capability.

The CMT process is adapted for many applications such as; low dilution cladding [19], welding materials with high heat conductivity [21], joining of dissimilar metals [22] and the state of art manufacturing method, AM. [23], Azar. [24] In the current study CMT is employed as a high deposition rate AM method to build Ti6Al4V alloy components. Deposition rate of the process depends on the wire diameter, feeding rate and travel speed since deposition rate is not the subject of the current study these parameters are not investigated during the experiments and set to constant values.

CMT process produced dense components similar to other AM methods that employed in the present study. Investigation of the micrographic structure of components their response to thermal processing and mechanical properties are shared in the current study.

Chapter 3. Titanium and Titanium Alloys

Titanium alloys became widely used after the second half of twentieth century since the modern industrial practice and design applications supported its use. Much of the use has come in military applications for aircraft such as the SR-71 Blackbird [25], B-1B bomber [26] and then followed by civil and commercial aerospace industry applications GE-90 aero-engine components, and the Boeing 777 [1-26]

In addition to low specific gravity, good corrosion resistance properties make titanium alloys preferred material for aerospace components. Excellent biocompatibility of titanium makes this metal available implant material in biomaterials. [27] Titanium alloys are used as implants for total hip and knee replacement surgeries. Formation of a stable, thin coherent titanium oxide (TiO_2) on the surface passivates the component against corrosion inducing media and provides superior corrosion resistance compared to stainless steel and Co-Cr alloys that are also used as implant materials. Furthermore, Ti6Al4V has better fatigue life time than stainless steel (316L) as a hip implant. [28] Besides these, titanium alloys match the closest modulus of elasticity of the bone and obvious choice for the femoral stem as they have relatively low modulus, and high strength. [27]

Since the target titanium alloys of the present study are mostly employed in aerospace and medical industry, examples are focused on these two specific industries but there are a number of uses for titanium and its alloys ranging from offshore structures to sporting goods and construction equipment in different industries.

Significant facts, important benefits, and some superiorities of titanium during material selection are listed as below;

- The density of titanium is only 60% of that steel or nickel base super alloys. (Ti6Al4V; 4.50 g/cm^3 vs. Stainless steel; 7,81 g/cm^3 and Inconel 718; 8.20 g/cm^3)
- The tensile strength of alloyed titanium can be comparable with lower-strength martensitic stainless steel and is better than that of austenitic of ferritic stainless.
- The commercial alloys of titanium can use at 538 °C to 598 °C dependent on composition alloy can be used even higher temperatures.
- Titanium often exceeds the corrosion resistance of stainless steel in most environments, and it has outstanding corrosion resistance in the human body.
- Titanium may be forged or wrought by standard techniques.
- It is suitable for casting production, usually preferred investment casting.
- It may be processed by means of P/M (Powder Metallurgy) technology. (Powder may cost more, yet P/M may offer property and processing improvements as well as over-all cost savings potential.)
- It may be joined by means of fusion welding, brazing, adhesives, diffusion bonding, and fasteners.
- It is available in wide variety of types and forms.
- However, the cost of titanium alloys are approx. four times of stainless steel, it is comparable to that of super alloys. [25]

3.1 Basic Properties

The melting point of titanium is 1668 °C and serves as a high strength component below 550-538 °C [3-25] Melting point above 1650 °C and low thermal conductivity make titanium useful as a refractory metal. It is paramagnetic and has fairly low electrical

conductivity. [30] Its coefficient of thermal expansion is lower than steel and less than half of aluminum. [25]

Titanium is a high oxygen reactivity element and according to Ellingham diagram it has the fourth highest oxygen affinity after calcium, magnesium, and aluminum. High reactivity with oxygen leads to immediate formation of a stable and adherent oxide surface when it is exposed to air. [1-27] However; this provides superior corrosion resistance especially in aggressive aqueous acid (dilute sulfuric acid, hydrochloric acid, chloride solutions and most organic acids) environments [1-29], Oxygen makes titanium production vulnerable in terms of oxide defects and requires controlled environment during manufacturing. Also at high temperature applications (above 600°C) the oxygen diffusion through the oxide layer increases significantly and excessive growth of the oxide layer cause embrittlement of the adjacent oxygen rich layer of titanium alloy. [1]

Titanium has ultimate tensile strength about 434 MPa in commercially pure condition [31] and has yield stress level around 1000 MPa in alloyed condition. Certain titanium alloys achieve tensile strength of over 1400 MPa. [25] Modulus of elasticity for titanium alloys is around 115 GPa at room temperature. [1]

Components made from titanium alloys have a fatigue limit [32] which means there is a limit of amplitude of cyclic stress that can be applied to the material without causing fatigue failure. [33] This fatigue limit in other words; endurance limit and fatigue strength is crucial for the components that are exposed to cyclic stress and dynamic loads.

Property	Description or value
Atomic number	22
Crystal Structure	
Alpha (≤ 882.5 °C)	Closed-packed hexagonal
Beta (≥ 882.5 °C)	Body-centered cubic
Color	Dark grey
Density	4.51 g/cm3
Melting point	1668 ± 10 °C
Solidus / liquidus	1725 °C
Hardness	70 to 74 HRB
Tensile strength	240 MPa min.
Young's modulus	120 Gpa
Poisson's ratio	0.361

Table 3.1 'Physical and mechanical properties of elemental titanium' (ASM International)

3.2 Crystallography and Structures

Titanium is an allotropic element that exists in two crystal forms in solid state; hexagonal close-packed alpha phase is stable at room temperature and body-centered cubic beta phase is stable above beta-transus temperature (≥ 882.5 °C)

Hexagonal unit cell of the α-Ti is shown in Fig.3.1 the lattice parameters of unit cell is ***a*** = 0.295 nm and ***c*** = 0.468 nm. Ratio of ***c/a*** is 1.59 which is slightly squashed compared to the ideal close packed ratio, 1.63. Three mostly dense planes of HCP is shown; (0002) basal plane, $\{10\bar{1}0\}$ one of the three prismatic planes, and one of the six pyramidal planes, $\{10\bar{1}1\}$ The unit cell of the BCC β-Ti is also demonstrated in Fig. 3.1 Lattice

parameter for BCC is ***a*** = 0.332 nm and most densely packed plane {110} also shown in the figure. [1]

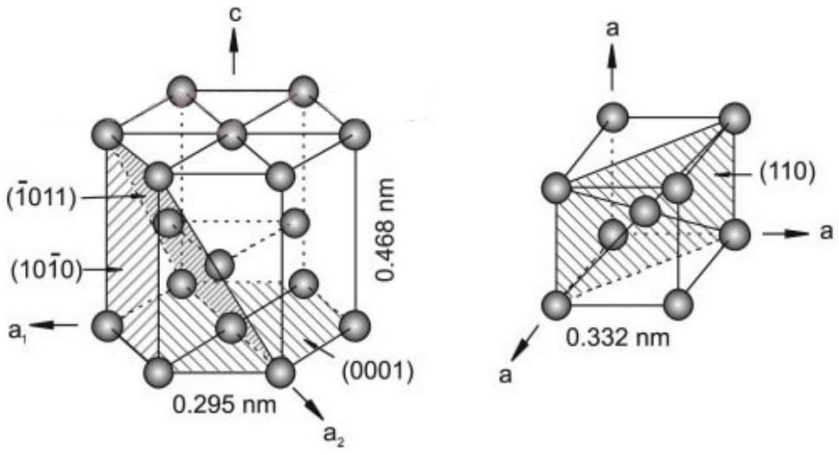

Fig 3.1 'Unit cell of α-Ti (HCP) and β-Ti (BCC)' [1]

Different phases have their own lattice structure due to the atomic arrangements, grains formed by the aggregate of similar lattice structures. Within each grain the orientation of the lattice structure is the same with distance, but across a grain boundary the next grain has a different spatial lattice orientation. [25] There is also an orientation relation during the allotropic transformation of the phases. Bieler, Trevino and Zeng showed the idealized orientation relationship between α-phase (thin lines) and β-phase (dashed lines) with the figure below, Fig. 3.2 [3]

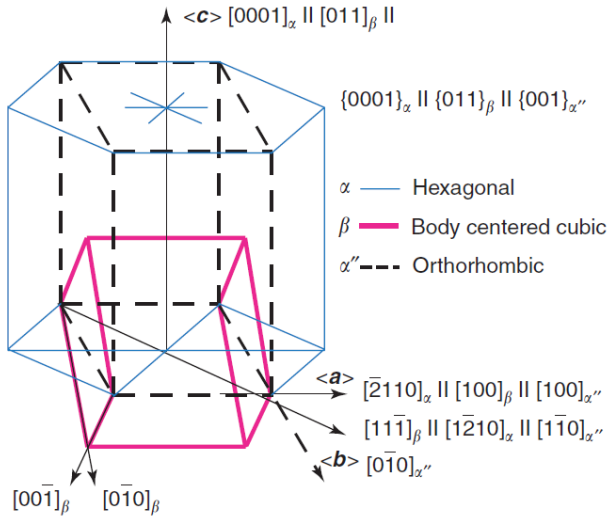

Fig. 3.2 'Orientation relationship between α-phase and β-phase during allotropic transformation' [3]

Fig. 3.2 shows perfect matching of the parameters between HCP and BCC. However it is a schematic view and lattice spacings for α and β do not match perfectly. Fig 3.3 shows the mismatch in between α, β, and α″. [3] Overlapped view of the atomic lattice positions shown in Fig. 3.3

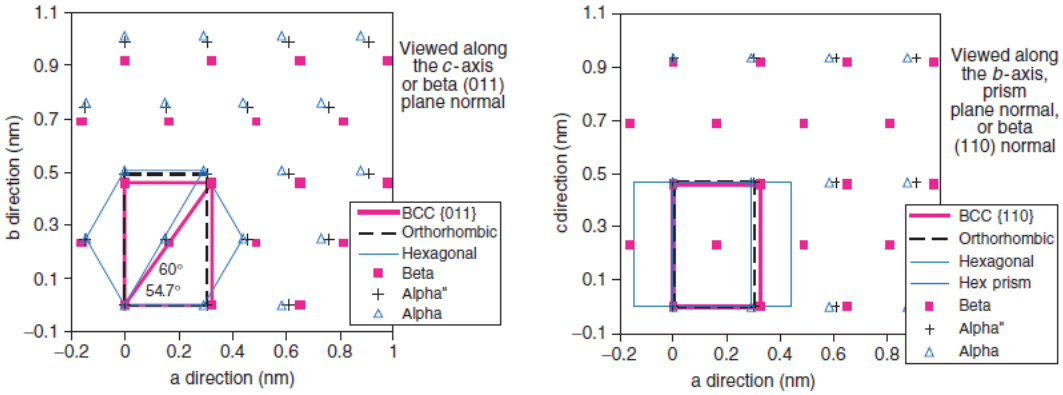

Fig. 3.3 'Atomic lattice positions of α, β, and α″ crystal structures' [3]

The α → β transformation happens with heating above the β-transus temperature, phase transformation requires lattice strains approximately 10% expansion along the $[2\bar{1}\bar{1}0]_\alpha$ to become a $[100]_\beta$ direction, approximately 10% contraction along the $[0110]_\alpha$ to become $[01\bar{1}]_\beta$, and approximately 1% contraction along $[0001]_\alpha$ that becomes $[01\bar{1}]_\beta$. Due to mismatch relations, one of the two $<111>_\beta$ directions in the {110} plane will be rotated ~5° to align itself with one of the $<\bar{2}110>_\alpha$ directions, leading to six possible variants of β from one α orientation, shown in Fig. 3.4.

Transformation of the α→β→α occurs regardless of the production process. However, microstructure can be manipulated by controlling the cooling rate from β→α+β region and also manipulated thermomechanical processing. α-phase precipitates from the β-matrix in the forms of laths or plates due to the process parameters. (cooling rate, strain value etc.) Precipitation of α-phase is explained with Burgers orientation relations between α and β. [34] According to the symmetry of the parent β and product α phases and their Burgers orientation relationship, there are twelve possible orientation variants of α precipitates within a single prior β grain. [35] The crystallographic relationship between α-Ti and β-Ti that obeys the Burgers orientation is

$$\{110\}_\beta \,//\, \{0001\}_\alpha$$
$$<1\bar{1}1>_\beta \,//\, <11\bar{2}0>_\alpha \quad [34]$$

Due to the symmetry of the BCC structure there are 6 distinct {110} planes in each β crystal and according to the Burgers orientation relationship all of them can act as the basal plane of the inherited α phase during transformation, Fig. 3.4. Since each of these planes, {110} contains two <111> direction, that determines $<11\bar{2}0>$ directions of the

inherited α phase. As a result, 12 unique α variants can be formed from a single β crystal. [36] Bieler mentioned that transformation variants preferred on $\{110\}_{\beta}$ planes which have high dislocation populations. As a result, it is possible to control the transformation process by controlling the dislocation density in the β-phase. [3]

The amount and the distribution of crystal orientation can have a large impact on both elastic and plastic properties. Even pure titanium has different properties according to the crystal orientation with respect to shear stress, any crystal can be either hard or soft. [3] For instance; HCP has considerable elastic and plastic anisotropy, for Young's modulus along c-axis has 143 GPa on the other hand a-axis has 104 GPa. The difference is higher than 35%. [3]

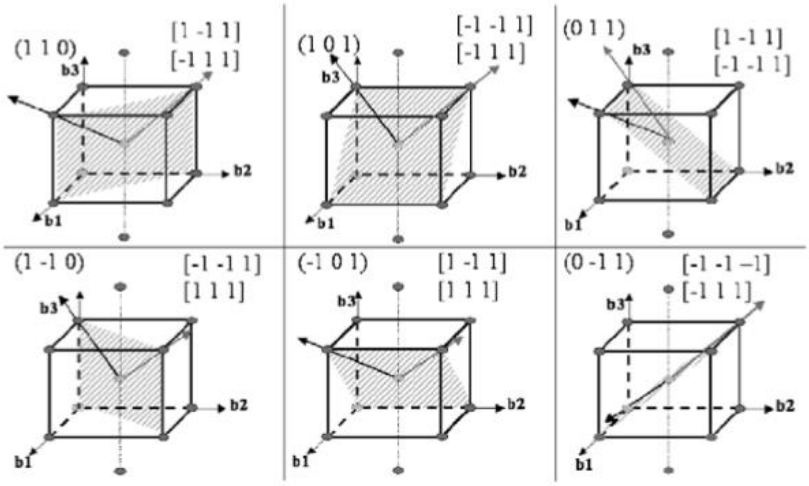

Fig 3.4 'Schematic demonstrating the formation of 12 α variants from a single β crystal following the Burgers orientation relationship' [36-37]

The amount and the distribution of the phases define the mechanical properties which are results of the process, thermal and thermomechanical history and chemical composition of the material. Titanium alloys are classified in three groups due to the phases that are existing at room temperature.

The alloying elements may form solid solutions and compounds with titanium. Substitutional elements that have a size factor are within ± 20%. [38] Allotropic transformation can be affected by the additional alloying elements in titanium. According to their effect elements can be classified in three gruops; α-stabilier, β-stabilizer, and neutral.

α-stabilier elements dissolves preferentially in the α phase and raising the β-transus temperature. [37] Aluminum is a solid solution strengther. It also reduces density snd improves oxidation resistnace. Al is the most widely used alloying element in titanium alloys, since it is only common metal raising the transition temperature and having large solubilities in both α and β-phase. [1] Carbon, nitrogen and oxygen are interstitial α stabilizer and they strength the α phase. [3]

β-stabilizer elements divided into β-isomorphous and β-eutectoid elements, Gua. β-isomorphous; molybdenum, vanadium and niobium lower the β-transus temperature. β-eutectoid stabilizers produce an eutectoid reaction. With increasing amount of these two kinds of β stabilizing elements, the β-transus temperature reduces continously until it is interrupted by compound formation to produce a two-phase structure at room temperature. [37-39-3] β-isomorphous elements are miscible in β-phase and β-eutectoid elements decrease eutectoid temperatures as much as 333 °C below the transformation temperature

of unalloyed titanium. [25] Chromium: β-eutectoid stabilizer. Cobalt: β-eutectoid stabilizer. Copper: β-eutectoid stabilizer, improves weldability, α and β strengthner. Hydrogen: β-eutectoid stabilizer, interstitial element. Nickel: β-eutectoid stabilizer. Silicon: β-eutectoid stabilizer, Si atoms tend to segregate at dislocations and thus effectively prevent dislocation climb, improving creep resistance, also strengths α phase. [3]

Neutral element have minimal effect on allotropic transformation and β-transus temperature. Zirconium: neutral stabilizer, solid solution strengthener of α-phase, Zr also tends to homogenize fine silicide precipitates. Tin: neutral stabilizer, improves weldability, solid solution strengther of α-phase. [3]

Titanium is has a mix structure of α+β below β-transus temperature if it contains β-stabilizer elements which make β-phase stabil at lower temperautres. As a result the β-transus temperature decreases. β-transus is critical in defromation processing and heat treatment. β-transus temperature will be shown later chapters in phase transformation section.

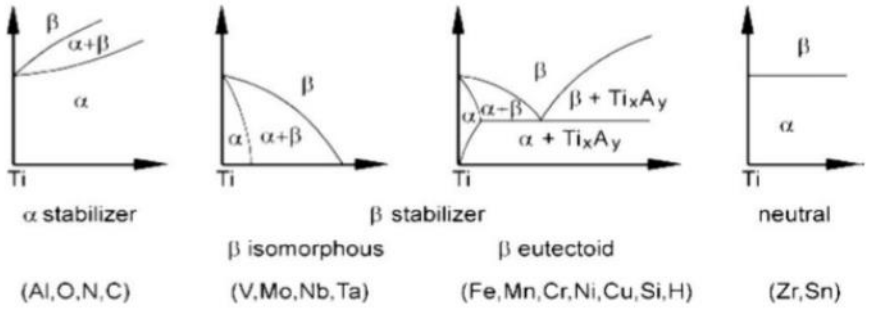

Fig. 3.5 'Effect of alloying elements on phase diagrams of titanium alloys' [1]

Titanium alloys commonly classiffied in three groups; α and near α alloys, α+β alloys, and β alloys.

3.3 α and Near α Titanium Alloys and Commercially Pure Titanium

Since the present study aims investigation of heat treatment response of CP:Ti in terms of microstructure and mechanical properties, this α titanium alloys are described with emphasis on CP:Ti. Oxygen is the main alloying element that determines the grade and strenght of the alloy. Oxygen and nitrogen, interstitial elements have great influence on strenghting the CP:Ti. [25] Four different grades of CP:Ti differ with respect to their oxygen content from 0.18% (grade1) to 0.40% (grade4) in order to increase the strength level, Tab. 3.2. Grade designations are taken from the American Society for Testing and Materials. (ASTM) [3-1]

CP Titanium	**Alloy Composition (wt%)**	**Tβ (°C)**	**σ0.2 (MPa)**
Grade 1	0.2 Fe / 0.18 O	890	170
Grade 2	0.3 Fe / 0.25 O	915	275
Grade 3	0.3 Fe / 0.35 O	920	380
Grade 4	0.5 Fe/ 0.40 O	950	480

Table 3.2 'CP:Ti grades compostion, β-transus temperature and yield stress values' [1]

There are also two more CP:Ti grades exists in addition to Tab. 3.2 which have better corrosion resistance: Grade 7 (Ti-0.2Pd) and Grade 12 (Ti0.3Mo0.8Ni) their Fe and O content is identical with Grade 2. [1]

Oxygen effect and oxidation is always of concern at elevated temperatures. Heating titanium in air at high temperatures results not only oxidation also solid solution hardening of the surface as a result of inward diffusion of oxygen, and nitrogen. When CP:Ti or any titanium alloys heated in an O_2 or N_2 containing environment, a surface hardened zone is formed. This surface-hardened layer is referred to as alpha case since oxygen and nitrogen stabilize the α-phase. Alpha case, or in other words; air contamination layer, is hard and brittle and invariably detrimental to service application. This layer should removed by chemical milling, pickling or machinig because alpha case drastically reduces fatigue, strenght and ductility. The effect of interstitial content on mechanical properties shown in the Fig. 3.6. [25]

All α titanium alloys stable in the hexagonal allotropic form of titanium at room temperature form single α-phase or α-phase containing only a trace amount of β-phase according to the interstitial and impurity level. It should be apparent that once a chemistry has been selected, microstructures in titanium alloys usually are developed by heat treatment or other processing (wrought/cast/powder metallurgy) which often uses heat and /or is followed by heat treatment.

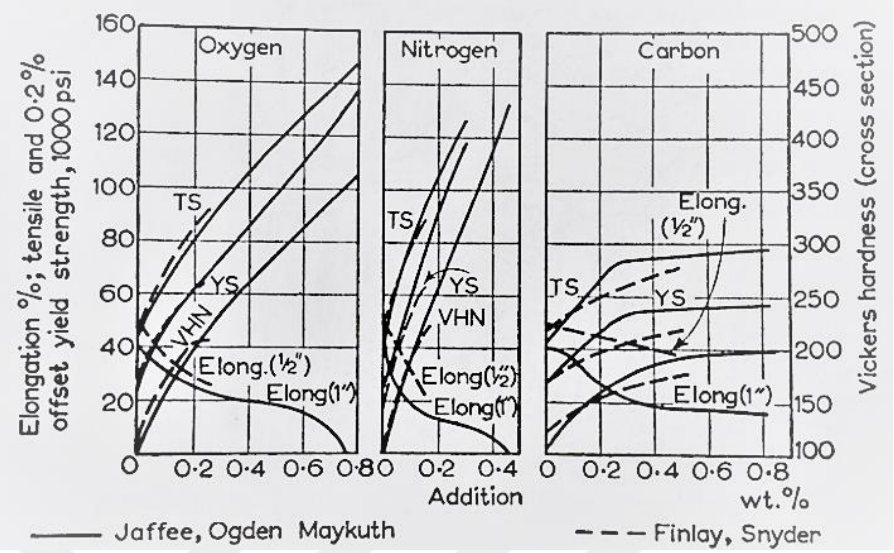

Fig. 3.6 'Interstitial effect on tensile and hardness of αtitanium alloys. Data of Jaffee are for samples annealed at 850 °C and the data of Finlay are for samples at 700 °C' [25]

With exception of CP:Ti and alpha alloys, microstructural changes are invariably produced through transformation of some or all of the alpha phase to beta phase. The microstructure that results is a function of the way in which the subsequent changes in beta or in residual (primary) alpha occur. Microstructural change is limited to grain refinement and possibly to grain shape changes in CP:Ti and α titanium alloys. [25]

CP:Ti is selected for its excellent corrosion resistance, especially in applications where high strength is not required. Yield strength of CP:Ti grades may vary from 170 MPa to about 480 MPa. [25] If it is compared to stainless steel, it is more attractive material for chemical and petrochemical processing equipment. In addition it has also become popular for heat exchangers and other piping applications because of its weldability and good general fabricability, both into tubing and the subsequent shaping of the tubing for

specific applications. When one of the other α titanium alloy selected rather than CP:Ti, this is usually because CP:Ti has insufficient strength for the intended application. The effects of composition on mechanical properties, especially strength, usually are a secondary consideration relative to the corrosion resistance. [1]

Titanium alloys have small number of alloying elements that they essentially do not respond to heat treatment, but this characteristic contributes to excellent weldability of these alloys. Thermomechanical processing of these alloys is done to control the crystallographic texture and grain size, but is not used to manipulate the microstructure in a similar manner done in α+β titanium alloys. [1]

Ti6Al4V is now the most common titanium alloy in the market. Alloying elements aluminum and vanadium are harmful metals for human body health. Implant producers want to remove these metals in their implants and research if it is possible to have mechanical requirements without alloying elements. Recently CP:Ti is investigated to use in biomedical applications. However, it has excellent corrosion resistance and the best biocompatible metal it has lower strength for service conditions of internal implants. Hip and knee implants are exposed to cyclic loadings during their life time and they require certain level of tensile strength, toughness and also fatigue properties. In the current study it is investigated that the SLM produced CP:Ti microstructure response to different heat treatments and the comparison of the initial condition and heat-treated conditions in terms of mechanical properties.

α titanium alloys are mainly used as sheet materials for fabrication. Processing route for CP:Ti shown in the Fig. 3.8 schematically. The microstructure of α alloys after

processing consist of recrystallized α grains with dispersed β-phase. This β-phase is present since there always is small amount of Fe present in all grades of CP:Ti. Fe has very low solubility in the α-phase and it therefore is rejected to form the β-phase, either during solidification or subsequent cooling. This β-phase remains stable down to room temperature.

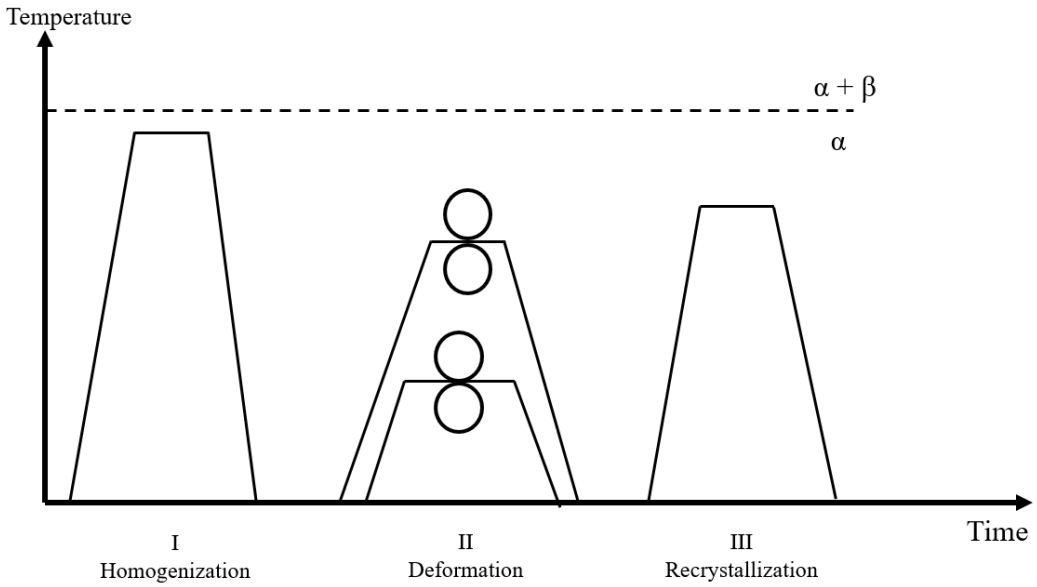

Fig. 3.8 'Schematically process route of CP:Ti and α titanium alloys.' [1]

3.4 α+β Titanium Alloys and Ti6Al4V

As their names suggest, α+β alloys are always mixture of both phases at room temperature. α+β titanium alloys contain elements to stabilize and strengthen the α-phase, together with 4-6% of β stabilizing elements which allow substantial amounts of β-phase

to be retained on quenching from β and α+β phase fields [39-37] The effect of the β stabilizer elements concentration to the equilibrium of the alloy shown in Fig. 3.9.

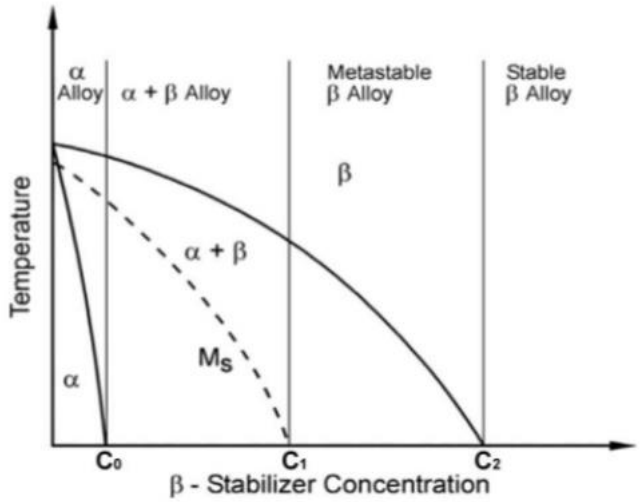

Fig. 3.9 'Pseudo-binary section through a β isomorphous phase diagram' [1]

The most important titanium alloy in this group is Ti6Al4V, represents more than 50% of the titanium market. [3] This alloy has found application for a wide variety of aerospace components and fracture critical parts. Ti6Al4V is the other titanium alloy that current study focused to investigate the microstructure changes due to heat treatments and the investigation of mechanical properties. Because of this α+β titanium alloys will described with emphasis on Ti6Al4V.

α+β titanium alloys can be solution heat treated, quenched, thermomechanical processed, and aged to medium/high-strength levels and have good formability, but the creep resistance and weldability are lower than α and near α titanium alloys since the

presence of the β-phase. This phase has a much higher diffusivity and more slip systems. [3-37]

α+β titanium alloys has three different microstructures due to thermomechanical processing route; fully lamellar, fully equiaxed, and bi-model (duplex) microstructures containing equiaxed primary α in lamellar α+β matrix. This subject will be elaborated in the section of microstructure with figures. Difference between these three microstructure depends on the processing route, the recrystallization temperature and deformation temperature. Fig. 3.10 showed the schematically view of the process route for fully lamellar microstructure. Tensile mechanical properties of Ti6Al4V for different process conditions are shown in Table 3.3.

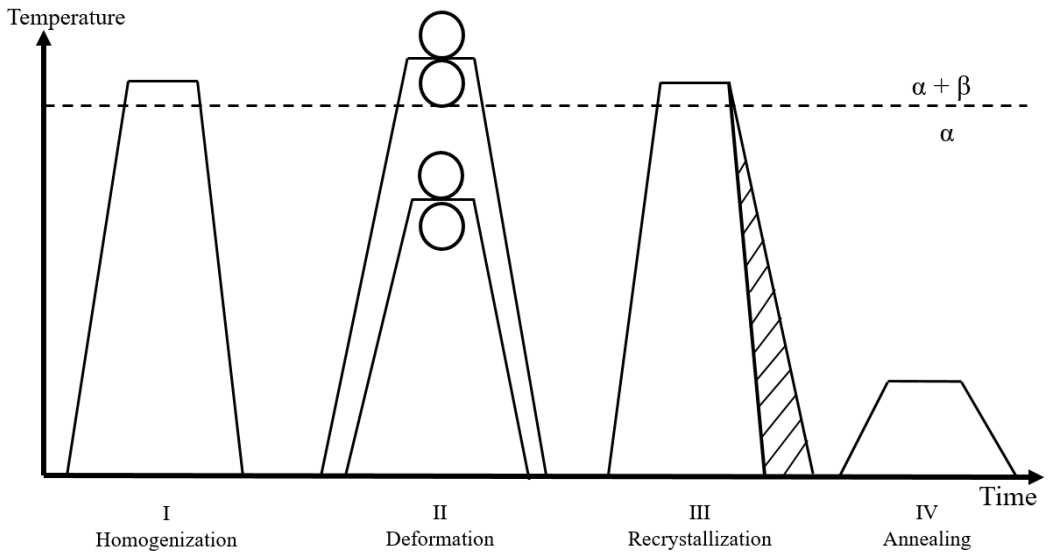

Fig. 3.10 'Schematically process route of α+β titanium alloys for fully lamellar microstructure' [1]

Condition	Yield Strength (MPa)	Tensile Strength (MPa)	Elongation (%)
Mill annealed	945	1069	10
Duplex annealed	917	965	18
Solution treated and aged	1103	1151	13

Table 3.3 'Ti6Al4V tensile mechanical properties' (at 25°C) [25]

Ti6Al4V contains 6 wt% Al and 4 wt% V. Typically uses include aerospace applications, pressure vessels, aircraft gas turbine disks, cases and compressor blades, as well as surgical implants. Ti6Al4V has an excellent combination of strength and toughness along with excellent corrosion resistance. The properties of this alloy are developed by relying on the refinement of the grains upon cooling from the beta region, or the alpha + beta region, and subsequent low temperature aging to decompose martensite formed upon quenching. During slow cooling from the beta region alpha begins to form below β-transus temperature around 980 °C. Alpha forms in plates with a crystallographic relation to the beta in which it forms. The alpha forms with their basal plane parallel to a special plane in the beta phase. Upon slow cooling nucleus formation, the alpha planes thicken relatively slowly perpendicular to this plane but grows faster along the plane because of the close atomic matching structure along this common plane. Thus, plates are developed. The microstructure consists of parallel plates of alpha delineated by beta phase between them. Where alpha plates formed parallel to one specific plane of beta meet alpha plates formed on another plane, a high angle grain boundary exists between the alpha crystals. Metallographic etching using HF acid reveals a line separating them. [25]

Upon cooling rapidly, beta may decompose by a martensite reaction, similar to that for pure titanium and form a Widmanstätten pattern. The structure presence after quenching to 25 °C depends on annealing temperature. [25]

The presence of some beta in structure after quenching from above the β-transus temperature is due to the fact that the temperature for the end of the martensite formation, M_f, is below room temperature for this alloy. That is because vanadium is a β-stabilizer, and the addition of 4% V to Ti6Al alloy is sufficient to place the M_f below 25 °C. Thus, upon quenching to 25 °C, not all of the beta is converted to alpha prime or alpha double prime. [25]

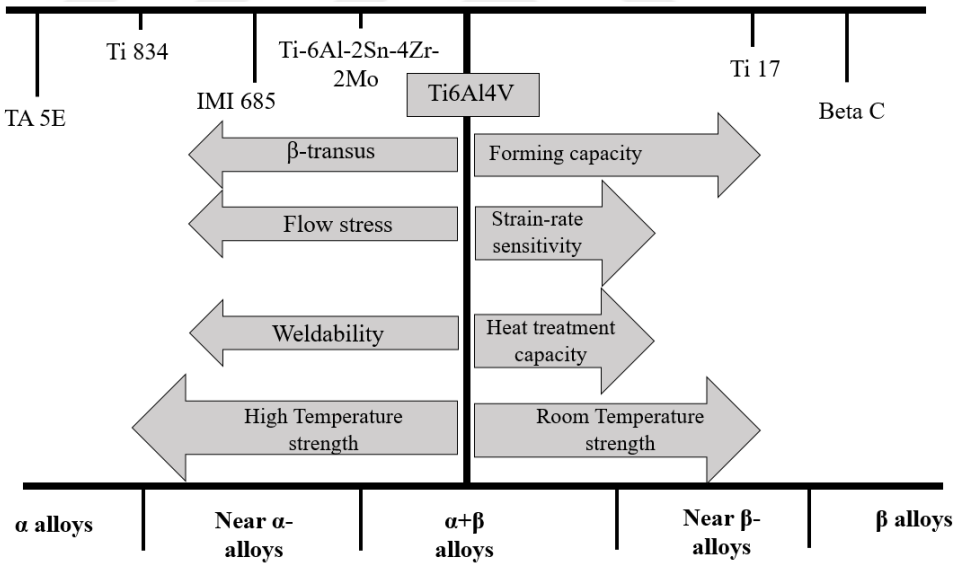

Fig. 3.11 'Main characteristics of different titanium family groupings' [25]

3.5 β Titanium Alloys

Motivation of the present study is built on CP:Ti and Ti6Al4V which are classified α titanium alloys and α+β titanium alloys respectively. Because of this β titanium alloys will not be subjected to investigation however brief information about this class is shared in this section.

β titanium alloys are, by definition, those which enable the β-phase to be retained after cooling to room temperature. Classification of metastable and stable β titanium alloys depend on the amount of the β-stabilizer alloying element. [37]

In contrast to α+β titanium alloys, β alloys do not transform martensitically upon quenching to room temperature, resulting in a metastable β-phase. The α-phase can be precipitated from the metastable β-phase as very fine, undeformable particles with a high-volume fraction. Therefore, the main characteristic of β alloys is that they can be hardened to much higher yield stress levels than α+β titanium alloys. Besides, β alloys can be processed at lower temperatures than α+β alloys, and some heavily stabilized β alloys are even cold deformable. Additionally, the β alloys have equal to better corrosion resistance than α+β alloys. The β alloys are good at environments especially where hydrogen pickup is possible since the β-phase has higher hydrogen tolerance than the α-phase. [1]

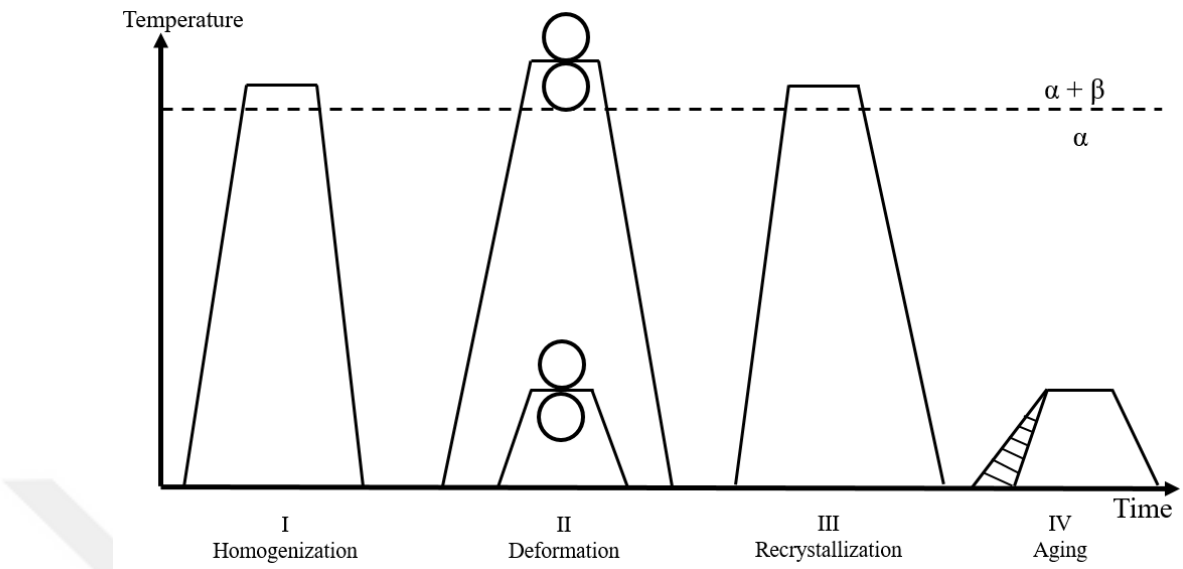

Fig. 3.12 'Schematically process route for heavily stabilized β titanium alloys' [1]

β titanium alloys are superior to other metallic implant materials and other titanium alloy groups in terms of mechanical biocompatibility. For instance, when metals implanted in bone, the difference between the Young's modulus of the bone and the metal causes stress shielding. This effect wears away the bone and causes the implant to loosen and eventually lose function ability. The Young's modulus of bone is around 30 GPa, while the modulus of stainless steel, cobalt-chromium and titanium are 200, 230, 127 GPa respectively. However, with proper alloying element additions, the modulus of beta phase titanium can be reduced to as low as 40 GPa. [40]

3.6 Phase Transformations of Titanium and Titanium Alloys

Many elements exist in different crystal structures in their solid states under different conditions of temperature, pressure, or external field. The transition of one

modification, allotrope, to another is termed phase transformation or polymorphous transformation. [38]

Phase transformation may occur in two orders; first order is the discontinuous changes in the first derivatives of the Gibbs free energy, G = H – TS, while second order transition is characterized by discontinuous changes in the second derivatives of the Gibbs free energy and there are no jump-wise changes in the first derivatives. In both type of transition, the crystal structure undergoes a discontinuous change at transition point. It is not necessary to have a symmetry relationship between the parent and the product phases in a first order transition. However, in second order transition a group / subgroup relationship can always be found in relation to symmetry groups associated with the crystal structures of the two phases. [38]

Stabilization and lattice stability should be explained to make a better understanding of phase transformation mechanism in titanium. There is a correlation between crystal structure and the group number of the transition elements and electron to atom ratio (e/a) in the case of alloys. The e/a ratio is a parameter which relates to many properties of binary transition metal alloys, particularly Ti-X alloys where X is a transition metal. In the content of Ti-X alloys α-stabilizer are generally non-transition or simple metals, on the other hand β-stabilizers are generally transition metals and noble metals. When a simple X metal is dissolved in Ti, most of the electrons belonging to X atoms occupy states in the lower part of the band and only very few appear at the fermi level. The d-shell electrons belonging to the host (solvent) tend to avoid the solute atoms and this leads to a dilution of the Ti sub-lattice. As a result of this is pre-existing any Ti-Ti bond

directionality preserves the hcp structure characteristics of Ti. As more additional X atoms the field of Ti α-stability terminated by the appearance of an intermetallic phase of the stoichiometry Ti_3X which is based on related to the hcp structure. For the case of β-stabilization we know crystal structures of transition metals change from hcp to bcc as the e/a ratio increases from 4 to 6 [40] It is possible to rationalize this stabilization of the bcc structure with electron screening model that stipulates a high concentration of conduction electrons, by enhancing the screening ion cores, may cause a symmetrical crystal structure to be favored. Thus, an increase in the electron density will tend to symmetrize the screening, thereby enhancing the stability of the bcc structure. [41-37]

Phases can be classified in two; equilibrium phases and non-equilibrium phases. Equilibrium phases; are the phases that exist when the system reaches steady state conditions. Composition of equilibrium phases at certain temperatures can be roughly predicted with phase diagrams. α-phase, β-phase, and α_2-phase are the equilibrium phases for titanium. α-phase has the hcp lattice structure that explained in the former sections of present study, it can be classified as primary α (α_p) and secondary α (α_s) depending on the formation of the phase due to the heat treatment. α_p is the α precipitate retained from the last high temperature processing or heat treatment. [37-42] Morphology of α_p can be lamellar, equiaxed or mixed due to thermomechanical history. Lamellar morphology obtained with cooling rate medium-to-slow from temperatures that are higher than β-transus or higher α+β regions. [43-37] Width of the α lamellae is correlated with the cooling rate. Transformation of the lamellar structure to equiaxed cannot be done by heat treatment itself, heavy working requires for this transition below β-transus temperature. Secondary

alpha, α_s, arises during annealing below β-transus temperature. [37] β-phase; is the phase that is more stable at elevated temperatures (above β-transus) and has structure of bcc. It is more stable at higher temperatures since it has more space to accommodate higher vibrational entropy required at high temperatures. [38] α_2-phase has an ordered hcp structure with chemical formula of Ti_3X, where X corresponds to simple metals like; Al, Ga, In, and Sn. Most common α_2-phase is Ti_3Al. α_2-phase forms at elevated temperature ageing of alloys which have higher Al content than 6 wt%. [37]

Upon rapid cooling from above β-transus temperature, β-phase is transfer to martensitic phases or metastable phases, depending on alloy composition. Four different type of martensite can be formed due to their crystal structures, hexagonal, orthorhombic, face-centered cubic and face-centered orthorhombic. [44] Among these martensites hcp and orthorhombic crystal structures are common and named as α' and α", respectively. ω is another metastable phase which can be either hexagonal or trigonal structure depending on whether the transformation is complete or in the initial stages. [45] Fig. 3.13 shows the effect of β-stabilizer elements on microstructure with quenching. Increase of the β-stabilizer transformation product changes from α' to α". Martensite start, M_s, temperature decrease with increase of the β-stabilizer. Higher cooling rates that suppressed M_s, below room temperature ω-phase forms. [38]

Martensitic α' phase is a supersaturated α-phase which is the product of diffusionless transformation. It has the same structure with α-phase and the same Burgers orientation relationship with the β-phase as does the α-phase. [45-37]

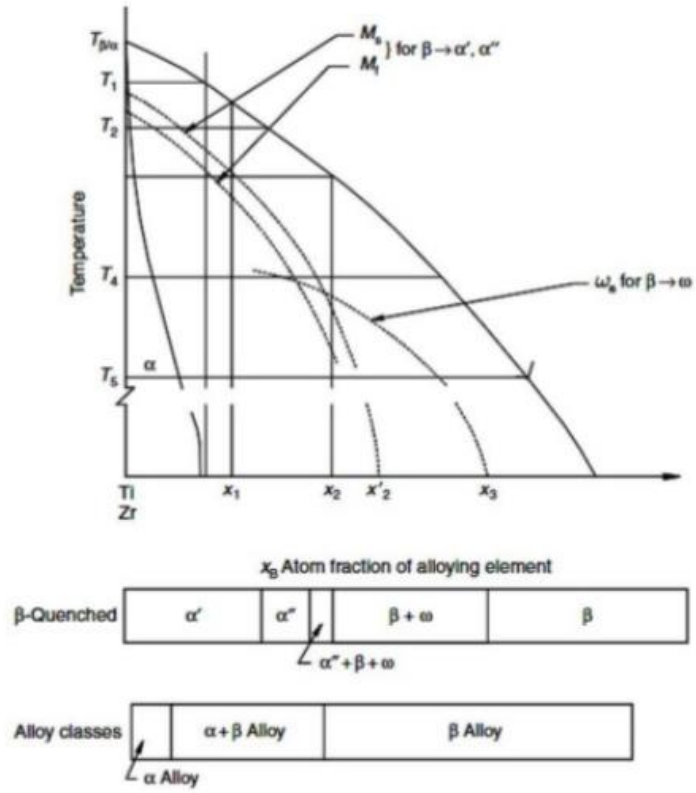

Fig. 3.13' β-stabilizer effect on microstructure with quenching' [38]

It is hard to distinguish α' phase and α-phase (acicular) because of the similar crystal lattice parameters. Fig. 3.14 shows lattice overlay of β-phase with α'/ α-phase. During the transformation from bcc to hcp, contraction of lattice a, protraction in lattice b, and minor protraction in lattice c are needed.

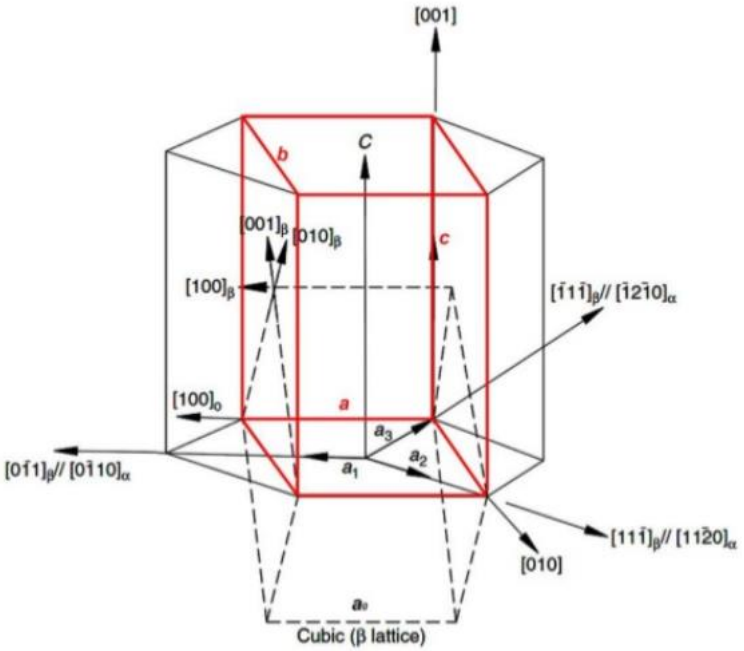

Fig. 3.14 'Lattice correspondence between bcc and hcp. Dashed lines show the position of the bcc unit cell, red lines show the tetragonal unit cell' [38]

On the contrary to steels, martensitic α' in titanium alloys does not significantly increase hardness since the martensite is supersaturated in substitutional stabilizing elements. [37] Its fine size increases hardness slightly.

α' phase has usually (massive) lath martensite and/or acicular martensite morphologies. Lath martensite consists of colonies which are optically resolvable, and its habit planes vary with alloy composition. Acicular martensite occurs with increasing solute content and decreasing M_s temperature. It looks like the mixture of individual plates, each being a different variant according to the orientation relation. [44] Detailed views of morphologies shared in microstructure section of the current study.

Martensitic α" has orthorhombic structure which has four atoms per unit cell, shown in Fig3.15. It can distinguish from α/α' with X-ray diffraction. Martensitic α" formation depends on the concentration of the β-stabilizers. With increase of the β-stabilizer content martensite structure changes from hexagonal α' to orthorhombic α" (Ti-Nb system) [46] For Ti-V systems addition of Al stabilize the orthorhombic phase, martensitic α". [47] Additionally, fast cooling rates may introduce martensitic α" by stress and strains. [48-49]

Symmetry of the β and the α" is similar to β→α transformation α" variants inherited from one prior β grain with 12 possible orientations. Lattice overlay of β and α" shown in Fig. 3.15. Since the ration between b_0/a_0 of orthorhombic α" is smaller than ideal value of hcp, √3, α" is always considered as an intermediate structure between β and α phases. [50-51]

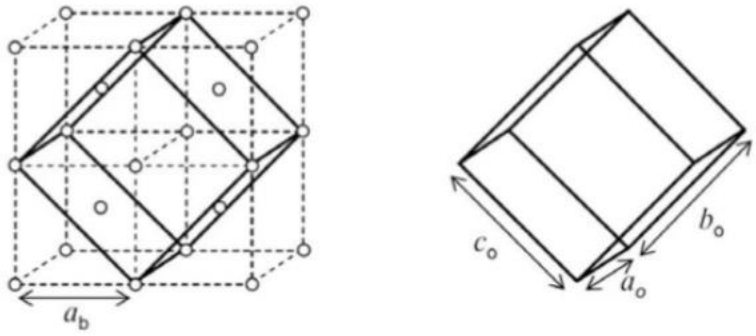

Fig. 3.15 'Schematic showing how the lattices of the β and α" phases are related.' [52-37]

Compared to other martensite phases α" is softer and have higher ductility at room temperature. [50] For instance Ti6Al4V has the modulus at around 70 GPa. [53-54]

Explanation of the low hardness of martensitic α" is not clear and could be attributed to a number of factors. Structure change from bcc to orthorhombic leads to less work hardening since smaller residual stresses. In addition to that a transition from a dislocated to twinned substructure may also leads to a drop-in hardness. [50]

Third metastable phase in titanium alloys ω-phase has hcp structure and its relationship with β-phase is $a_\omega = \sqrt{2}\, a_\beta$ and $c_\omega = (\sqrt{3}/2)\, a_\beta$. Basal plane is oriented parallel to the $\{111\}_\beta$ planes which gives four ω variants in one β crystal. [55]

ω-phase classified in two categories according to formation condition; first, athermal ω-phase that forms upon quenching metastable β alloys for which M_s is just below room temperature. Transformation from β to athermal ω is completed by the collapse of atoms in $\{111\}_\beta$ planes along $<111>_\beta$ to form coherent precipitates which are extremely small and no distinct shape. [1] The formation of athermal ω-phase cannot be suppressed on quenching and it forms without change in composition. [55] Second ω-phase precipitates isothermally as a very fine particle from metastable β when β is aged at temperature in the range of 100-500 °C [39-56] Isothermal ω forms rapidly as homogeneously nucleated, coherent precipitates with volume fraction of up to 80%, this characteristic complicates controlling of the amount of ω-phase. [55]

Type and concentration of β-stabilizers determine the morphology of the ω-phase. Ta, Nb, and Mo reduce the lattice parameter of the β phase by a small amount compared to elements such as Fe, Mn, Cr, and V. [57-37]

3.6.1 Phase Transformation Mechanisms

Solid-state phase transformations are very important since combination of different phase transformations can be used to optimize the mechanical properties of the materials. [37] α+β titanium alloys have two notable transformation mechanisms; Diffusional transformation from β-phase to α-phase and diffusionless transformation from β-phase to martensitic α' or α".

3.6.1.1 Diffusional Transformation (β→α)

Mechanism of this transformation is the diffusional nucleation and growth of α-phase. Location of the α precipitates determine the nucleation of α. Grain boundaries; α grows from the grain boundary into the β grains, and primary and secondary α that nucleate and grow within the β-phase. [51]

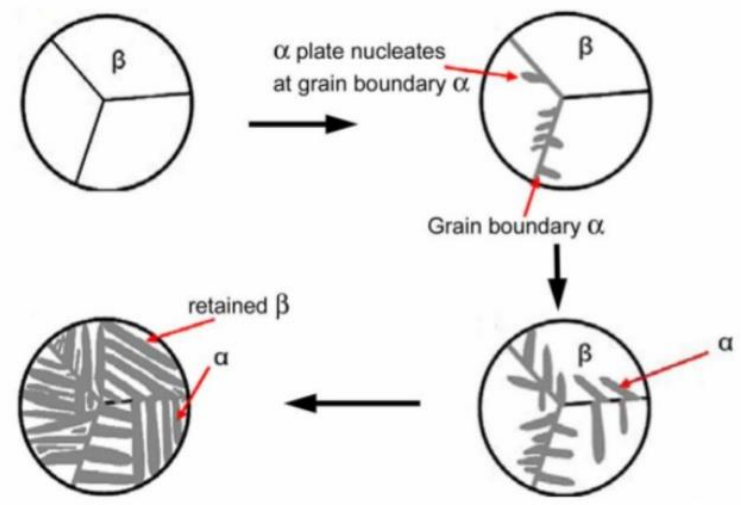

Fig. 3.16 'Schematic view of diffusional β→α transformation' [37]

Cooling with slow cooling rate from above β-transus temperature to α+β region, α nucleates preferentially at prior β grain boundaries. [58] When cooling continues, α plates nucleates either at the interface of the grain boundary α or at the β grain boundary itself, and grow into the β grain as parallel plates belonging to the same variant of the Burgers relationship which is called α colony. [1-37] The α colony, together with the retained β phase in between the individual α plates within the colony, continues to grow into the β grain until being blocked by other α colonies. [37] Cooling rate determines the number of the colonies, the width and the length of the individual α plate. α colonies length can be hundreds of microns in investment casting which has relatively slow cooling rate. [25] In the slow cooling condition, the α and β plates are often called α and β lamellae and the resulting microstructure is then designated as lamellar. [37] In faster cooling rate processes the colony sizes decrease until they contain only one or a few α plates. This microstructure is commonly referred to as basket-wave or Widmanstätten. [37] With high cooling rates colonies nucleated at β grain boundaries cannot fill the whole grain interior anymore and colonies start to nucleate also on boundaries of other colonies. To minimize the overall elastic strains, the new α plates nucleating by 'point' contact on the broad face of an existing α plate tend to grow nearly perpendicular to that plate. This selective nucleation and growth mechanism in combination with smaller number of α plates within the colonies leads to characteristic microstructure called basket-wave or Widmanstätten. [1] This basket-wave or Widmanstätten structure observed more frequently in alloys with higher contents of β stabilizers, especially with slow diffusing elements. [1]

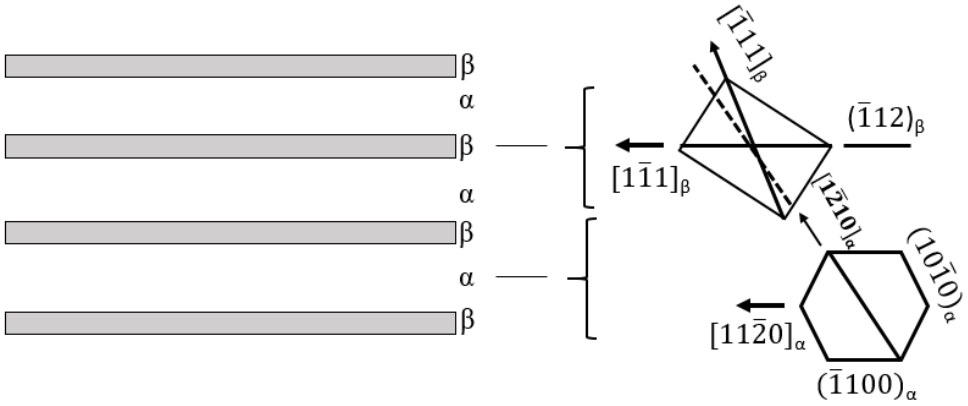

Fig. 3.17 'Schematic representation of the crystallographic relationship between α plates and β matrix in α colonies' [1]

3.6.1.2 Martensitic Transformation (β→α'/α")

The martensite transformation or diffusionless transformation involves the cooperative movement of atoms by a shear type process resulting in a microscopically homogeneous transformation of the bcc into the hexagonal crystal lattice over a given volume. [1] The extremely fast speed makes martensite able to grow independently of thermal activation [59] The first and foremost condition of a martensitic transformation is that the product phase inherits the composition of the prior β-phase. [1]

Generally, the martensitic plates contain a high dislocation density and sometimes twins. The hexagonal α' martensite is super saturated in β stabilizers and, upon annealing in the α+β phase field, decomposes to α+β by precipitating incoherent β particles at dislocations or β-phase layers at plate boundaries. [1]

With increasing solute content, the hexagonal structure of the martensite becomes distorted and, from crystallographic viewpoint, the crystal structure loses its hexagonal symmetry and must be described as orthorhombic which designated as α". [1]

One of the characteristic of martensitic transformation is that there are strict lattice correspondence and orientation relation between parent and product lattice. The orientation relationships between β and α'/α or α" Burgers proposed that transformation from bcc to hcp occurred by heterogeneous shear on $(21\bar{1})[1\bar{1}1]$, which transforms the (011) bcc plane to (0001) plane of the hcp structure. Such a transformation of structure is demonstrated in Fig. 3.18 after shear, the change in structure is then completed by a shuffle of the atom in the position O into the position B or C to obtain the hcp stacking. [37-60]

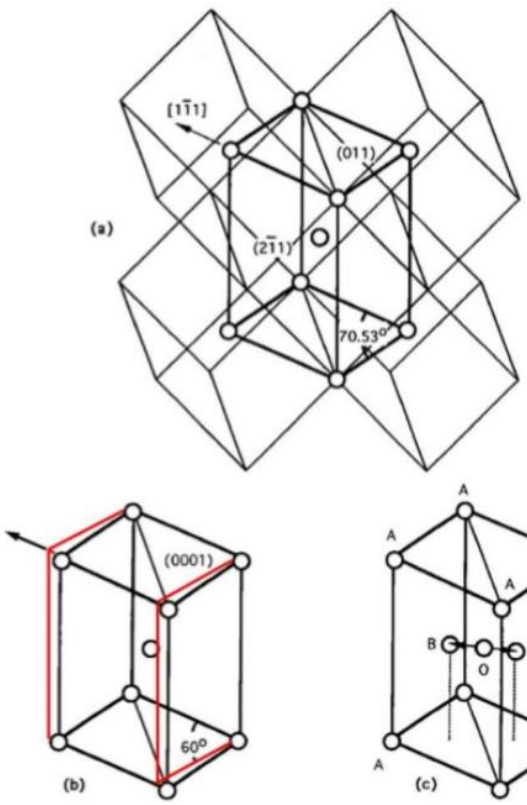

Fig. 3.18 'Structure transformation from β to martensitic α'; (a) a basis cell for hcp structure outlined within five bcc unit cells before transformation. (b) shear along [111] minishes the angle between the basal axes of the cell to transfer it to a hexagonal unit cell. (c) Shuffle of the atom to obtain the final hexagonal structure' [60]

As it is mentioned before there are 12 possible variants that can form from prior β-phase due to the Burgers orientation relationship, these 12 variants are not always equally favoured. The choice of the variant is generally made by selecting one which involves the minimum distortion and rotation of corresponding lattice vectors. [37] A study on pure titanium showed that some transformation variants are preferred over others. Some martensite plates whose mutual strain coupling effect can significantly reduce the overall strain energy are formed preferentially. [61]

3.6.2 Binary Ti-X Systems

Margolin and Nielsen [62] classified β-stabilized Ti-X systems in three groups; 1) α-β isomorphous systems in which X is completely soluble in the α as well as β-phases (e.g. Ti-Zr, Ti-Hf), 2) β-isomorphous systems where X is completely soluble in the β-phase and has limited solubility in the α-phase. (e.g. Ti-V, Ti-Mo) and 3) β-eutectoid systems where X has a limited solubility in the β-phase which decomposes eutectoidally into the α-phase and an appropriate intermetallic phase, Ti_mX_n, on cooling. [38] Later then this Molchanova (1965) classified Ti-X binary systems in four categories which is a simpler classification of the earlier three main groups with subgroups version. 1) β-isomorphous, 2) β-eutectoid, 3) Simple peritectic, 4) β-peritectoid. (Fig. 3.19) [38]

Aluminum is an α-stabilizer, the binary phase diagram of Ti-Al shown in the figure 3.20. It is obtained that increasing aluminum content the Ti_3Al (α_2) phase will be formed and that the two region (α+ Ti_3Al) starts about 5%Al at around 500 °C. To avoid any appreciable amount of coherent Ti_3Al precipitates in the α-phase, the aluminum content in most titanium alloys is limited around 6%. [1]

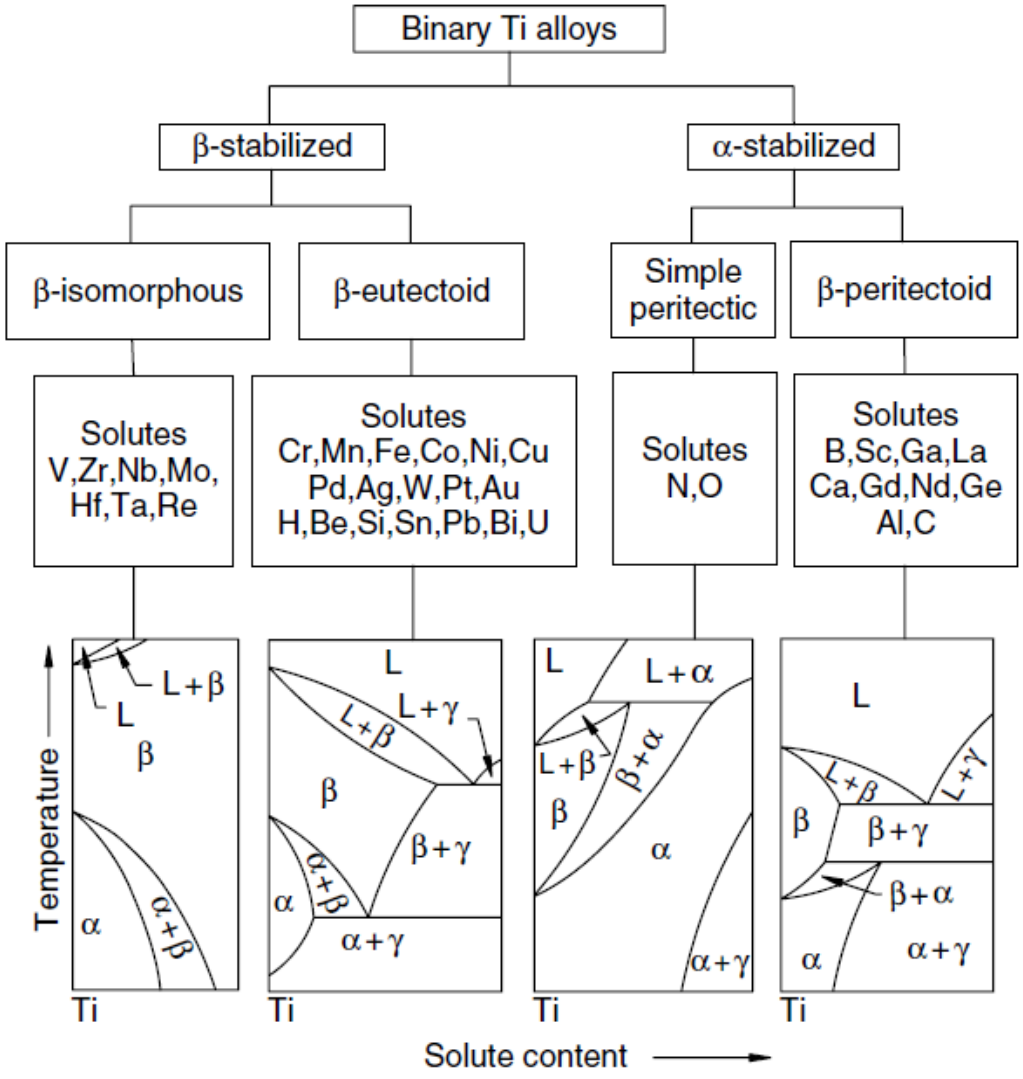

Fig. 3.19 'Classification of Ti-X binary systems' (Legend γ stands for the pertinent intermetallic phase) [38]

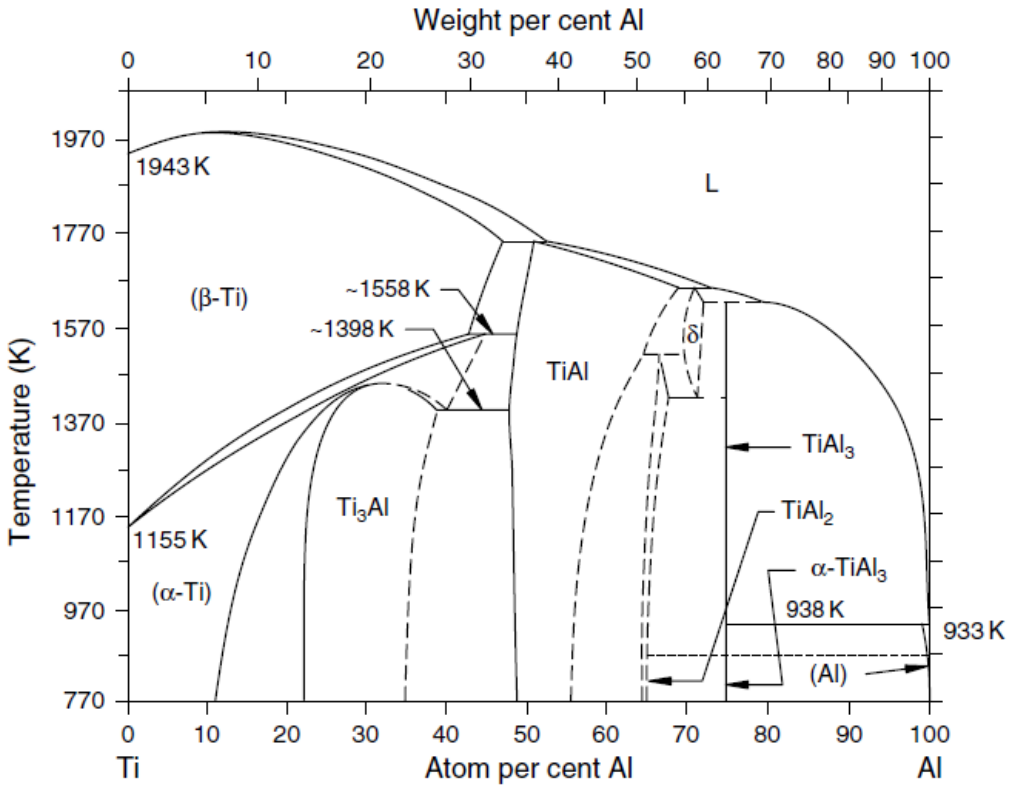

Fig. 3.20 'Ti-Al equilibrium phase diagram' [38]

3.6.3 Ternary Systems – Ti6Al4V

Ternary phase diagram for Ti-Al-V and pseudo binary equilibrium diagrams Ti-V for fix amount of Al can be found in literature [38-63] Also simulation for any amount for each element can be done with different software programs. Therefore, the amount of equilibrium α and β-phase and their chemical compositions at certain temperature can be deduced from the phase diagrams. [37] Fig. 3.21 shows the calculated data for Ti6Al4V. It can be seen 100% β-phase obtained at 1000 °C, consisting with β-transus temperature reported as 995 ±20 °C [45] At 1000 °C, β-phase contains approx. 6 wt% Al and 4 wt% V. When the β→α transformation starts, Al diffuses into the α phase, and at the same time V

is expelled from the α. [37] Therefore the amount of V in the β-phase increases during the formation of α. The observations by transmission electron microscopy and the results of energy dispersive spectrometry analysis indicates that the β→α phase transformation is mainly controlled by V diffusion. [58]

Cooling rate has significant effect on microstructure as mentioned earlier. Final microstructures of Ti6Al4V due to different cooling rates shared in microstructure section of the present study. The effect of cooling rate with different quenching temperatures shown in Fig. 3.22

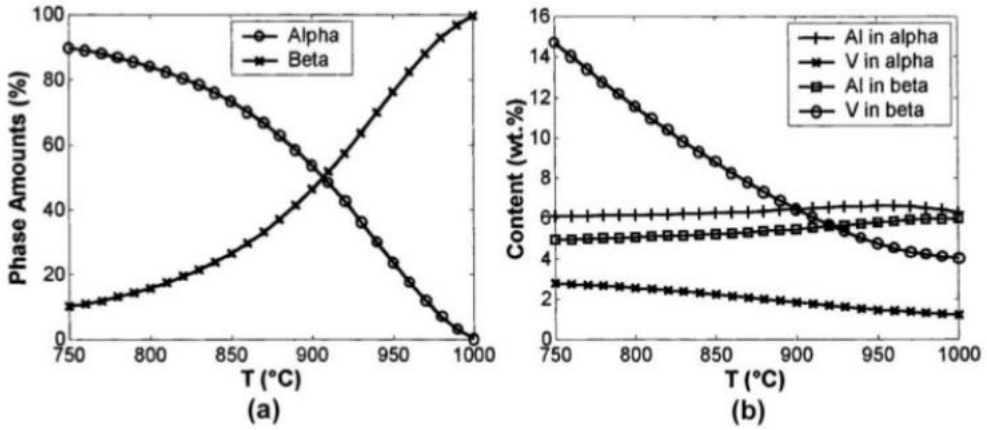

Fig. 3.21 '(a) Volume fraction of phases vs temperature. (b) Al-V equilibrium concentration in each phase vs. temperature' [64]

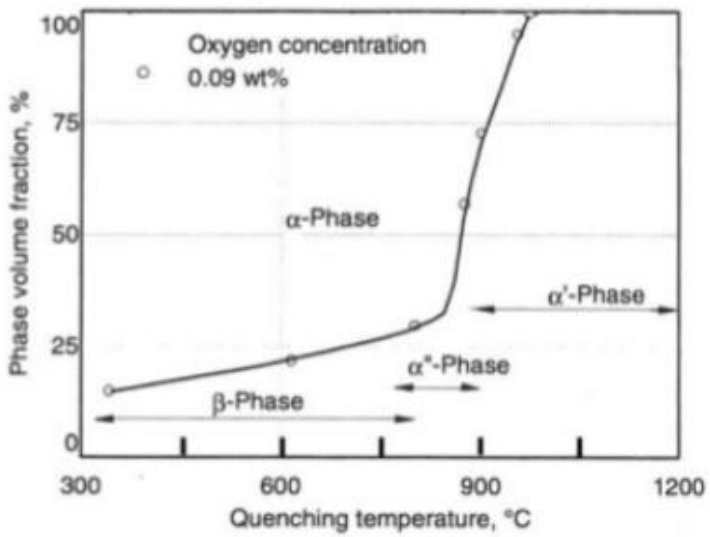

Fig. 3.22'Quenching effect with different cooling rates on phase transformations at constant oxygen concentration (0.09 wt%)' [53]

3.7 Microstructure

In this section the basic correlations between processing, microstructural features, and partially mechanical properties of titanium alloys are shared. The mechanical properties of titanium alloys shared more detailed in the mechanical property section of the current study.

Microstructure of materials determines the mechanical properties of the components as a result of both chemical composition of the alloy and thermomechanical process history. Processing can be classified in three major steps for titanium. First, casting of titanium alloys for ingots in the chemical composition of the component produced. Second, shaping process of the component such as forging, extrusion, hot-rolling, cold-rolling, machining or welding/joining. Shaping process is defined due to the geometrical

complexity (desired dimensions) of the component and the required mechanical properties, by design & production engineers. Finally, third major step is the heat treatment. This step ensures final mechanical properties required from the component like grain refinement stress relieving. The microstructural features like grain size/shape are primarily governed by thermomechanical processing and heat treatment. It is possible to manipulate and design the processes to produce different microstructures with distinct combinations of properties. [37]

3.7.1 Microstructure of α Titanium Alloys and Pure Titanium (CP:Ti)

Properties that are defined by microstructure of α titanium alloys are depend on composition (i.e. oxygen content for CP titanium). Processing history also has effect on microstructure, but not for the phase distribution or phase fraction of microstructure only effects the grain size and the texture orientation. [1] the properties of α titanium are more direct dependent to chemical composition as opposed to α+β and β titanium alloys.

Generally, the sheet products show continuous variation of the yield strength and elastic modulus between the longitudinal and transverse directions. In α titanium alloys, elastic constants are higher on the c-axis compared to perpendicular direction. This difference in elastic constants increases in Ti-Al alloys, since Al is a substitutional element which contracts the α-phase lattice. On the contrary oxygen which is an interstitial element has no essential effect on modulus of elasticity. Thus, the composition dependence of texture effects on modulus is smaller in CP titanium than for alloys such as Ti5Al2.5Sn.

[1] At this juncture it is good to explain what texture means in microstructure features. Texture is pronounced orientation of certain crystallographic planes in certain directions depending on the processing direction. Crystallographic texture in other words preferred orientation in a polycrystalline is represented by {hkl} <uvw> where {hkl} means the planes of crystal lie parallel to the rolling plane, and <uvw> directions point parallel to the rolling directions for rolled sheet materials. [37] Texture variant between α and β phases is based on the Burgers orientation relationship (BOR). However, some experiments demonstrated that variants between two phases do not occur in equal probability (six possible variants α→β and twelve possible variants β→α) For instance, β texture may not fit BOR with the originally α-phase in Ti6Al4V during α→β transformation. [65-66]

CP titanium typically produced as coil and during coil production the rolling is largely unidirectional, and the type and intensity of texture present is attributable to this working practice. [1] The typical texture present in CP titanium has the maximum concentration of basal poles lying along the direction that connects the sheet normal and the sheet width (transverse direction).

Interstitial elements such as oxygen and nitrogen have significant effect on CP:Ti microstructure. As it is mentioned earlier sections increase of the amount of oxygen and nitrogen decreases toughness. On the contrary the tensile strength increases. (Fig. 3.6) Comparison of the microstructure with oxygen and nitrogen added pure titanium shown in the figure below.

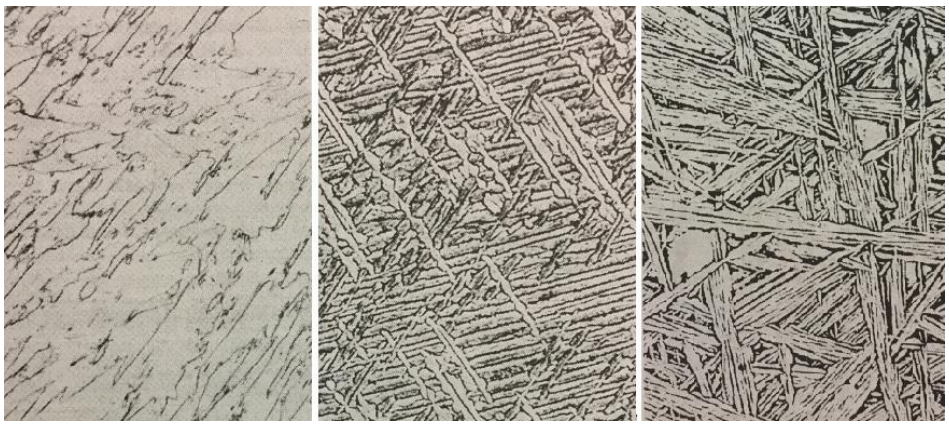

(a) (b) (c)

Fig. 3.23 'Microstructure comparison of CP:Ti and interstitial added titanium (a) relatively pure titanium (b) 0.3 wt% O added microstructure after annealing in the β region, (c) 0.3 wt% N added' [25]

Equiaxed microstructure of CP:Ti after annealing at 800 °C (below β-transus temperature) is shown in the figure below. (Fig. 3. 24 (a)) For annealing from above the β-transus temperature, 1000 °C, and quenching to 25 °C. The structure is shown in Fig 3.24 (b). It shows that in pure titanium even with rapid cooling, quenching does not suppress the β→α transformation final structure transformed entirely to α-phase. Note that the alpha grain boundaries are serrated and quite irregular. This structure is stronger than the equiaxed structure developed by annealing only alpha region. In Fig. 3.24 (c) slow cooling structure shows it is also fully alpha but the grain boundaries are less irregular than those produced upon cooling rapidly. This structure is weaker than fast cooling structure but still stronger than the equiaxed structure. [25]

(a) (b) (c)

Fig. 3.24 'CP:Ti microstructure at different cooling conditions from different annealing temperatures; (a) annealed 1 h at 800 °C water quenched 0.2% yield strength = 124 MPa Tensile strength = 248 MPa, elongation = 80%, (b) Annealed 1 h at 1000 °C water quenched 0.2% yield strength = 228 MPa, Tensile strength = 290 MPa, elongation = 60%, (c) Annealed at 1000 °C furnace cooled 0.2% yield strength = 165 MPa, Tensile strength = 262 MPa, elongation = 60%, all images taken with light microscope at x100' [25]

3.7.2 Microstructure of α+β Titanium Alloys and Ti6Al4V

There are three typical microstructures in α+β alloys; fully lamellar, bimodal, and fully equiaxed. Fig. 3.25 shows each microstructure below.

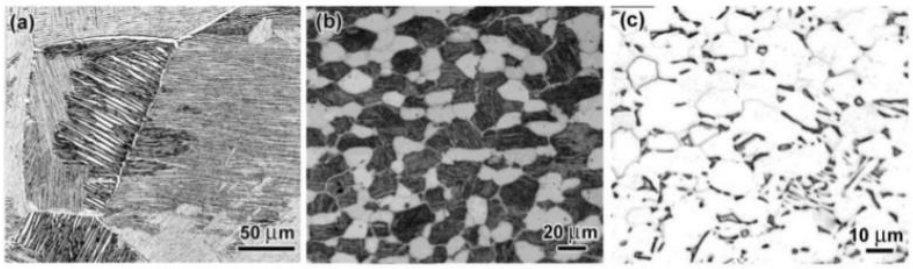

Fig. 3.25 'Typical microstructure of α+β titanium alloys; (a) Fully lamellar, (b) Bimodal, (c) Fully equiaxed' [67]

3.7.2.1 Fully Lamellar Structure

Lamellar structure can be obtained easily with an annealing treatment in the β-phase at final steps of the processing. This treatment is also called β recrystallization. [1] Whole processing route schematically shown in Fig. 3.10. Recrystallization treatment in the β region is step III. Deformation can be done either in the β region or α+β region. Deforming in the β region preferred in industrial practice since lower flow stress exists compared to the α+β region and to avoid the large β grain size. [1] Recrystallization temperature is kept slightly over β-transus temperature (+ 30-50 °C) with the same reason: avoid the β grain growth. As a result, β grain size of fully lamellar microstructures is around 600μm. [1]

Features of the lamellar structure such as size of the α lamellae, the size of the α colony, and thickness of the plates (α layers) at the β grain boundaries are highly dependent to the cooling rate from the β region. Fig 3.26 shows the microstructures of Ti-6242 alloy with different cooling rates.

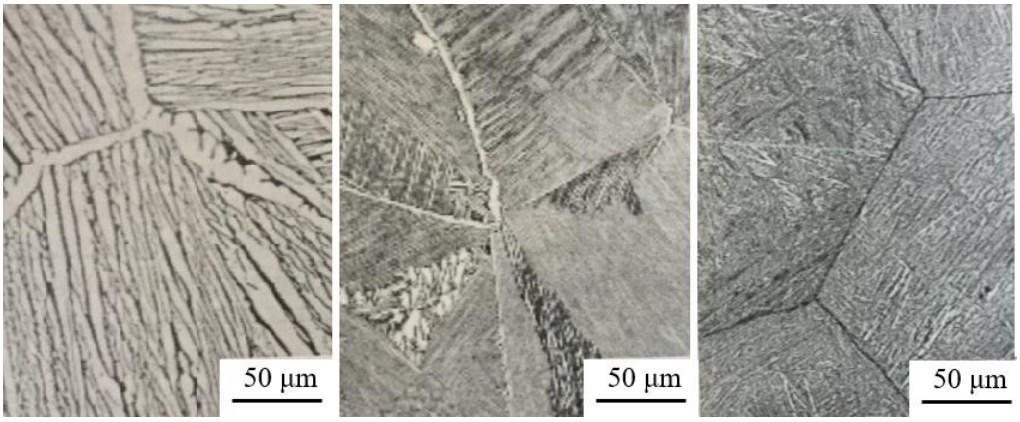

(a) (b) (c)

Fig. 3.26 'Cooling rate effect from β region on microstructure, Ti-6242, (a) 1 °C/min, (b) 100 °C/min, (c) 8000 °C/min' (LM) [1]

Majority of the commercial cooling rates have typical microstructures which are shown in Fig. 3.26 (b). Cooling rate of 100 °C/min occurred at water quenched thick section forgings or forced air cooling of thin sheets. The change of colony or Widmanstätten type microstructure to martensitic structure, with critical cooling rate that avoids the nose in CCT diagram, is naturally alloy dependent. For the most common α+β alloys; Ti6Al4V and Ti-6242 this change occurs at cooling rates that are faster than 1000 °C/min. Therefore, martensitic microstructure is rarely present in structural components. [1]

The width of individual α plates and the α colony size decrease with increasing cooling rate. The change of the size is not linear with the change of the cooling rate. The width of the α plates decreases drastically from 5μm in slowly cooled material to 0.5μm for a cooling rate of 100 °C/min. For the further increase on cooling rate only leads reduction to 0.2μm with a fair amount of thicker martensite plates present in the structure. [1]

Decrease of the colony size is not as significant as the decrease of the individual α plate thickness. α colony size can be half of the β grain size around 300μm in slowly cooled components, at a moderate cooling it decreases to 100μm. (cooling rate 100 °C/min.) [1]

Final step of processing route for the α+β titanium alloys is annealing, Fig 3.10. Temperature is the most important parameter for annealing since temperature determines whether age hardening of the α-phase by Ti_3Al particles occurs or not. For instance; Ti_3Al solvus temperature in Ti6Al4V is 550 °C. Treatment at 500 °C will cause Ti_3Al precipitation on the other hand heat treatment at 600 °C or above will be only cause stress

relieving. In the final annealing step, it is pointed out that martensitic microstructures can be changed to fine lamellar α+β microstructure in the temperature range around 700-850 °C. By this annealing treatment, β-phase is formed as a continuous layer between martensitic plates. [1]

3.7.2.2 Bimodal Microstructure

Bimodal microstructures obtain from a processing route schematically shown in Fig. 3.27, where only homogenization treatment done above β-transus temperature. Bi-model microstructure consists both globular primary α and transformed β grains.

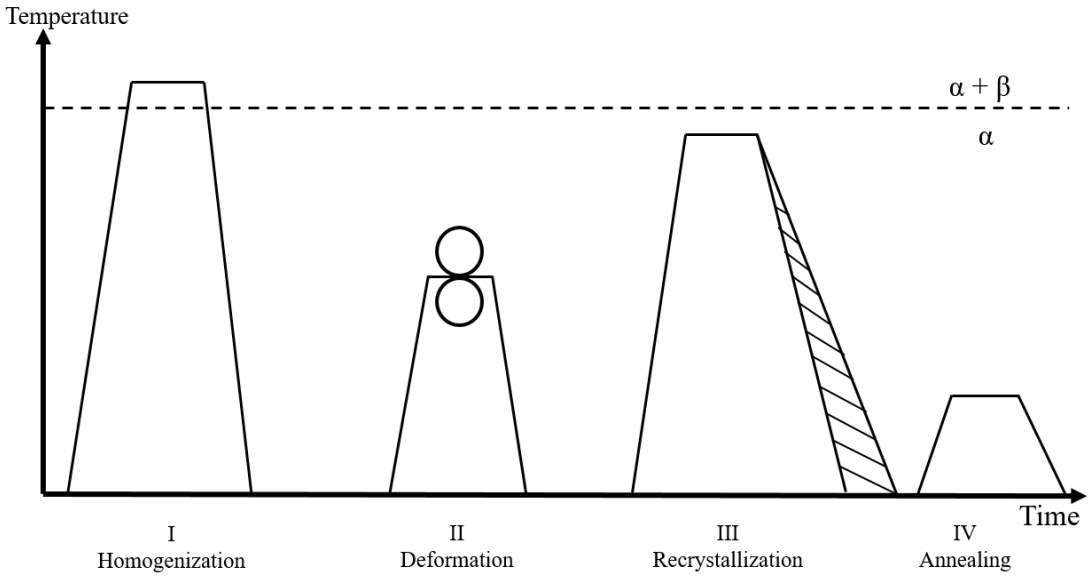

Fig. 3.27 'Schematically processing route for bimodal microstructures of the α+β titanium alloys' [1]

Cooling rate from above the β-transus temperature is a critical parameter to determine the width of the α lamellae. The difference between two different cooling rate with same processing route is shown in Figure 3.28, and difference in between equiaxed primary α size can be seen. [1]

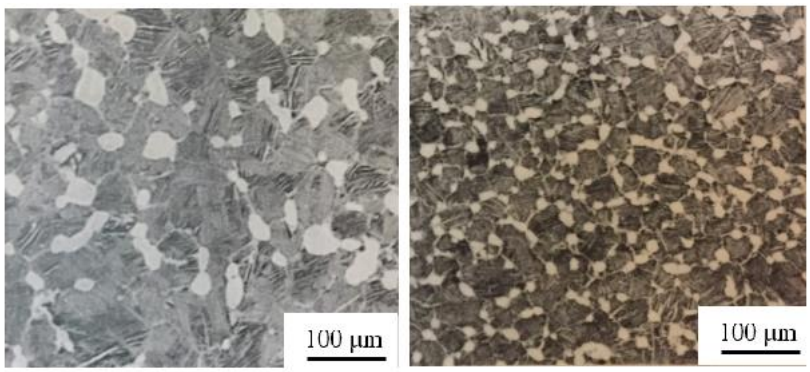

(a) (b)

Fig. 3.28 'Cooling rate of homogenization effect on bi-model microstructure grain size, (a) slow cooling rate, (b) fast cooling rate' (LM, IMI834 alloy) [1]

Temperature is the most important parameter for step III of the bimodal microstructure processing route in α+β titanium alloys. This step determines the volume fraction of the recrystallized equiaxed primary α located at the "triple-points" of the recrystallized β grains. Together with α_p volume fraction and the α_p size defines the most important microstructure feature of the bimodal structure, namely the β grain size which is about equal to the distance between primary α. (Fig. 3.28) [1]

3.7.2.3 Fully Equiaxed Microstructure

Fully equiaxed microstructure can be obtained with the same processing route of bimodal microstructure up to recrystallization process, step III. If cooling rate from the recrystallization annealing temperature is sufficiently low, only the α_p grains will grow during the cooling process and no α lamellae are formed within the β grains, resulting in fully equiaxed structure with the equilibrium volume fraction of β phase located at the "triple-points" of the α grains. Typical processing route for fully equiaxed microstructure shown in the figure below. (Fig. 3.29) An example for such a fully equiaxed microstructure is shown in Fig. 3.30. In this case the α grain size will be large and always be larger than the α_p size of the corresponding bimodal structure which would have been formed upon faster cooling. [1]

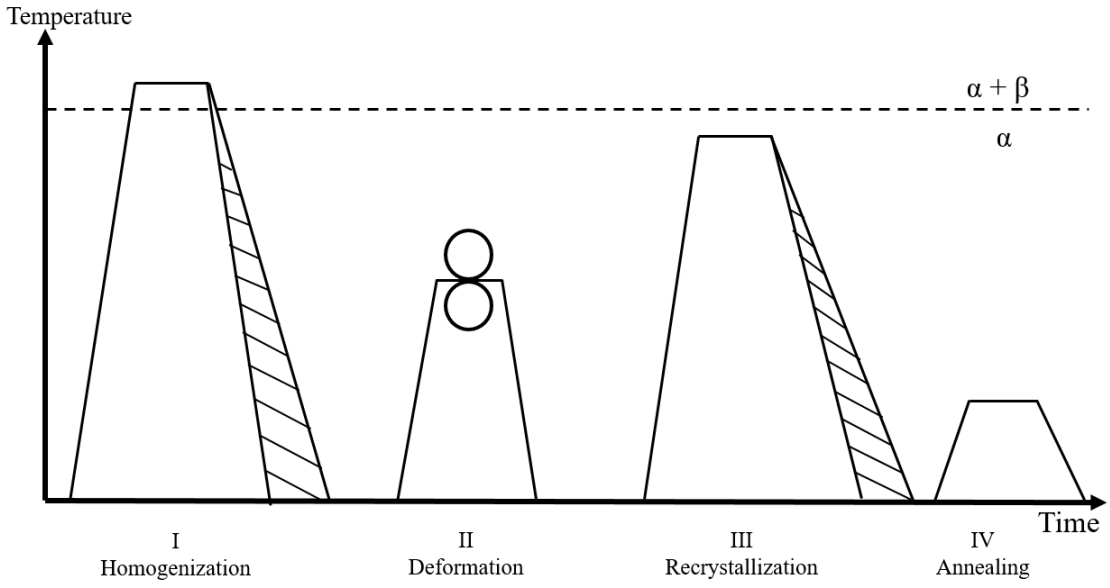

Fig. 3.29 'Schematically processing route for fully equiaxed microstructure for α+β titanium alloys' (slowly cooled from the bimodal recrystallization annealing temperature) [1]

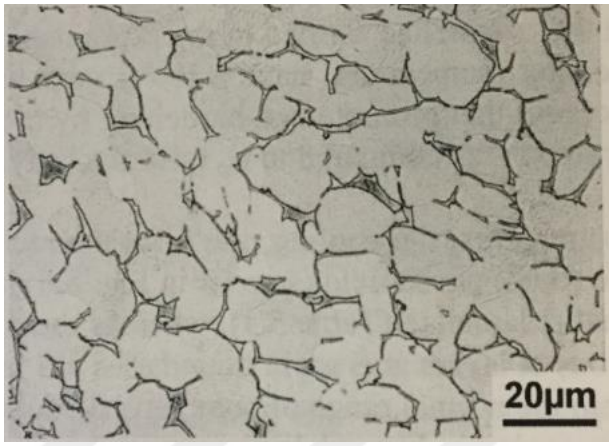

Fig. 3.30 'Fully equiaxed microstructure of the Ti-6242 alloy slowly cooled from the bimodal recrystallization temperature' (LM) [1]

Another possibility to obtain a fully equiaxed microstructure is recrystallization at a low temperature that equilibrium volume fraction of α-phase at the temperature is high enough to form the fully equiaxed microstructure directly from the formed lamellar structure during the recrystallization process. [1] α-phase penetrates along β/β grain boundaries into the recrystallized β. Using this second processing route (Fig. 3.31) with low recrystallization and annealing temperature (i.e. 800-850 °C for Ti6Al4V) smaller α grain sizes can be achieved as compared to the first method described above. For instance, recrystallization temperature at 800 °C for Ti6Al4V results with fully equiaxed microstructure in laboratory conditions with grain size around 2µm. [1]

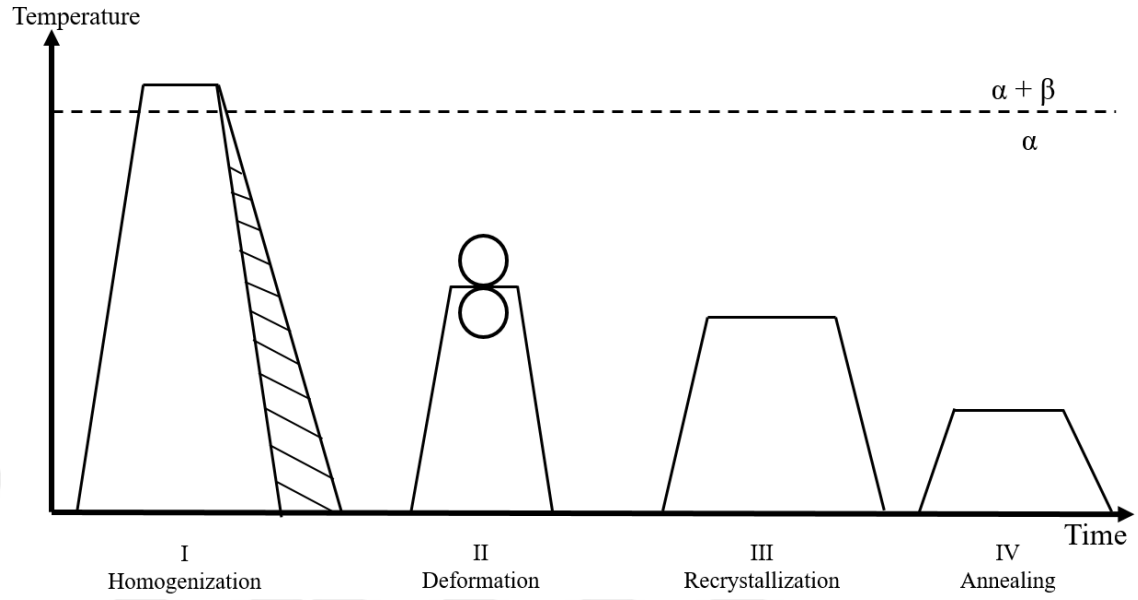

Fig. 3.31 'Schematically processing route for fully equiaxed microstructure for α+β titanium alloys' [1]

As it is mentioned several times cooling rate is one of the most important parameter that defines the microstructure features. Fig. 3.32 shows different microstructures at annealing conditions of Ti6Al4V, cooling with different rates from the same temperature. Slow cooling, the microstructure morphology consists of sets of parallel α plates surrounded by β-phase precipitates between them. (Fig 3.32 (c)) Higher cooling rate enhances the formation and growth of these α platelets however decreases the individual width. Higher cooling rates promote the nucleation of α inside β grains and lead to formation of the basket-weave structure. (Fig. 3.32 (b)) Increasing cooling rate even higher rates leads to martensitic transformation.

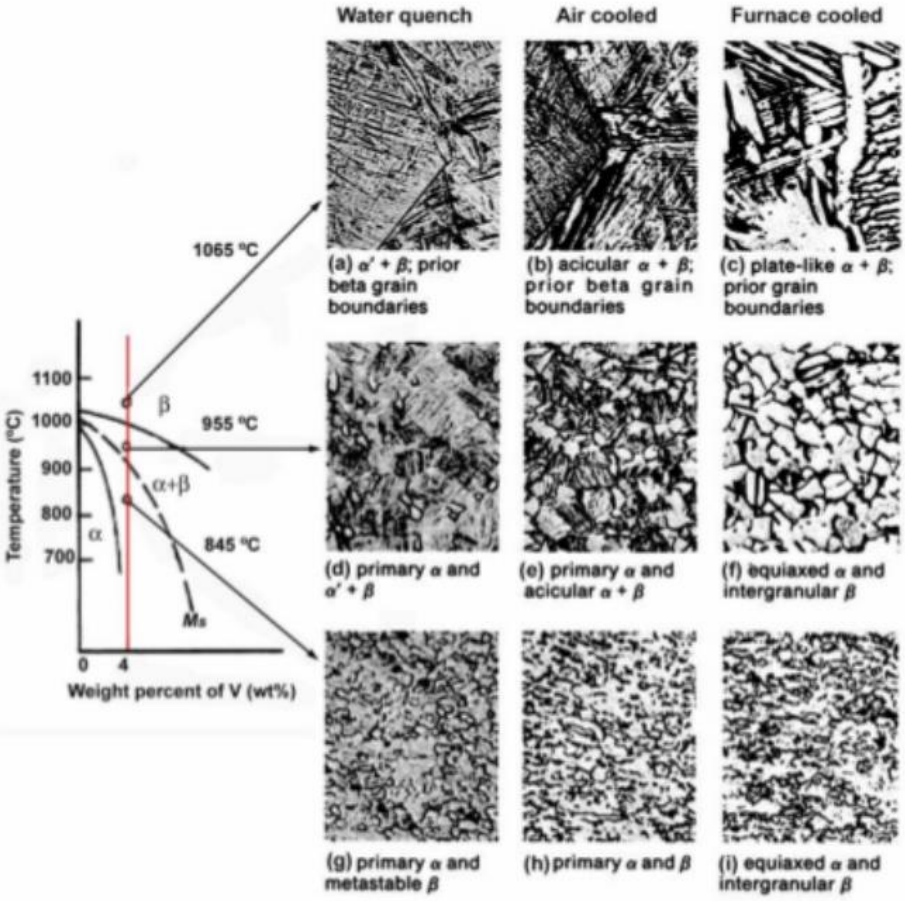

Fig. 3.32 'Effect of cooling rate on the microstructure of Ti6Al4V alloy.' [25]

3.7.3 Microstructure of β Titanium Alloys

β titanium alloys do not transform martensitically upon quenching in contrast to α+β titanium alloys. Metastable β-phase is formed after quenching and α-phase can be precipitated from the metastable phase as very fine and undeformable particles with a high-volume fraction. Therefore, the main characteristic of β titanium alloys are that they can be hardened to much higher yield strength levels than α+β titanium alloys. [1]

Key microstructural feature of all β alloys is β annealed structure, process route is shown in Fig. 3.33. Recrystallization is done in β region and aging is done in the α+β region to precipitate the α-phase in form of fine α platelets.

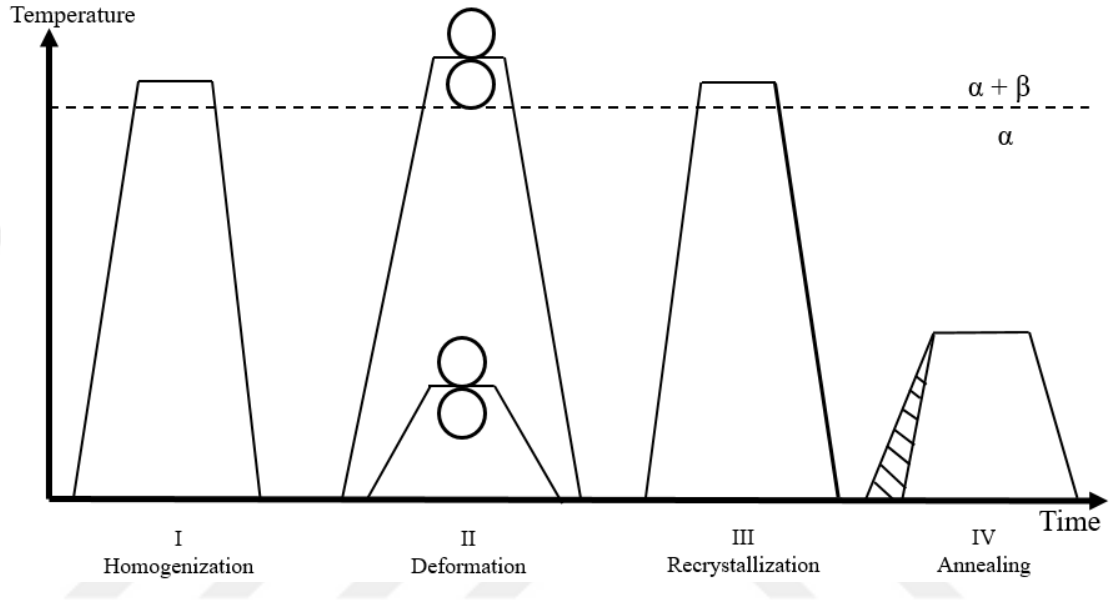

Fig. 3.33 'Schematically processing route for β annealed microstructure of β titanium alloys' [1]

α phase nucleates preferentially at β grain boundaries and forms a continuous α layer. Precipitate free zone layer (PFZ) is formed next to this continuous α layer which does not contain any α plates, so it is softer than the age-hardened matrix. (Fig. 3.34 (b)) [1]

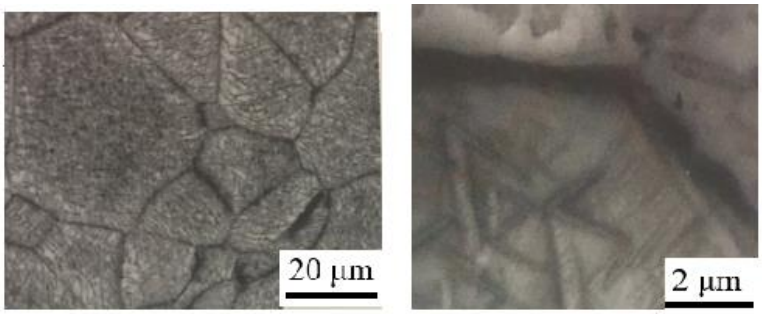

(a) (b)

Fig. 3.34 'Microstructure of β annealed and aged of heavily stabilized β alloy; (a) LM (b) TEM' [1]

It is difficult for heavily stabilized β titanium alloys to obtain a homogeneous distribution of α platelets by the normal aging treatment which is shown in Fig. 3.33. Pre-aging at lower temperatures can create more homogeneous distribution of α platelets. The effect of the pre-aging on microstructure is shown in the figure below. (Fig. 3.35)

Since the present study does not focus on β titanium alloys other microstructure features of these group is not covered

.

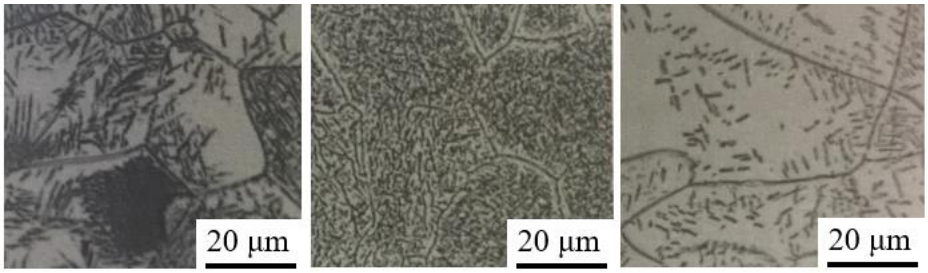

(a) (b) (c)

Fig. 3.35 'Pre-aging effect on heavily stabilized β titanium alloy; (a) 8h 690 °C + 8h 650 °C, (b) 8h 500°C + 24h 725 °C, (c) 24h 725 °C' [1]

3.8 Mechanical Properties

Microstructure of titanium was covered in the previous section. Microstructure is a direct result of composition, processing, and heat treatment. Therefore, microstructure is the key thing to determine the mechanical properties of titanium alloys. Tensile strength, ductility, toughness are particular mechanical properties that the present study interests and investigates. In addition to these low & high cyclic fatigue properties are also covered in this section for a future study, research can be widened with additional fatigue testing application on the heat-treated samples with a sequel study.

The most important factors that affect the mechanical properties of titanium are listed below, properties can either be affected just by one of these or by a combination; [25]

- The amounts of specific alloying elements and impurities
- Melting process that used to make primary ingot

- Number of melting steps
- Method for mechanically working of ingots into mill products
- Steps in the forging process
- Casting process and volume of cast articles additional densification techniques, such as hot isostatic pressing (HIP), to reduce casting porosity
- Powder metallurgy (P/M) process, including the method of making powder
- Joining process which used to fabricate a structure
- Post processing heat treatment or employed final step
- Machining process and surface treatment

Titanium alloys are attractive since their strength to density ratio compared to steel and high-strength aluminum and magnesium alloys. (Fig 3.36)

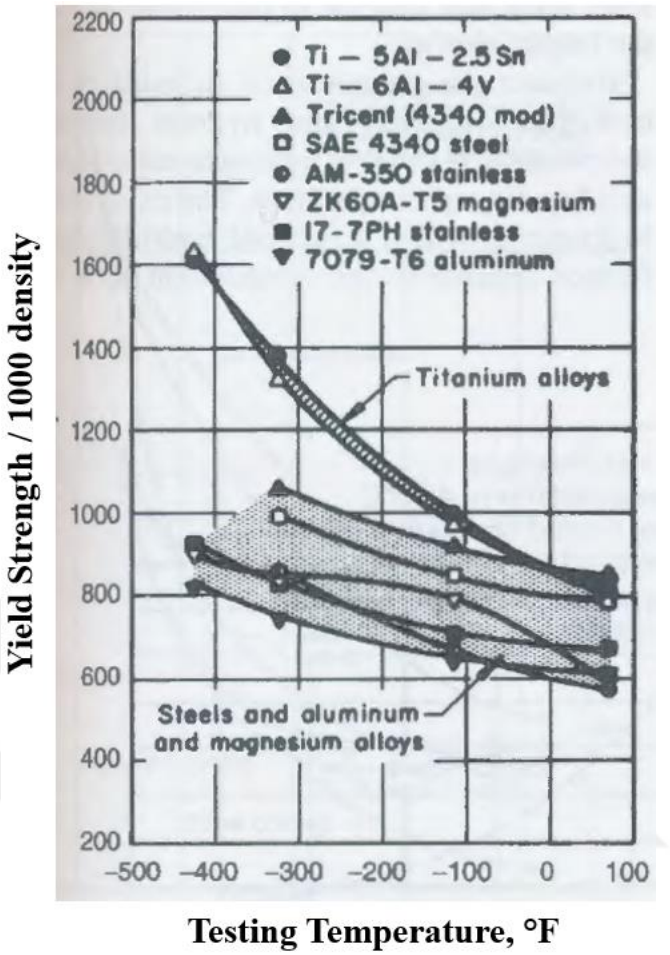

Fig. 3.36 'Ratio of yield strength to density vs temperature for some titanium alloys, some steel, aluminum and magnesium' [25]

3.8.1 Mechanical Properties of α Titanium Alloys and CP:Ti

Properties for α titanium alloys are depend on mostly the composition with comparison to α+β and β alloys. Sheet products of α titanium alloys show variation of yield strength and elastic modulus between longitudinal and transverse directions. Since the crystallographic texture variation always presences in α titanium alloys. The elastic constants of α titanium are higher when it is measured parallel to the c-axis compared to a

perpendicular direction. This difference is higher in Ti-Al alloys since Al is a substitutional element which contracts the α phase lattice. [1] Oxygen on the other hand is an interstitial element in the α-phase and has essentially no effect on modulus of elasticity. [1]

Single phase titanium alloys like α alloys can be strengthened with relatively few techniques compared to α+β and β alloys. Solid solution strengthening is the basic mechanism for α titanium alloys. Both interstitial (oxygen, carbon, and nitrogen) and substitutional (aluminum, tin, and zirconium) solid solution can be done. Precipitation strengthening can be done with α_2 phase formation, also grain size strengthening and texture strengthening can be done in this titanium alloy group. [1] Solid solution additions and very small grains both restrict the operation of deformation twining and reduce the formability of the material. Texture strengthening is possible however it is highly directional. Texture that provides strengthening in the plane of the sheet also reduces the possibility for the improvement in formability which can be achieved form a basal texture type. Precipitation hardening by α_2 phase causes strain localization that decreases significantly the tensile ductility of the material. [1]

Grain size strengthening, and oxygen addition improve yield strength of CP:Ti Grade 4 as 480 MPa. Like other metallic materials the strength and ductility of CP:Ti are inversely related. Grain size effect on flow stress at different strains are shown in the figure below. (Fig. 3.37)

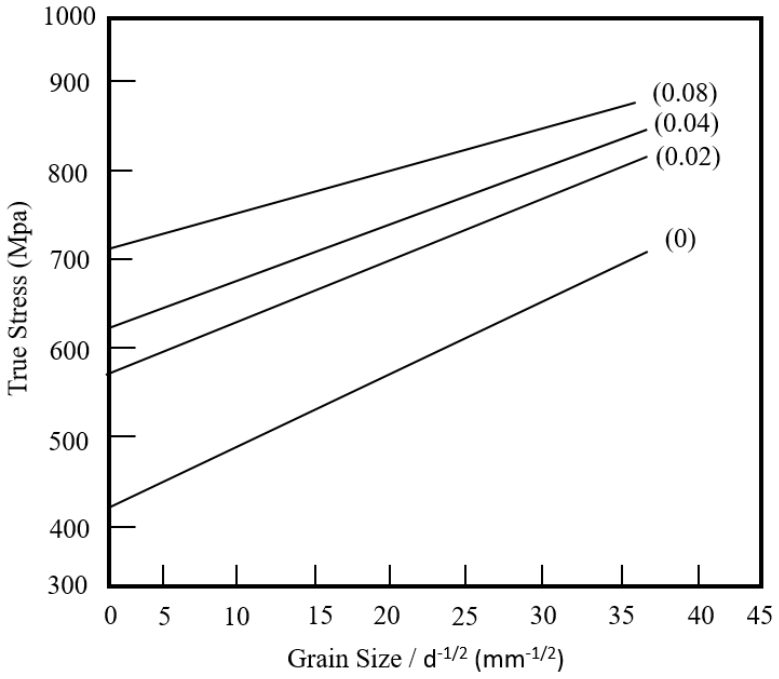

Fig. 3.37 'True Stress vs. grain size at different strain values' [1]

High cycle fatigue strength (10^7 cycles) for CP:Ti is about 70% of its yield strength. Since the CP:Ti selected because superior corrosion resistance and fabricability there are lack of fatigue and fracture data for CP:Ti. In addition to that; CP:Ti preferred for sheet materials rather than Ti6Al4V since the cost is lower. The good strength and fatigue behavior increase costs incrementally. [1]

CP:Ti have different fracture modes compared to α+β and β alloys. The significant difference is presence of large, elongated fracture features due to extensive plastic flow during crack extension and much larger void sizes in CP:Ti. Another difference in between the α alloys and α+β and β alloys is relatively low number of boundaries that are barriers to slip transmissions. In CP:Ti these boundaries are mostly α/α grain boundaries, whereas

they are α/β boundaries in high strength alloys. In fact, the high strength alloys derive much of their strength from boundary strengthening. [1]

At low temperature loadings, the α phase becomes very string, especially in grades 3 and 4. In these conditions plastic flow is limited, and the α-phase can fracture by cleavage. The impact resistance of CP:Ti and Ti3Al2.5V and Ti6Al4V are shown in the figure below. (Fig. 3. 38)[1] Cleavage fracture typically occurs when the local normal stress across the cleavage plane exceeds a critical value. This fracture criterion is in contrast to reaching a critical local plastic strain which causes nucleation of microvoid during ductile fracture. Thus, in the α-phase (hcp) the texture directly affects the propensity for cleavage because the relative orientations of the basal plane and loading axis affect the normal stress component across the cleavage plane. Nucleation of cleavage cracks are hard in smaller grain size microstructure. Thus, components serving in low temperature strengthened by finer grain sizes. [1]

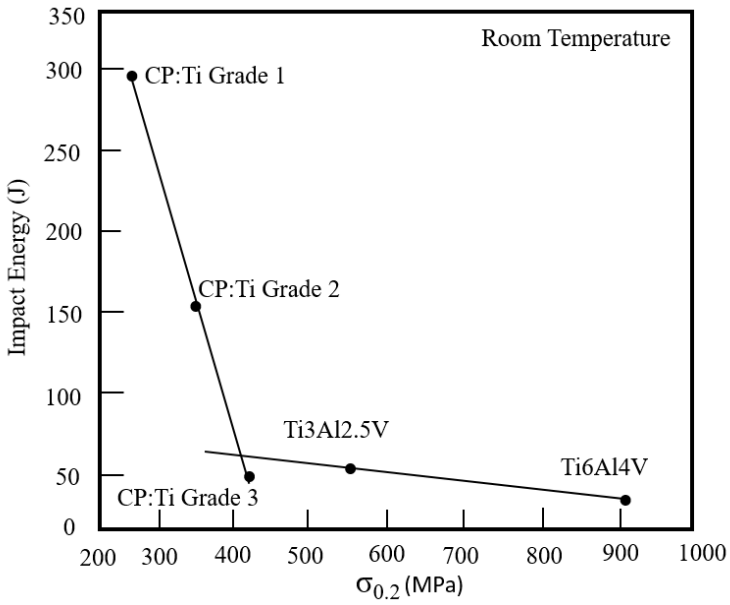

Fig. 3.38 'Charpy impact toughness vs yield stress comparison for different CP grades and two alloys (Ti3Al2.5V and Ti6Al4V)' [1]

Fatigue; the cyclic degradation of the strength capability of a material, depends on the composition, structure, surface treatment, and the stress levels and mode of application of stresses. Failure cycles in the range of less than $5x10^4$ cycles are termed as low-cycle fatigue (LCF) whereas failures at and above 10^6 cycles are termed as high-cycle fatigue (HCF) Fatigue life of unalloyed titanium depends on grain size, interstitial level, and degree of cold work. (Grain size effect Fig. 3.39) [25]

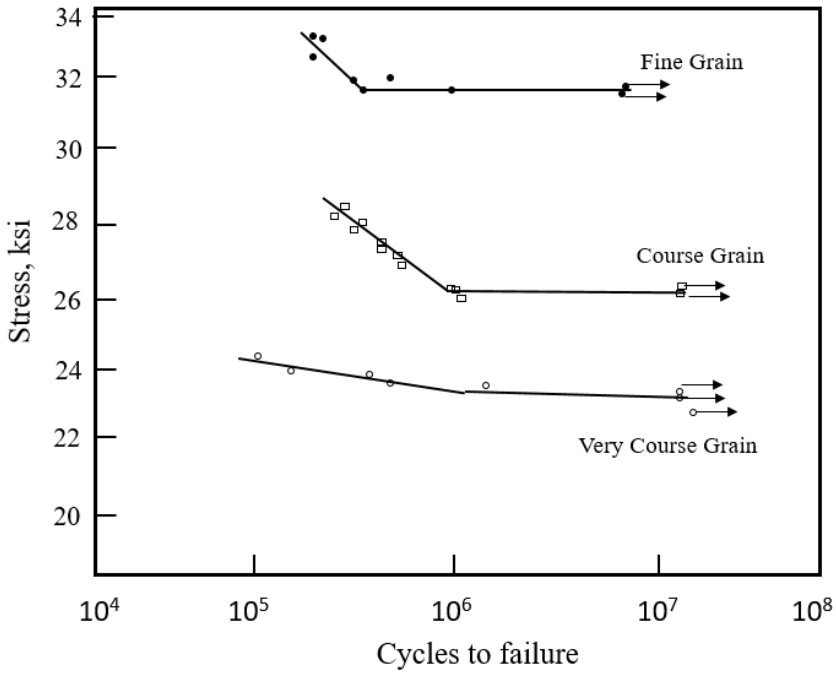

Fig. 3.39 'Fatigue performance of grain size in CP:Ti' [25]

3.8.2 Mechanical Properties of α+β Titanium Alloys

Mechanical properties are directly related with the microstructure of the titanium alloys, since α+β alloys have three different typical microstructures, mechanical properties are outlined with correlation of these microstructures. Emphasized mechanical properties are tensile, fatigue and fracture toughness.

3.8.2.1 Mechanical Properties of Fully Lamellar α+β Titanium Alloys

Fully lamellar microstructure consists of α colonies. The size of the colonies is the significant variant for this microstructure that determines the mechanical property of the alloy. Colony size depends on the cooling rate as mentioned early sections. Since α colonies

determine the slip length in lamellar microstructure, the size of colonies is the most important characteristic that affect mechanical property. Although the two phases have to deform independently, slip can be fairly easily transferred across the incoherent α/β interface, because the two slip systems in each phase are exactly parallel, (110) $[1\bar{1}1]_\beta \parallel (0002)\ [11\bar{2}0]_\alpha$ and $(\bar{1}12)\ [1\bar{1}1]_\beta \parallel (\bar{1}100)\ [11\bar{2}0]_\alpha$ and two others are off only 10°, (110) $[1\bar{1}2]_\beta$ and (0002) $[1\bar{2}10]_\alpha$ as well as $(1\bar{1}2)\ [\bar{1}11]_\beta$ and $(10\bar{1}0)\ [1\bar{2}10]_\alpha$. [1] Slip length and mechanical property relation shown in the figure below. (Fig. 3.39) Increase of the cooling rate decreased the α colony size with a commensurate reduction in effective slip length and increased the yield strength. [1]

In the annealed condition strength derived by substitutional and interstitial alloying elements. Interstitial elements; O, N, H, and C increase strength and decrease ductility. Al is the most important substitutional element that is a solid-solution strengthener. It has a linear effect on strength. Other, less important solid solution strengthening are interstitial solid solution strengthening, grain size effect, second phase (β) effect, ordering in alpha, age hardening, and effects of crystallographic texture. [25]

Effect of a commercially feasible cooling rate, up to 1000 °C/min, is only between 50 to 100 MPa. Large increase in yield strength was observed when the colony structure was changed to martensitic type of microstructure where slip length and colony size equal to the width of individual α plates. [1]

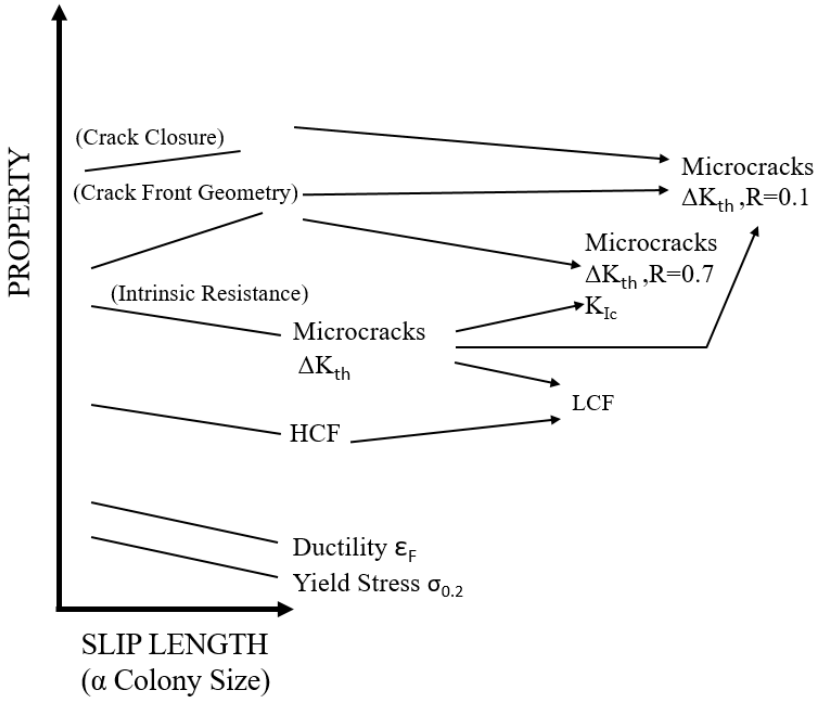

Fig. 3.40 'Slip length vs. mechanical property' [1]

Tensile ductility increases first with the increase of the cooling rate since the slip length decreases, Fig. 3.40. At low cooling rate, a ductile trans-crystalline dimple type of fracture is observed. At higher cooling rates, a ductile inter-crystalline dimple type of fracture is observed. [1]

Reducing β grain size increases largely the tensile elongation which is shown in the figure below for Ti6Al4V from 600μm to 100μm. Fig 3.41 shows the tensile elongation versus cooling rate of TiAl64V it is observed bimodal microstructures have higher ductility values at higher cooling rates. [1]

At room temperature Ti6Al4V consists 90% of alpha and the α-phase dominates the mechanical properties of the component. Alloys can be manipulated by heat treatment since there is some amount of β phase exists at room temperature. The beta to α+β reaction at low temperature leads to increase the strength. The key is to quench from high temperature at α+β region and then age at a lower temperature. A typical strengthening heat treatment consists of heating for 1 h at 955 °C and water quenching, followed by heating for 4 h at 540 °C and air cooling. [25]

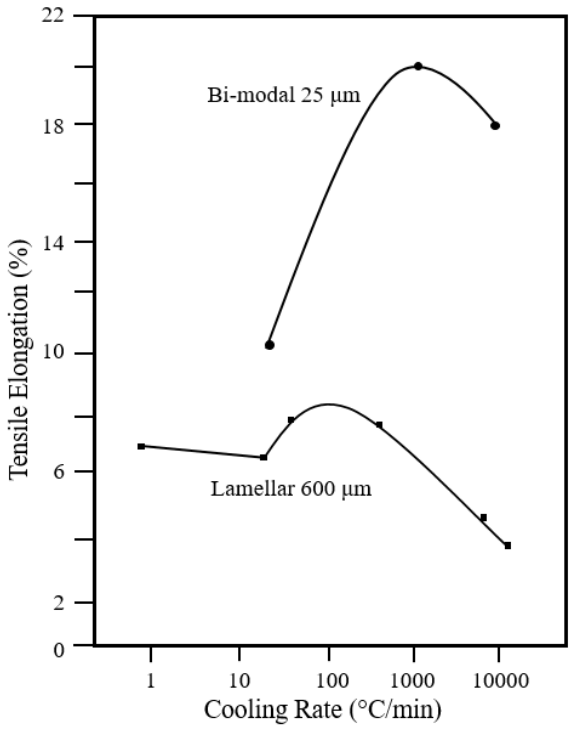

Fig. 3.41 'Elongation comparison of two microstructure of Ti6Al4V at different cooling rates.' [1]

Fatigue property of α+β titanium alloys determine by grain size, degree of aging, and oxygen content. Fatigue properties are strongly affected by the morphology and

arrangement of both α and β-phase. Important parameters of microstructure for fatigue are; prior β grain size, and colony size of the α/β lamellae. [25] Figure 3.42 shows the relation between fatigue and lamellae width of fully lamellar Ti6Al4V.

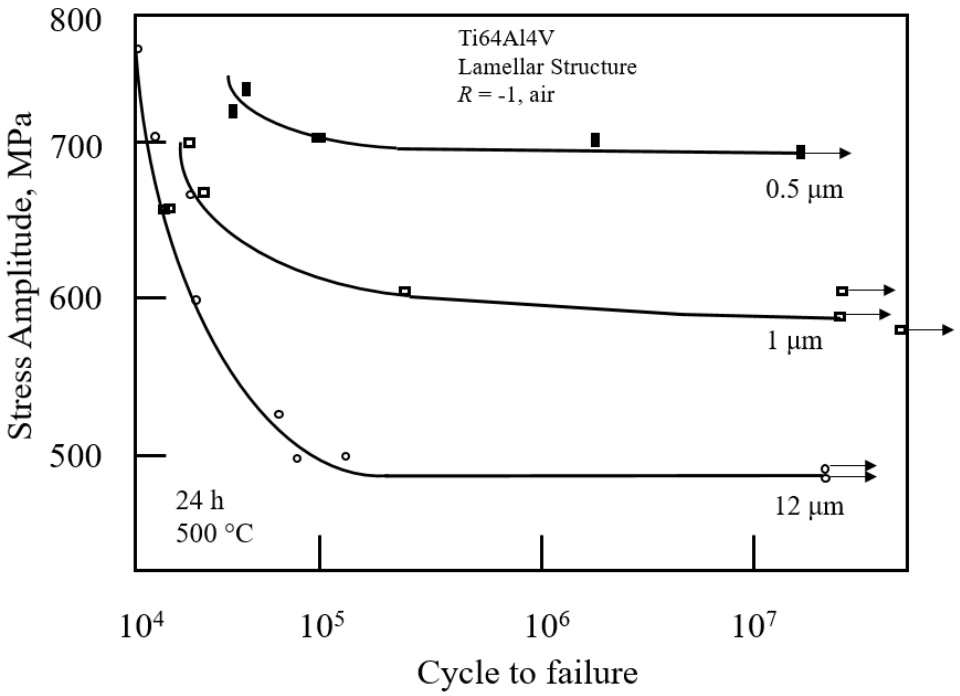

Fig. 3.42 'Fatigue performance of lamellae thickness in Ti6Al4V' [25]

3.8.2.2 Mechanical Properties of Bimodal α+β Titanium Alloys

Significant difference in microstructure parameters that affect the mechanical properties compared to others with bimodal type is the relatively small β grains. With correct set up of the process and recrystallization, dimensions are about equal to the distance between primary α grains or particles. In commercial bimodal microstructures β grain size is in the range of about 30-70μm. [1]

The second most important parameter for bimodal Ti alloys is the alloy element partitioning effect which increases with increased primary α volume fraction. This alloy element partitioning effect leads to a lower basic strength within the lamellar regions of the bimodal microstructure as compared to a fully lamellar microstructure. This has only a very small effect on ductility, crack propagation and fracture toughness. [1]

Yield strength usually has its maximum values at volume fraction of primary α is between 10-20%. For small volume fraction of primary α the α colony size effect dominates the strength. On the other hand alloy element partitioning dominates the strength for large volume fraction of primary α. At high temperature, 600 °C, smaller decline in yield strength for high primary α fraction indicates that the alloy element partitioning effect is less pronounced. At high temperatures it is probably the strengthening effect of oxygen reduced. [1] Comparison between lamellar and bimodal microstructure at different temperatures shown in Table 3.4

Microstructure	Test Temp	$\sigma_{0.2}$ (Mpa)	UTS (MPa)	σ_F (MPa)	El. (%)	RA (%)
Lamellar	RT	925	1015	1145	5	12
Bi-Modal (20 vol% primary α)	RT	995	1100	1350	13	20
Bi-Modal (30 vol% primary α)	RT	955	1060	1365	13	26
Lamellar	600 °C	515	640	800	10	26
Bi-Modal (10 vol% primary α)	600 °C	570	695	885	10	30
Bi-Modal (40 vol% primary α)	600 °C	565	670	910	14	36

Table 3.4 'Tensile properties comparison of IMI 834 alloy at different microstructures' [1]

Fatigue cracks are nucleated in the lamellar grains of bimodal structure. These lamellar grains are softer than primary α as a result of the alloy element partitioning effect.

Fig. 3.43 shows the fatigue behavior of two bimodal microstructures with different vol. % of primary α and lamellar structure. The continuous decline in HCF strength with increasing primary α volume fraction shows that, at low stress amplitudes with limited slip activity over short distances, the decline in basic strength of the lamellar regions has a stronger effect than the positive contribution due to the reduced α colony size. [1]

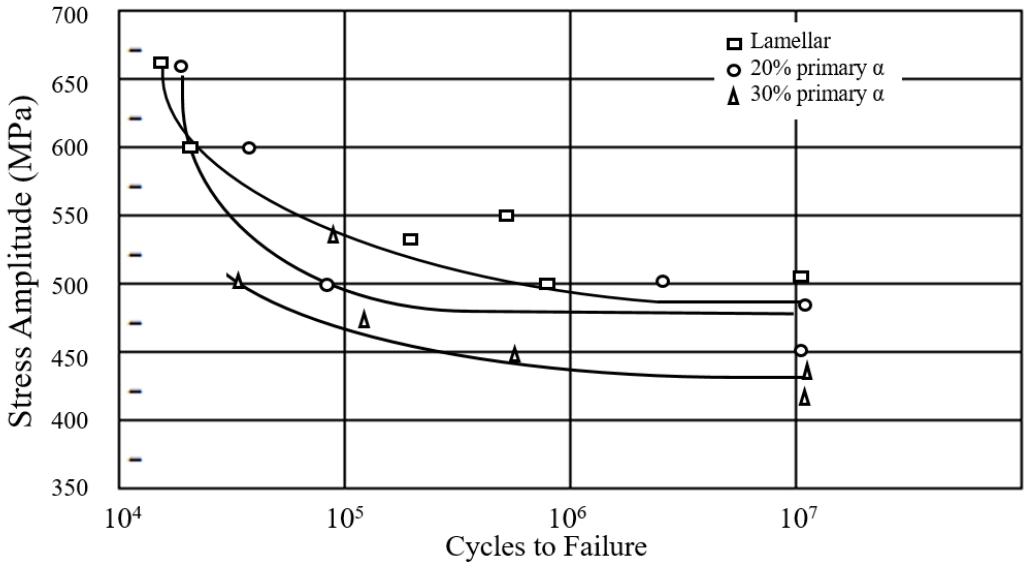

Fig. 3.43 'HCF curves of IMI 834 (α+β titanium alloy) at different microstructures.' [1]

3.8.2.3 Mechanical Properties of Equiaxed α+β Titanium Alloys

Most important microstructure feature for fully equiaxed α+β alloys that affects the mechanical properties is α grain size since slip length depends on α grain the relation between slip length and α colony size which is shown in the Fig. 3.40. Table 3.5 shows the

correlation between microstructure features and mechanical properties for equiaxed α+β alloys.

	$\sigma_{0.2}$	ε_F	HCF	ΔK_{th}
Small α Colonies α Lamellae (a)	+	+	+	+
Bi-Modal Structure (b)	+	+	-	+
Small α Grain Size (c)	+	+	+	+
(a) Compared to coarse lamellar structure				
(b) Compared to fully lamellar structure with same cooling rate				
(c) Compared to large α grain size of fully equiaxed structures				

Table 3.5 'Correlation of microstructures and mechanical properties of three α+β alloy microstructure' [1]

3.9 Thermal Processing of Titanium

Thermal processing is applied titanium alloys for several reasons. Different production processes cause residual stress during fabrication, heat treatment applied to reduce the residual stresses of the components. Optimization of the ductility, machinability, and dimensional stability (annealing) is another reason for titanium alloys heat treatments. In addition to these increasing mechanical properties like; the strength (solution treating and aging in α+β and β alloys), the toughness (fracture toughness), the fatigue properties, and high temperature creep resistance. Generally, heat treatment rearranges phase-volume fractions, phase boundaries in strategic way. [3] 5 main heat treatment methods are applied

to titanium alloys, Stress Relieving, Annealing, Solution Treating, Quenching, and Aging. Unalloyed α titanium alloys can be stress relieved and annealed, but cannot be heat treated to increase their strength. [3]

3.9.1 Stress Relieving

The aim of this process is to reduce the residual stress prior to the manufacturing process or prior to quenching heat treatment. For α and α+β alloys stress relieving temperature is between the range of 480 – 815 °C, and if these alloys β annealed, more rearrangement of phase boundaries is needed, and stress relieving temperature should be increased up to 55 °C. For α and α+β alloys stress relieving temperatures should be below β-transus temperature. For β alloys stress relieving must be taken care to avoid interfering with the final age-hardening treatment. If β alloy is in its final age-hardened condition, stress relieving temperature should be at or below the aging temperature to prevent strength reduction. [3]

Removal of such residual stresses helps maintaining the shape stability, and eliminates unfavorable conditions such as the loss of yield strength, commonly known as Bauschinger effect, which can be particularly noticeable in titanium alloys. [25]

None of the non-destructive testing than can measure the efficiency of stress relief. It is possible with direct measurement of residual stress by x-ray diffraction. Changes in microstructure due to stress relief cannot be detected by optical microscopy. While x-ray stress measurement is an effective way to determine the degree of stress reduction. The

residual stress vs time curves at each stress relief temperature for Ti6Al4V is shown in the figure below. (Fig. 3.44) [25]

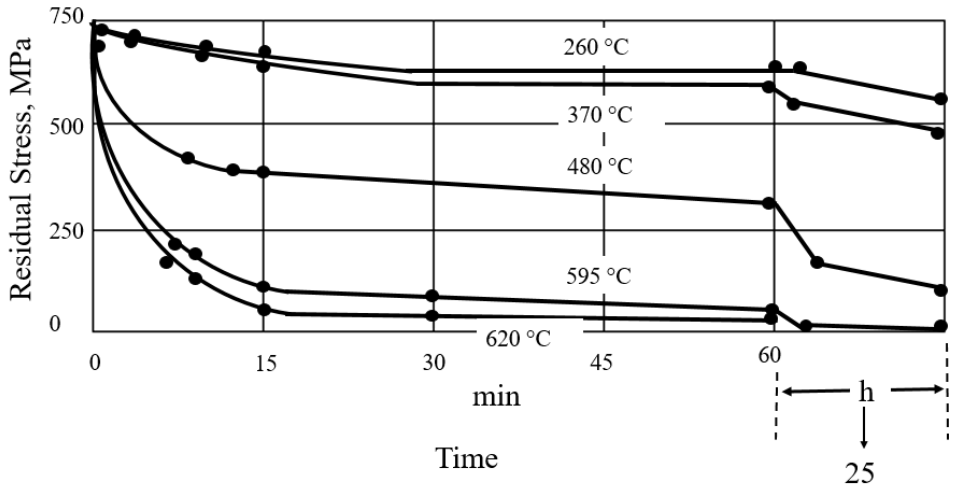

Fig. 3.44 'Residual stress vs. time curve for Ti6Al4V' [25]

3.9.2 Annealing

The annealing of titanium and titanium alloys serves primarily to increase the fracture toughness, room temperature ductility, dimensional stability, and high-temperature creep resistance. This HT is often the final HT for α and α+β alloys as it yields a good balance of properties. [3] Common treatments that identified as annealing are; Mill Annealing, Duplex Annealing, Recrystallization Annealing, Beta Annealing. [25]

α and α+β alloys are typically annealed in the temperature range of 700 – 900 °C whereas β alloys are normally annealed in the temperature range of 690-815 °C. Care must be taken when using β alloys in the annealed condition in service temperatures up to 400

°C, which could result in embrittlement. Service temperatures between the ranges of 400-600 °C could be age-hardened the β alloy, resulting in a strength increase at the expense of ductility. [3]

Duplex annealing improves the creep resistance and the fracture toughness in other words it improves the resistance to crack nucleation of the material. Recrystallization annealing provides high-damage tolerance properties (fracture toughness, crack growth resistance) that are crucial for fracture critical applications. Beta annealing is done at temperatures above β-transus temperature, leading to a large grain size followed by a subsequent mill annealing. For α and α+β alloys. Beta annealing maximizes the damage tolerance properties, since resistance to crack propagation is best when there are fewer grain boundaries. [3]

3.9.3 Solution Treating

Solution treating is used to transform desired amount of α to β phase in α+β alloys with heating the material to a temperature near β-transus and cooling strategically to produce a higher ratio of β-phase in a desired morphology. α+β alloys are solution treated slightly below the β-transus temperature and β- alloys treated above the β-transus temperature. For β alloys the object of solution treating is to retain 100% β-phase upon quenching, so that upon subsequent aging, decomposition of the metastable β -phase occurs to generate second-phase precipitates that provide strength. [3]

3.9.4 Quenching

Cooling rate from solution treating strongly affects the strength of the material. Slow cooling rates allow diffusion to occur, resulting in decomposition of the β-phase and may prevent effective strengthening during the aging process. Also quench delay time that is the time from the material is removed from the furnace and subsequently placed into the quenching media, can affect properties. Longer quench delays can lower the strength; this strength reduction is ascribed to the formation of coarse acicular α-phase. [3]

Thickness is one of the most significant parameter that defines the quenching effect on tensile strength of the component. Fig. 3.45 shows the relation of the as quenched thickness and mechanical properties.

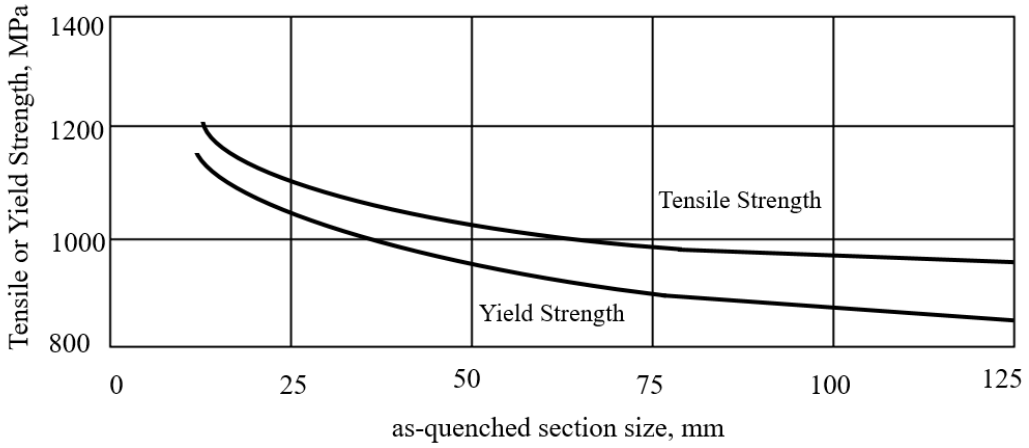

Fig. 3.45 'Section size effect on tensile properties of Ti6Al4V' [25]

3.9.5 Aging

The final step at titanium alloys heat treatments. Aging process of titanium is different than the aging process of aluminum and nickel. [25] Aging process of titanium alloys causes decomposition of the supersaturated β-phase retained upon quenching, through α-precipitation within the β matrix. Martensite decompose in a manner that sharpens interfaces or boundaries that provide strengthening. The aging temperature controls the size and volume fraction of the α-precipitates, and determines the final strength of the material. [3] α and α+β alloys aged in temperature range of 480-605 °C while β alloys aged in the range of 425-595 °C. [3]

Chapter 4. Experimental Methods and Materials

4.1 Materials

Materials used for the present study are CP:Ti and Ti6Al4V titanium alloys. Ti6Al4V alloy components were produced by EBM and CP:Ti components were produced by SLM process. Ti6Al4V contains 6 wt% Al and 4 wt% V. CP:Ti used in the current study is grade 1 which contains 0.2 wt% Fe, and 0.18 wt% O. β-transus temperatures are 995 ±20 °C [45], 890°C [1]respectively for Ti6Al4V and CP:Ti. Mechanical properties of Ti6Al4V and CP:Ti shared in the 'Mechanical Properties' section of the literature review. (see Section 3.8)

4.2 Heat Treatment

Two methods were used to investigate the heat treatment process for Ti6Al4V EBM produced samples. Slow rate: 100°C/min Differential Scanning Calorimetry (DSC) 100°C/min and rapid: 50 °C/sec, Gleeble®

4.2.1 Differential Scanning Calorimeter

DSC is a thermo-analytical technique that evaluates the amount of heat required to increase the temperature of a sample. A Reference sample is used to measure this heat value as a function of temperature. The reference and the sample exposed the same heating and their temperature difference is used to determine relative heat flow. DSC experiment

designed to increase the temperature linearly as a function of time and make analysis according to difference in between the reference and the sample heat flow.

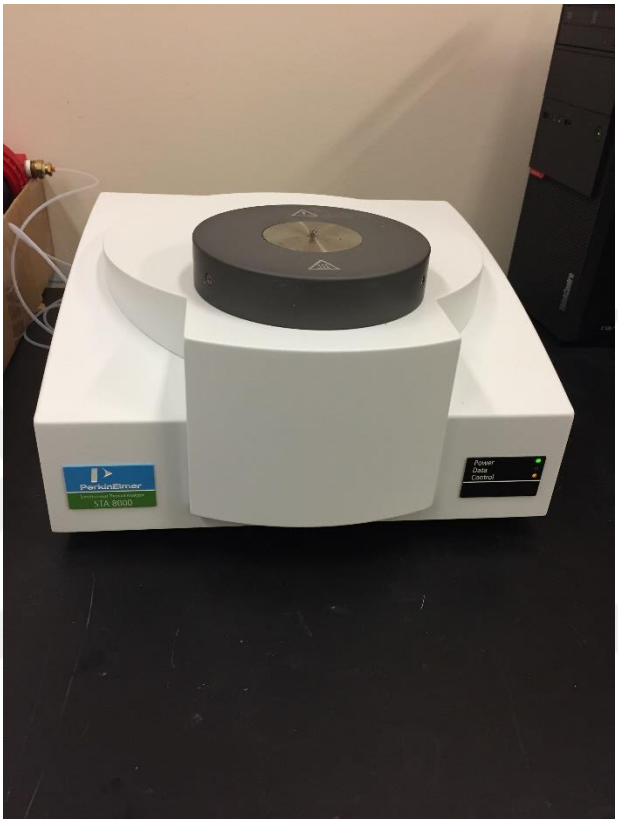

Fig. 4.1 'Differential Scanning Calorimetry, Perkin Elmer STA 8000'

The basic principle of this technique depends on the heat flow difference in between reference and the sample. Energy need for phase transformation provided by heat. When transformation happens, there is a difference in heat flow and heat of sample since sample used heat energy for transformation. By observing this difference DSC can measure the amount of heat absorbed or released during such transitions. [68-69-70]

Present study evaluated three different DSC experiments for EBM Ti64 to investigate the phase transformation trend between different HT conditions. Applied HT is shown in Table 4.1.

Applied HT	Number of Cycles	Heating Rate (°C/min)	Cooling Rate (°C/min)	Soaking Time	Temperature (°C)
1 x DSC EBM Ti64	1 time	100	100	5 min	1000
5 x DSC EBM Ti64 NH	5 times	100	100	No Soaking	1000 - 800
5 x DSC EBM Ti64 H	5 times	100	100	5 min	1000 - 800

Table 4.1 'Applied Heat Treatments to EBM Ti64 with DSC'

The Perkin Elmer brand DSC was used for the current study. The DSC chamber was backfilled with Argon to prevent the oxidation effect at high temperatures. 30 L/min gas flow was set as a default setting for each experiment. Schematics of heating and cooling curves for each experiment are shown in the figure below. (Fig. 4.2)

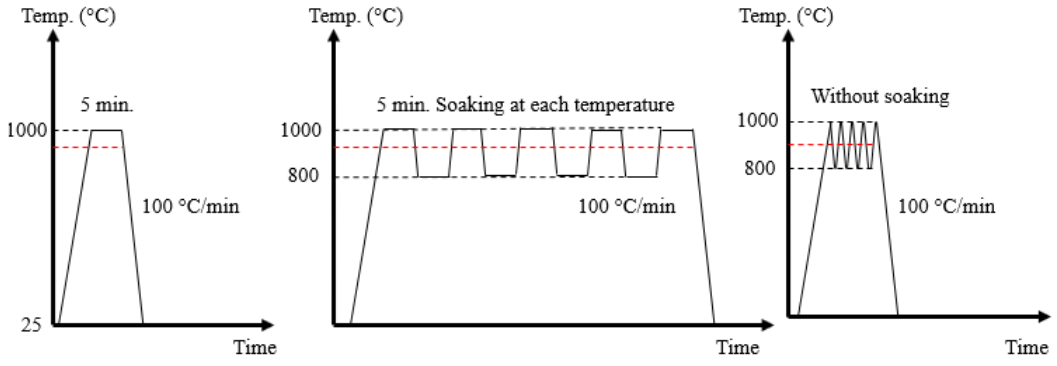

(a) 1 x DSC EBM Ti64 (b) 5 x DSC EBM Ti64 H (c) 5 x DSC EBM Ti64 NH

Fig. 4.2 'Schematic Heat Treatment Curves for DSC Experiments'

The aim of these experiments was to observe the effect of cyclic HT on microstructure and phase transformation phenomenon. As it is explained in the previous sections EBM process has high heating and cooling rates during solidification. When we compared the AM processes shared in the current study EBM has the highest heating and cooling rate. This caused high amount of residual stress in the EBM manufactured components. Inherited high residual stress may trigger the phase transformation mechanisms kinetically and affect microstructure change during cyclic HT. With this idea the residual stress can be used to improve mechanical properties of EBM manufactured Ti6Al4V components. The present study observed the phase transformation and microstructure change with 1-time HT slightly above the β-transus temperature. This sample is referred to as 1 x DSC EBM Ti64 and was compared to the initial condition, as build EBM Ti6Al4V. After that, cyclic HT was applied to the as received EBM samples between 1000 °C – 800 °C without soaking. This sample is referred to as 5 x DSC EBM Ti64 NH, NH referred no soaking. Heating above β-transus and cooling below the β-transus temperature triggers phase transformation and residual stress modification. During $\beta \rightarrow \alpha$ transition α-phase grows from the β grain boundaries. At higher cooling rates α-phase also grows from within the β grains. 5 x DSC EBM Ti64 NH cyclic HT aimed to transform α-phase to β but not let the microstructure transform 100% to β since the inherited β grains will be nucleation points for α-phase for 100 °C/min cooling rate. According to this theory 5 x DSC EBM Ti64NH sample should have finer α-grains and lower grain size compared to 1 x DSC EBM Ti64 and the as build condition sample.

Finally, cyclic HT with soaking for 5 minutes at each temperature was applied. This sample is referred to as 5 x DSC EBM Ti64H. In this experiment the sample was heated above β-transus and cooled below β-transus temperature and soaked 5 minutes for each temperature step as shown in the Fig. 4.1. This heat treatment should allow all α-phase transformed to β and in theory since this sample has more time compared to 5 x DSC EBM Ti64 NH. Final microstructure should have larger β grain size. Comparisons of these results are shared in the Section 5.

4.2.2 Rapid Heat Treatment

Gleeble® is a thermo-mechanical testing machine invented by Dynamic Systems Inc. It has a direct resistance heating system which provides up to 10,000 °C/sec heating rate. It is also capable of high cooling rates using high thermal conductivity grips to hold the specimen. Similar cooling rates can be achievable with an optional quench system. Since the Gleeble® has a unique heating system it can heat 3 to 10 times faster than conventional furnace equipped machines. [71]

Fig. 4.3 'Gleeble® 3500 Thermomechanical Treatment, Materials Research Lab. PSU'

Gleeble® can also simultaneously perform tensile and compression tests at high temperatures on many different geometries. Applications of Gleeble® include; hot ductility testing, Nil ductility testing, thermal / mechanical fatigue testing, creep/stress rupture. [71]

Thermocouples or optional infrared pyrometer provide signals for accurate feedback control of specimen temperatures. These provide accurate temperature measurements during testing. [71]

The Gleeble® 3500 model is located in PSU Materials Lab. The Gleeble® 3500 mechanical system is a complete, fully integrated servo hydraulic system capable of exerting as much as 10 tons of static force in tension or compression. Displacement rates as fast as 1000 mm/sec. can be achieved. Non-contact laser extensometer provides strain

feedback to insure accurate execution and repeatability of the mechanical test program. [71]

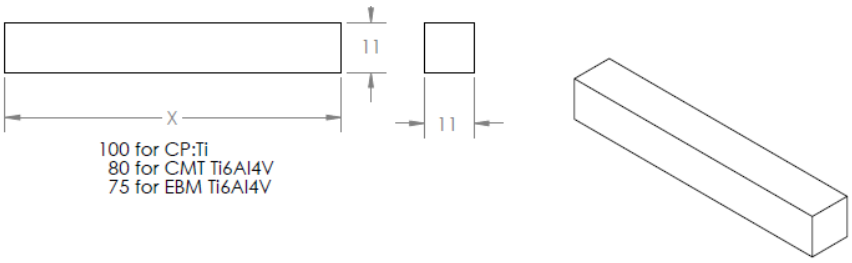

Fig. 4.4 'Rapid HT (Gleeble®) Sample dimensions for each sample'

Gleeble® HT is applied for EBM Ti64, CMT Ti64 and SLM CP:Ti. The aim of Gleeble® HT is to observe the effect of higher heating and cooling rate on phase transformation and microstructure. Applied heat treatments are shown in Table 4.2.

Applied HT	**Number of Cycles**	**Heating Rate (°C/sec)**	**Soaking Time**	**Temperature (°C)**
1 x GL EBM Ti64	1 time	50	10 sec	1000
1 x GL CMT Ti64	1 time	50	10 sec	1000
1 x GL SLM CP:Ti	1 time	50	10 sec	950
3 x GL SLM CP:Ti	3 times	50	10 sec	950 - 750
5 x GL SLM CP:Ti	5 times	50	10 sec	950 - 750

Table 4.2 'Applied Heat Treatments to EBM Ti64, CMT Ti64 and SLM CP:Ti with Rapid HT (Gleeble®)'

4.3 Charpy V-notch Impact Testing

Charpy V-notch impact was testing applied to the rapid heat treated samples and initial conditions of each EBM Ti6Al4V, CMT Ti6Al4V and SLM CP:Ti samples to make comparisons between processes . ASTM E23 [72] standard test was applied for each sample. Sample dimensions before notch cutting are shown in Fig. 4.4 and after notch cutting in Fig. 4.5.

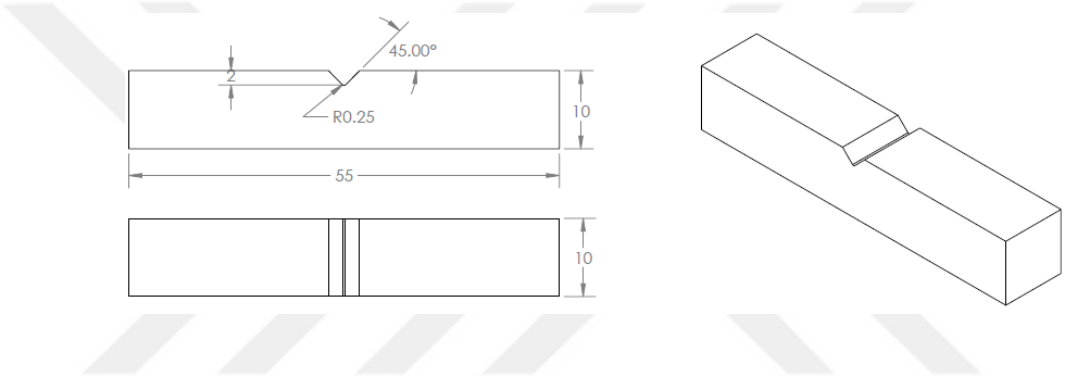

Fig. 4.5 'Charpy v-notch impact test sample dimensions, ASTM E23'

Goal of the impact test is to monitor the toughness values at different heat treatment conditions and make a connection between the microstructure response to HT and mechanical properties. Each test was executed at room temperature. Results are shared and compared in section 5.

Fig 4.6 ‘Charpy v-notch impact test pendulum, Materials Research Lab. PSU’

4.4 Microstructure Examination

Microstructure examination for the current study was executed with a Zeiss Sigma VP® FEG Scanning Electron Microscope which is located in the Centre for Electron Microscopy & Nanofabrication (CEMN) at Portland State University. Zeiss Sigma VP® microscope is equipped with an Electron Back Scatter Diffraction (EBSD) detection that provides imaging for microstructure examination. AZtech® software is used for EBSD

image processing in SEM sessions. Channel 5® software used for further interpretation of EBSD data and additional analysis such as grain size, recrystallized fraction, grain orientation spread etc. These maps and results are shared in section 5.

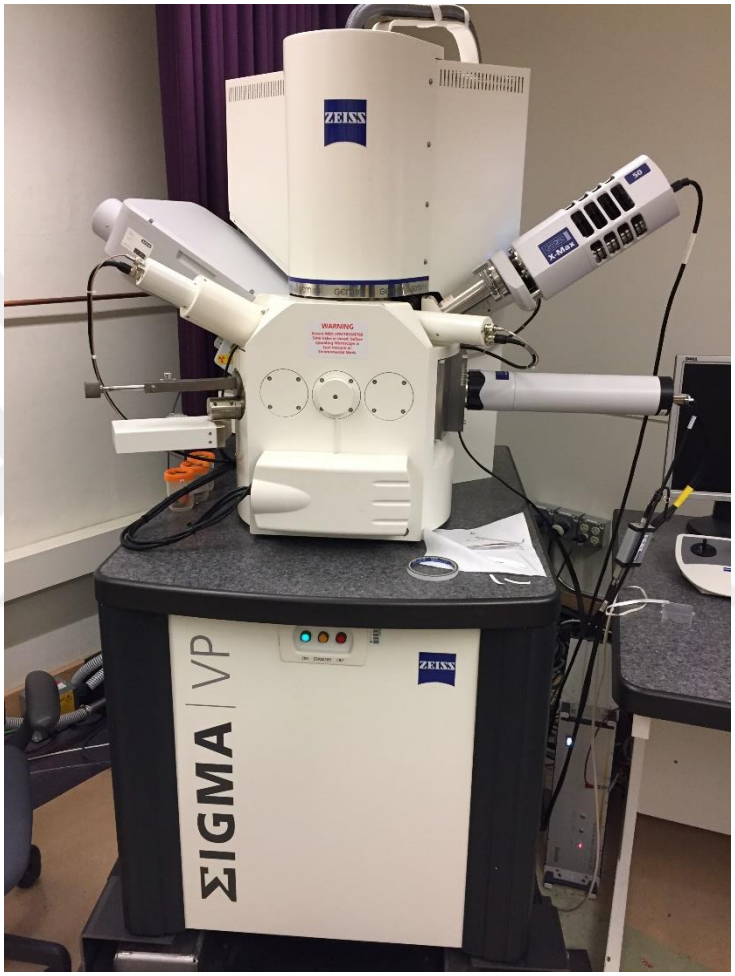

Fig. 4.7 'Zeiss Sigma® Scanning Electron Microscope, CEMN PSU'

Applied acceleration voltage for EBSD imaging is 15kV. Magnification for DSC samples and initial condition of Ti6Al4V was 2.5kx. Frame of the scanned area for same sample group was 53µm x 70.8µm or 489 x 652 pixels.

Samples prepared with Struers® polishing machine. (Fig. 4.8) Multiple sample holder used for every sample preparation. Sequence of 200mm, 9µm, 3µm and 0.4µm polishing applied at different force and time values. Final oxide polishing suspension (OPS) applied at the last step. Samples are ultrasonically cleaned in between every polishing step for 5 minutes.

Fig. 4.8 'Struers® polishing machine, Materials Research Lab. PSU'

Chapter 5 Results and Discussion

5.1 Initial Microstructure Evaluation

During EBM process titanium powders are exposed to an incident very high energy electron beam and that causes rapid heating above the liquidus temperature. With high beam resolution very small confined regions melt and solidification happens with rapid cooling rates. The microstructure of the EBM process has very fine grains due to this rapid solidification. When EBM Ti6Al4V microstructure is compared with conventional produced wrought Ti6Al4V microstructure in IPF maps depicted in Fig. 5.1

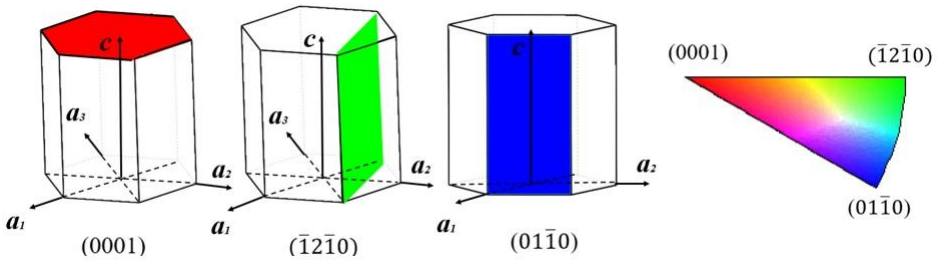

(a)

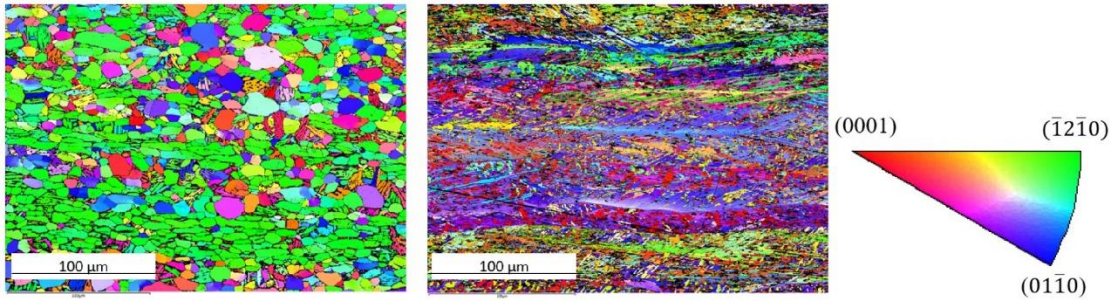

(b) (c)

Fig. 5.1 '(a) IPF coloring and HCP Lattice index, (b) IPF microstructure map of wrought Ti6Al4V, (c) IPF microstructure map of EBM Ti6Al4V'

Wrought material has more equiaxed grains rather than EBM microstructure which is mostly α-phase plates and Widmanstätten structure, and sometimes Basket-weave

shaped microstructure. At higher cooling rates the microstructure becomes more martensitic (>1000 °C/s). EBM process has 150-250 °C/s cooling rates during solidification of the powders on the other hand conventional methods have 10s of °C/s cooling rates.

Initial microstructure of EBM Ti6Al4V samples have texture which is oriented 90° to the building direction of the process. Fig. 5.2 shows the building direction of the samples and the coordinates.

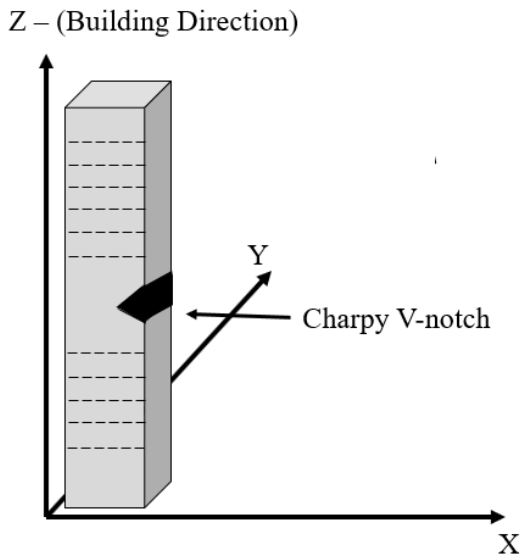

Fig. 5.2 'Building direction and coordinates with V-notch location for EBM Ti6Al4V samples'

Microstructure texture causes different mechanical properties in different directions which may limits the application of EBM components. For instance; component may satisfy the required tensile strength on the XY plane however it can failed in the Z direction. The tensile strength in the XY direction is higher than the strength in Z direction. This as build condition should be considered during the design process of the component or

production process should be improved with additional steps (post processes, post heat treatments, etc.) or manufacturing process should be modified (pre-processes, pre-heat treatments, heated chambers, etc.) Microstructure of EBM Ti6Al4V at different orientations are shown in the figure below (Fig. 5.3)

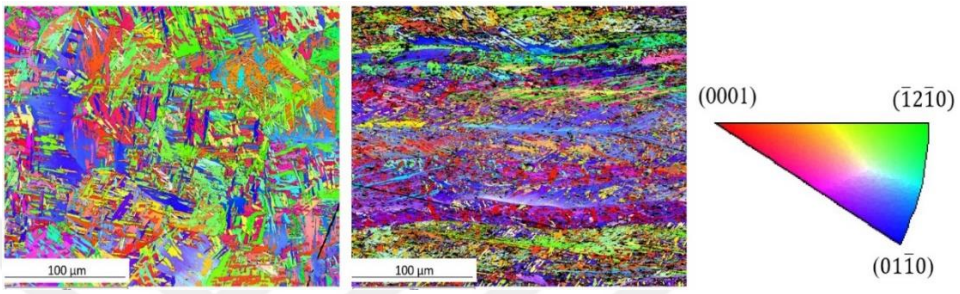

(a) (b)

Fig. 5.3 'EBM Ti6Al4V IPF microstructure images (a) XY direction, (b)YZ direction'

Another AM process for Ti6Al4V in the present study is CMT. However, CMT process has higher cooling rates compared to conventional production methods, but its cooling rates are lower compared to EBM process. As a result of this; CMT microstructure is finer than wrought Ti6Al4V, but more coarse than EBM Ti6Al4V. (Fig. 5.4)

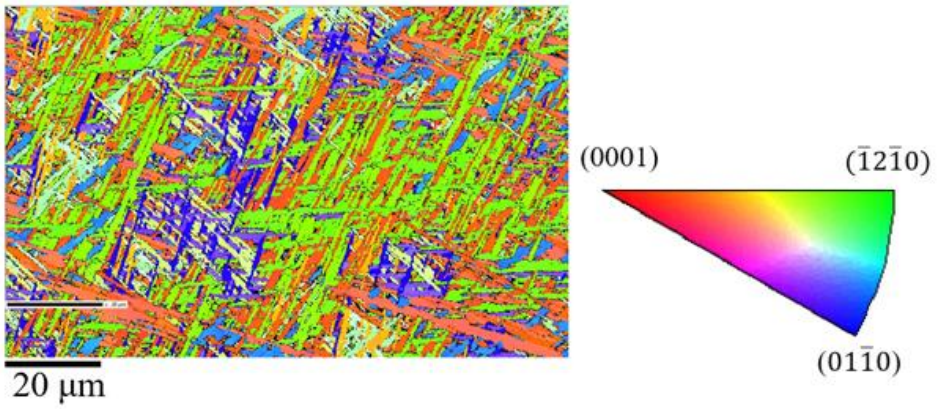

Fig. 5.4 'CMT Ti6Al4V IPF microstructure image of YZ direction'

Compared to EBM, CMT microstructure texture is more independent to building direction. Since there is not significant difference between cooling rates of coordinates in CMT process, microstructure orientations are random, so we cannot say that the CMT microstructure has a texture like EBM microstructure. However; microstructure of the CMT does not show texture, mechanical properties effected by building direction since layer interface may have defects. Building direction and interfaces are shown in Fig. 5.5. Defects are mainly related with oxidation of titanium and volumetric defects that affect surface quality. Since the process is not executed in vacuum chamber oxide formation occurs on the surface of the beams this oxide layer should be removed before the other beam build on.

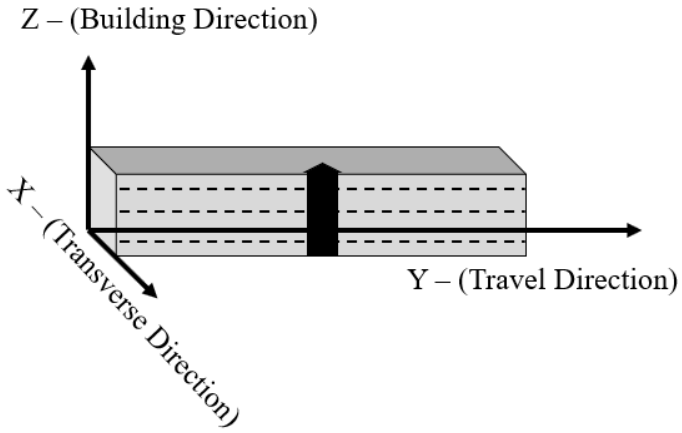

Fig. 5.5 'Building direction and coordinates with V-notch location for CMT Ti6Al4V samples'

The third additive manufacturing method was SLM and CP:Ti material was investigated in this study. The SLM process has higher porosity ratios compared to other

method even CMT process. Since the chamber conditions are not sophisticated like EBM there are very tiny porosities spread throughout the microstructure. As a result of this EBSD imaging technique cannot be applied to SLM CP:Ti. Surface topography of SLM CP:Ti degraded signal collection. This is caused by pores that block pattern determination of scattered electrons. SLM CP:Ti has 160% more porosity compared to the EBM Ti6Al4V sample. An optical microscopy image of SLM CP:Ti without etching is shown in Fig. 5.6. Charpy V-notch orientation and building direction of the SLM CP:Ti samples have the same orientation as EBM build samples shared in Fig. 5.2.

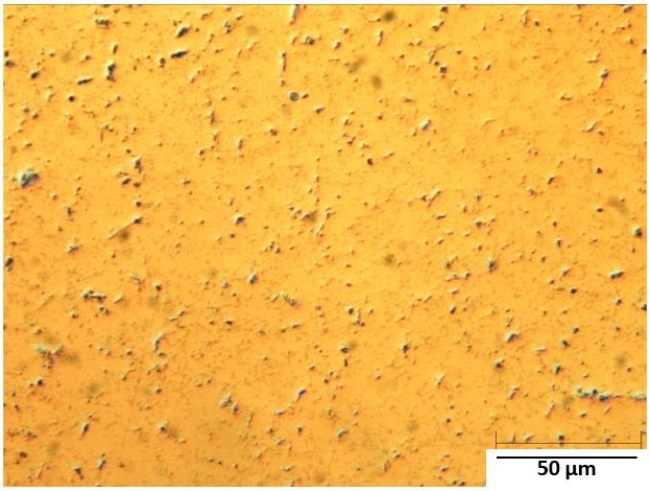

(a)

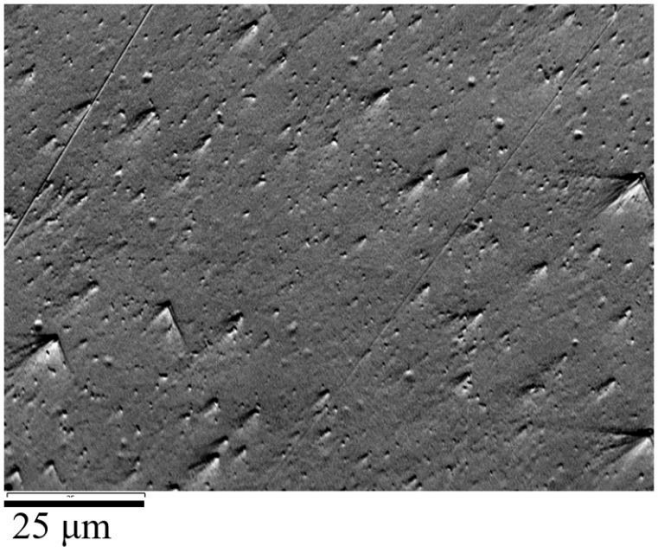

(b)

Fig. **5.6** 'Initial SLM CP:Ti microstructure, (a) OM, (b) SEM'

5.2 Microstructure Response and Toughness After Heat Treatments

5.2.1 EBM Ti6Al4V Microstructure Response After DSC Heat Treatments

Intrinsic high cooling rates of EBM builds the finest microstructure among the studied AM methods. α grain growth starts from the prior β grain boundaries and at higher cooling rates, and α phase grains also nucleate inside the β grains. As a result, the final microstructure of α+β titanium alloy, Ti6Al4V, has thinner α laths/plates compared to lower cooling rate production methods.

Allotropic transformation from β to α has multiple variants, 12 α formation variants from a single β crystal due to BOR shown in Fig. 3.4 in section 3. The β → α+β transformation mechanism effected by cooling rate, thermomechanical processing (strain value), and dislocation population. Since α-phase HCP and β-phase BCC lattice structures

do not have a perfect match, contraction and expansion occurs during the phase changes which effects the residual stress and strain values of the microstructure. At high cooling rates phase transformation happens rapidly without ideal expansion or contraction in between the two-phase lattice. In rapid transformation mechanism atomic movements are suppressed due to high cooling and transformation happens at higher angle orientations. (Fig. 5.7) Fig 5.7 (a) shows the population of the grains according to orientation of the basal plane of BCC to c-axis of the HCP lattice. In ideal conditions there is 45° angle in between c-axis and base plane, Fig. 3.2. Besides these strains, this microstructure is less stable and requires post treatments to improve the properties.

In addition to lattice stress, strains, and microscopic scale transformation, highly localized heating and cooling during EBM process cause unevenly expansions and creates macroscopic scale thermal stresses inside the microstructure which is still present after cooling. This residual thermal stress decreases the mechanical properties of the EBM produced components. This high residual stress inside the microstructure has a direct effect on phase transformations. At higher temperatures components expands evenly and during expansion the residual stress relieves with strain. This is how stress relieving heat treatment is done. In case of EBM process heat treatment, localized stress on lattice structures and macroscopic thermal residual stress trigger different phase transformation mechanisms above β-transus temperature improving the mechanical properties of the component.

The starting point to investigate the HT effect on EBM Ti6Al4V microstructure is one-time HT to above β-transus temperature and cooling to room temperature. Theoretical β-transus temperature for Ti6Al4V is 995 °C and in the experiment, it is heated to 1000 °C

and soaked 5 min. This experiment is done at DSC and same heating and cooling rate applied to the sample; 100 °C/min. This rate can be achieved with conventional HT furnaces. This sample is labeled as 1 x DSC EBM Ti64, and subjected to the HT curve shown in the Fig 4.2 (a). The heat flow vs temperature curve from DSC is shown in Fig 5.8

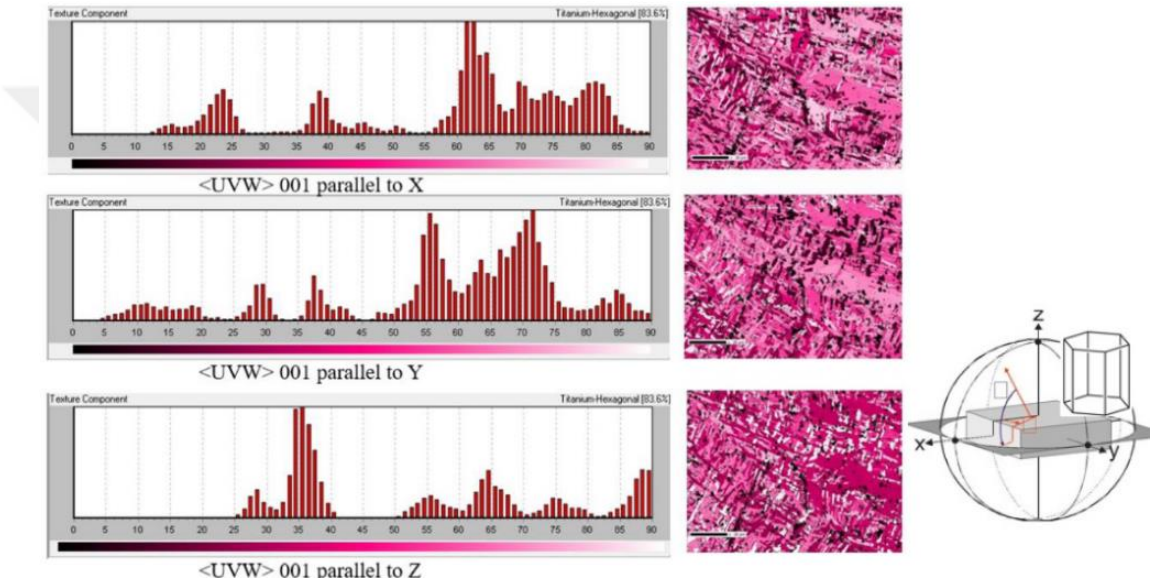

Fig. 5.7 'Texture component of initial EBM Ti6Al4V, (a) X parallel to basal plane, (b) Y parallel to basal plane, (c) Z parallel to basal plane'

Heat flow curve of the 1 x DSC EBM Ti64 shows the cooling from 1000 °C. Phase transformation for 100 °C/min cooling rate occurred at the temperature approximately at 950 °C. (peak point in Fig 5.8) Phase transformation from β → α occurred at lower temperature compared to theoretical temperature this is because of the cooling rate difference between theory and experiment.

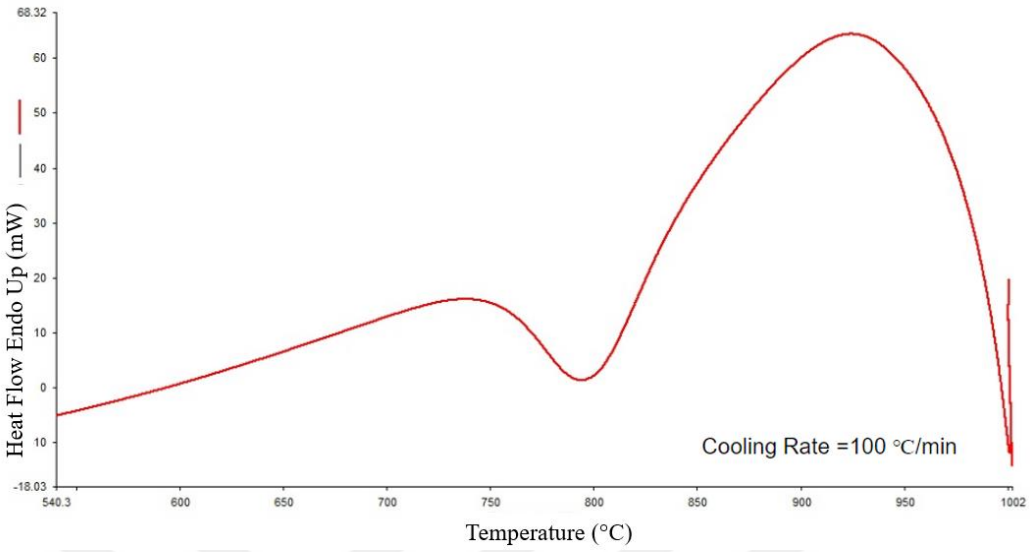

Fig. 5.8 'Heat Flow Curve for 1 x DSC EBM Ti64'

After one-time heat treatment microstructure responded with bigger grain size and the texture of the EBM microstructure decreased. 5 minutes soaking time not only let microstructure fully transform from α → β, but also caused β grain growth. Figure 5.9 shows EBSD images of the 1 x DSC EBM Ti64. Large prior beta grain in the center can easily be distinguish.

When we compared the one-time heat treatment microstructure and initial condition the most significant difference is the grain size. Average grain size in initial condition was 3.38μm^2 and after the one-time HT, average grain size became 1211.7 μm^2. Comparison of the grain size maps between initial EBM and 1x DSC EBM Ti64 is shown in Fig. 5.9.

Second significant difference between initial and one-time HT sample is the texture component. There is a texture orientation in initial EBM build samples related with building direction that is shown in Fig. 5.3 and Fig. 5.7. After one-time HT the texture of the microstructure decreased.

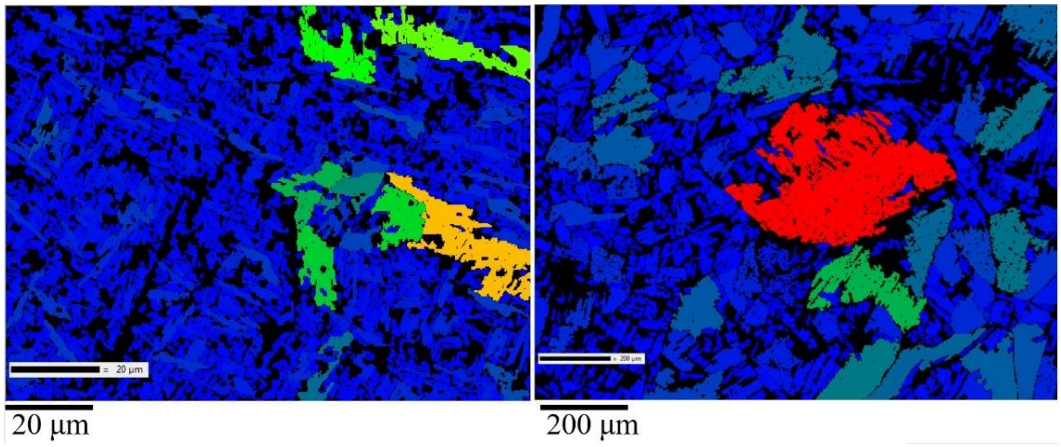

(a) (b)

Fig. 5.9 'Grain size EBSD map, (a) Initial Condition, (b) 1 x DSC EBM Ti64'

1 x DSC EBM Ti64 has more random grain orientation. Population of the grains with lower angle oriented with reference to the c-axis is more than the initial condition which means that mechanical properties in 1 x DSC EBM Ti64 is much independent than as build condition. Grain population spread relative to c-axis orientation is shown in Fig. 5.10

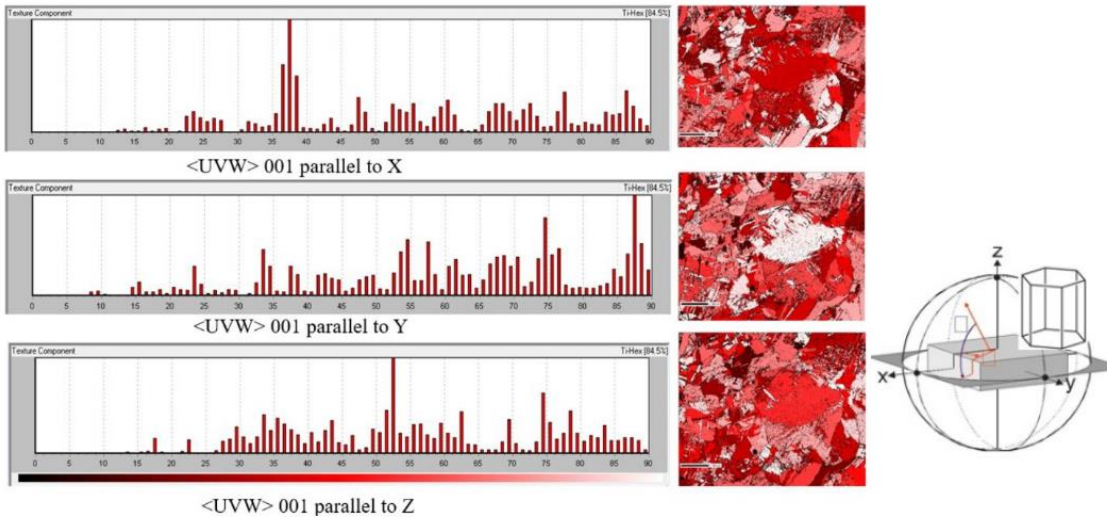

Fig. 5.10 'Texture component of 1 x DSC EBM Ti64, (a) X parallel to basal plane, (b) Y parallel to basal plane, (c) Z parallel to basal plane'

Texture improvement of the microstructure should change the strain values of the sample. Strain map compared in between two conditions. EBSD data can be analyzed to describe the strain contour of the microstructure. Comparison of the initial and one-time heat treatment strain contour is shown in the figure below. (Fig. 5.11)

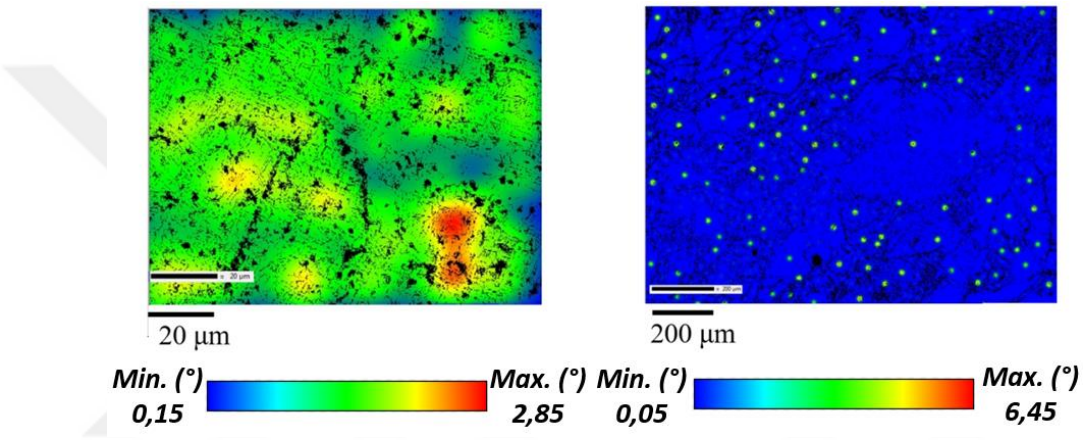

(a) (b)

Fig. 5.11 'Strain Contour, (a) Initial EBM Ti64, (b) 1 x DSC EBM Ti64'

Strain contour maps have different scale so interpreting according to color scale of Fig. 5.11 may be misleading. Quantitative data is shown below, Fig. 5.12.

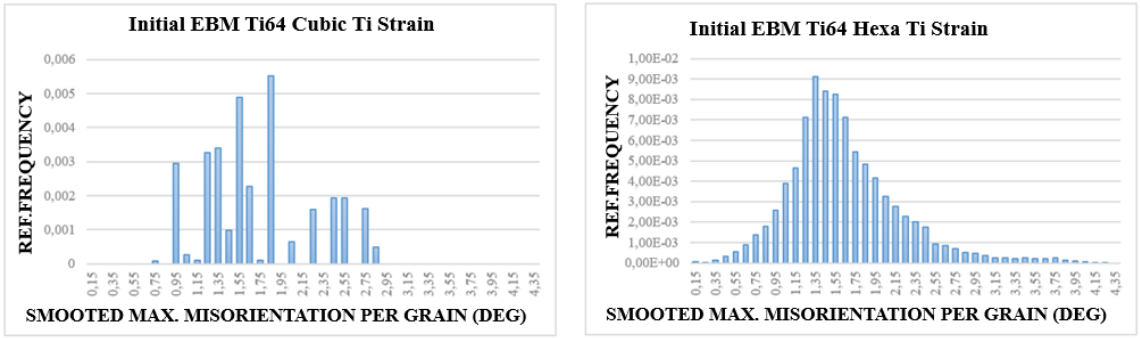

(a)

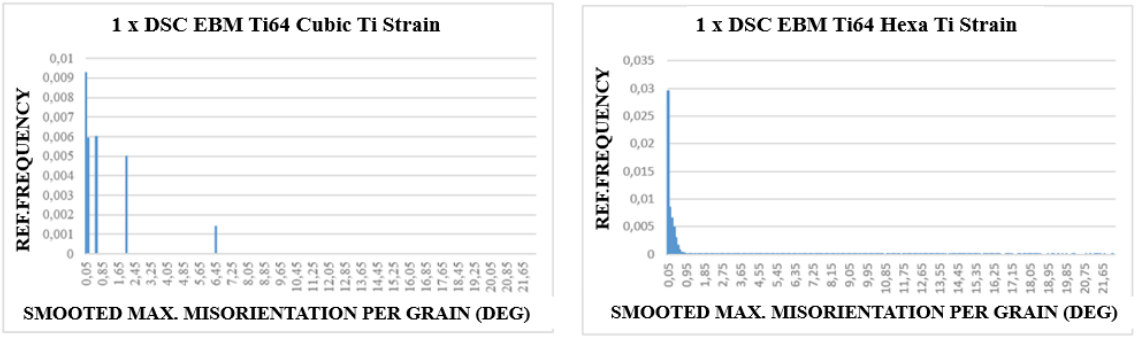

(b)

Fig. 5.12 '(a) Strain contour for initial condition α and β phases, (b) Strain contour for 1 x DSC EBM Ti64 α and β phases'

When we compared the initial strain distribution we observed the strain value decrease for α phase with applied the HT. For the β phase comparison, we observed that strains are accumulated at higher misorientation angles.

In addition to grain size, texture component, and strain contour, grain orientation spread (GOS) maps were compared in between initial and one-time HT sample. GOS technique consists of calculating the average orientation of each grain then comparing the misorientation of each pixel in the grain from its average orientation to determine the average orientation spread. The spread is the average deviation between the orientation of each point in the grain and the grain average. Red-like colors on the color scale means more misorientation of the grains. Fig. 5.13 shows initial EBM sample has highly misoriented grains colored with red and orange on the other hand after HT, high angle oriented grains disappeared. Since the cooling rate of the HT is lower, phase transformation mechanism is more diffusion controlled, the orientation between grains have lower angle and the GOS map of one-time HT sample has no red-like colored grains.

When we compared the two pole figures of initial and one-time HT sample it is observed there is random grain distribution. Fig.5.14. This is attributed to the lower cooling rate and slow diffusion controlled transformation.

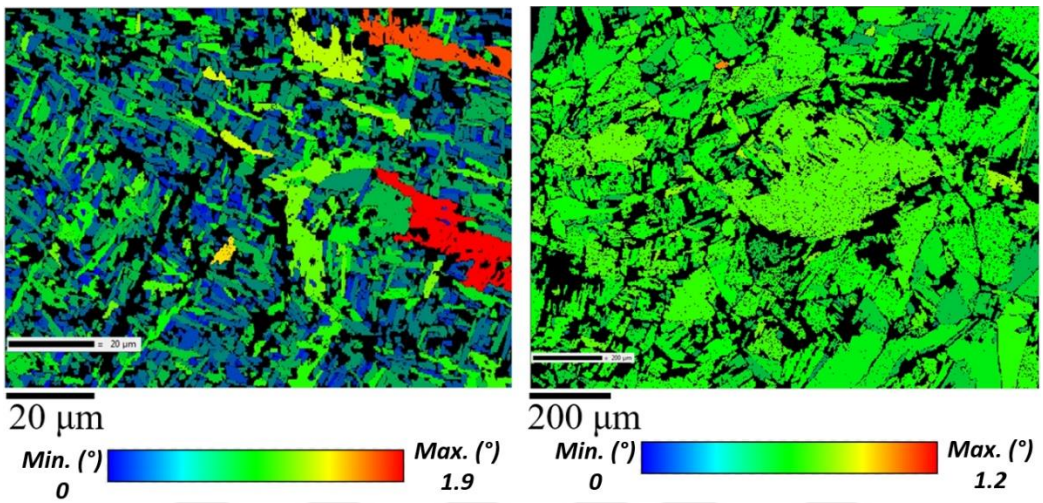

(a) (b)

Fig. 5.13 'Grain orientation spread (GOS) map (a) Initial EBM Ti64, (b) 1 x DSC EBM Ti64'

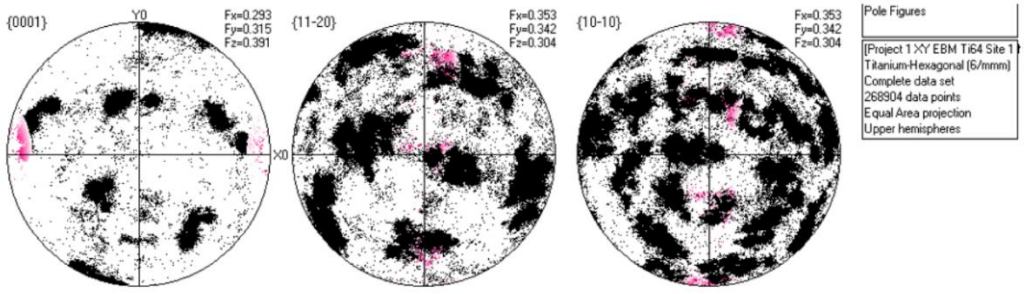

(a)

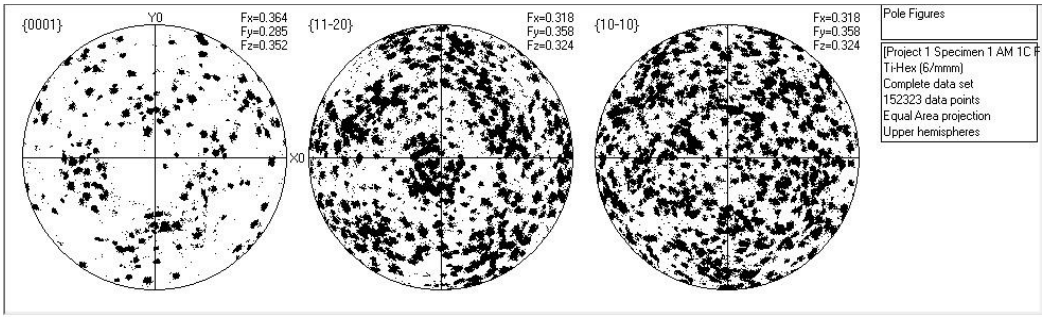

(b)

Fig. 5.14 'Pole figures (a)) Initial EBM Ti64, (b) 1 x DSC EBM Ti64 '

Microstructure change observed with one-time HT is related with phase transformation mechanism and grain characteristics determined by cooling rate. Further investigation using DSC is applied cyclic heating and cooling near β-transus temperature. The second experiment applied to EBM Ti6Al4V is 5-time cyclic HT in between 1000 - 800 °C. Heating and cooling rates are 100 °C/min. Schematic view of the HT shown in Fig. 4.2 (c). This sample labeled as 5 x DSC EBM Ti64 NH.

The goal with the 5-time cyclic HT is to trigger more phase transformations and have well distributed finer α-phase laths/plates and decreased residual stress. In this experiment soaking was not applied to avoid fully transformed microstructure from α to β-phase. The inherited small β-phase grains provide more nucleation points for α-phase. Band contrast and grain size map of 5 x DSC EBM Ti64 sample shown in Fig. 5.15.

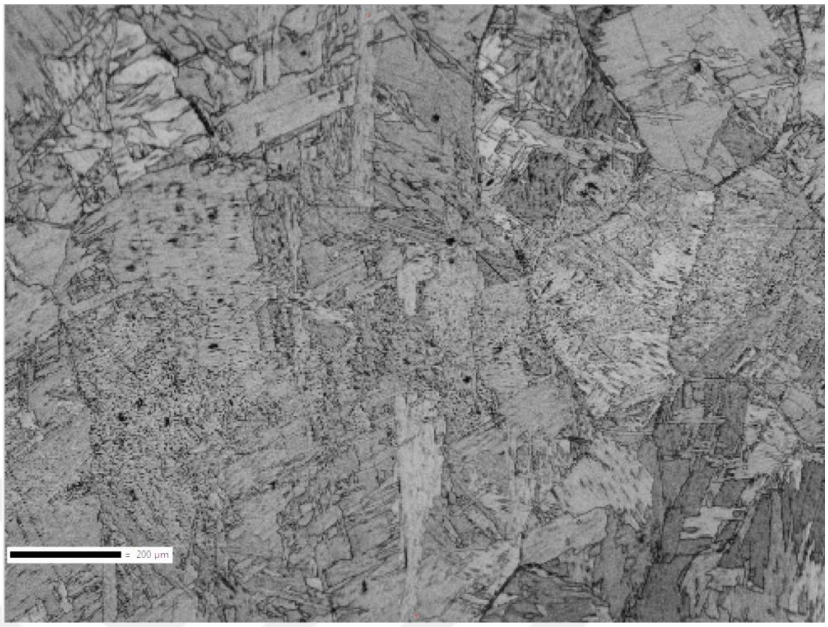

(a) Band Contrast

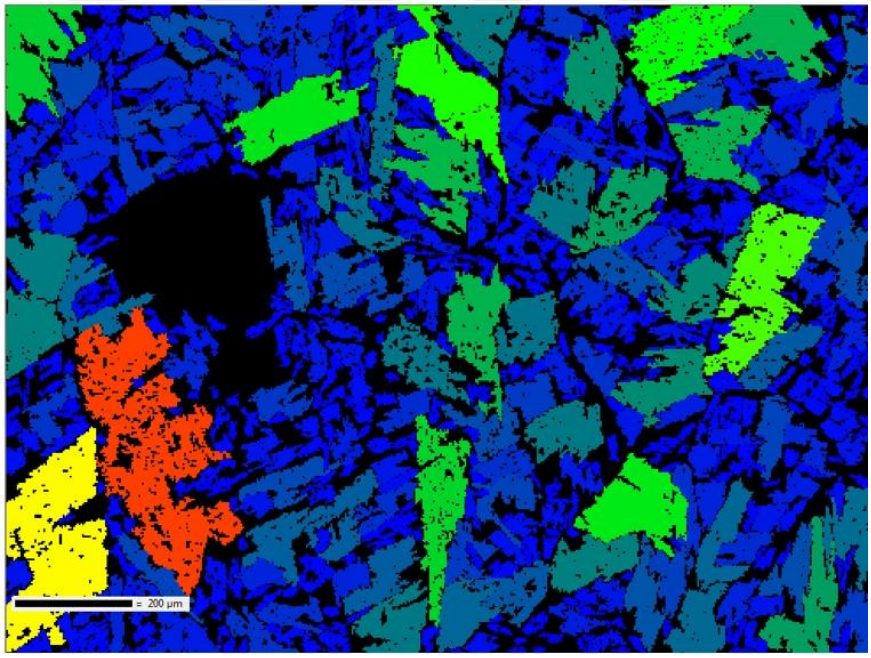

(b) Grain Size Map

Fig. 5.15 '5 x DSC EBM Ti64 NH sample microstructure'

The 5-time HT sample heat flow curve shows phase transformation occurred at a slightly higher temperature compared to the one-time HT, but still lower than the

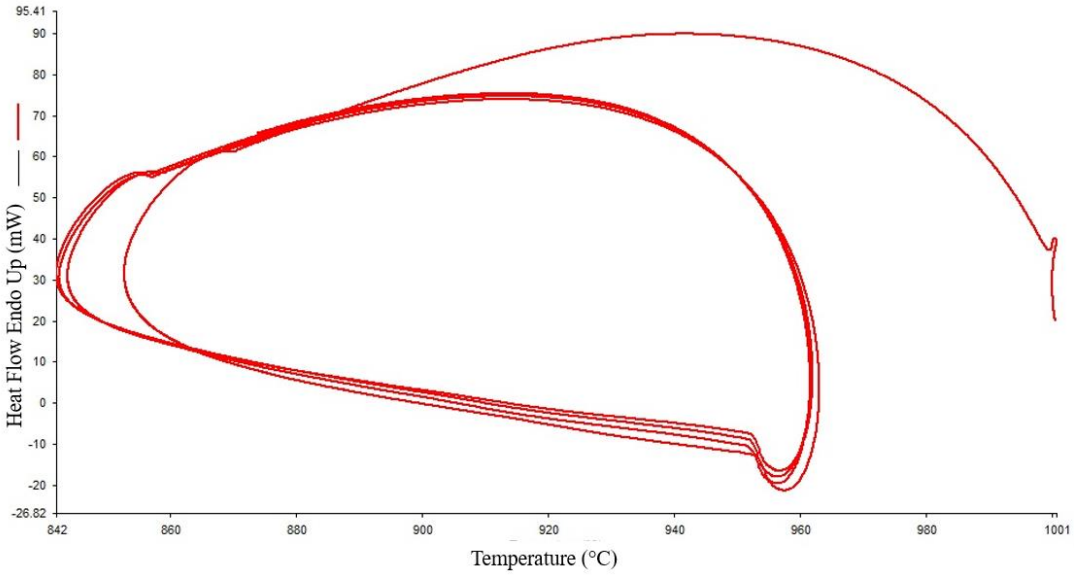

Fig. 5.16 'Heat Flow Curve for 5 x DSC EBM Ti64 NH'

theoretical temperature. It is observed that a slight shifting occurs in between each cycle cooling and it is related the amount of the transformed phased during cycles. It is considered that the amount of β-phase is not the same for each cycle.

The average grain size increased with cyclic heat treatment. The grain size area was 1211.7 μm^2 for one-time HT and increased to 1545 μm^2.

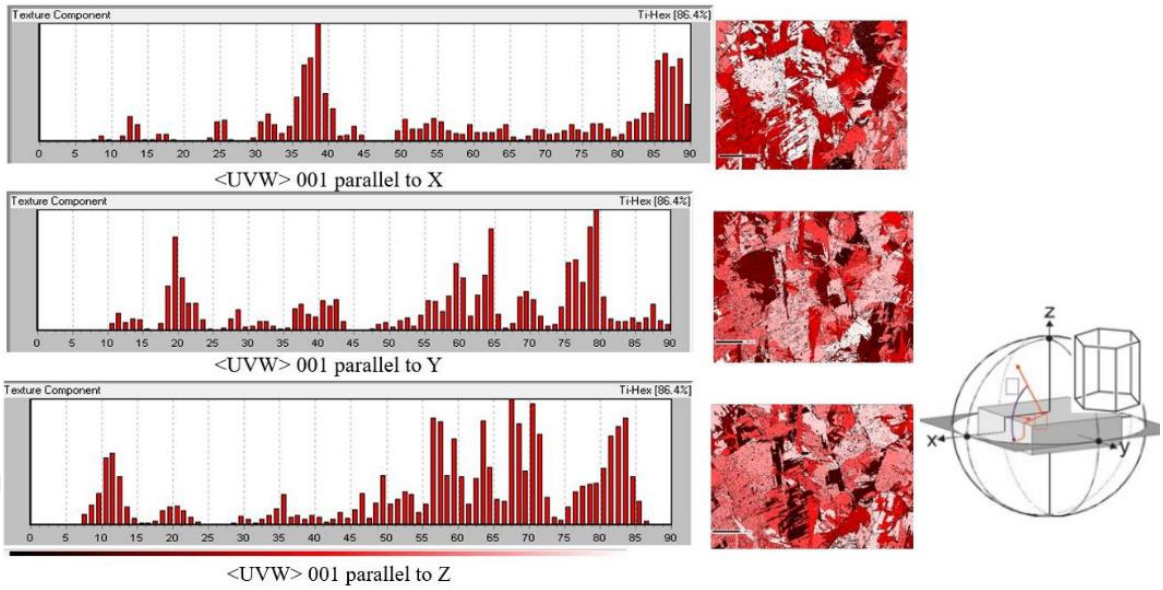

Fig. 5.17 'Texture component of 5 x DSC EBM Ti64 NH, (a) X parallel to basal plane, (b) Y parallel to basal plane, (c) Z parallel to basal plane'

Texture component of 5-time HT shown in Fig.5.17. It is observed that there is an increase on the population of the high angle orientated grains in <UVW> 001 parallel to X position. This means that the number of the grains which have >85° angle increased.

The orientation change of the microstructure is a result of preferred or ideal phase transformations. When we were comparing the 5-time and 1-time HT; we observed that the microstructure had different grain distribution however grain size increased, the grains distributed more evenly and had lower standard deviation. This can be related to the 5-time cyclic HT allowing microstructure to transform from phase to phase more ideally rather than the one-time HT in terms of preferred β→α variants but still affected by highly inherited residual stress which occurred during production of the sample. For further investigation the strain contour map of the one-time HT compared with strain contour map of the 5-time microstructure, shown in Fig 5.18.

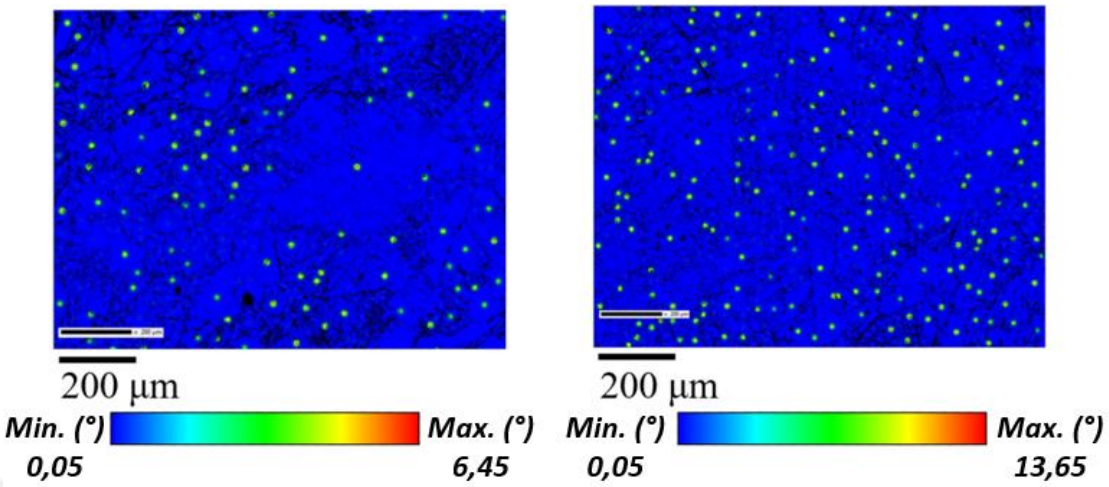

(a) (b)

Fig. 5.18 'Strain contour map, (a) 1 x DSC EBM Ti64, (b) 5 x DSC EBM Ti64 NH'

Comparison of the two stain maps in Fig. 5.18 shows that 5 x DSC EBM Ti64 NH sample has more strained regions. The number of green-red dots are more and randomly distributed all around the microstructure. We observed after a number of HT microstructure release the residual stress with increased strains and grain orientation change become more stable. During stress release, strain values were increased while expansion and contraction happened with phase transformation and the microstructure tried to get to a stable form. Since as build condition is highly stress loaded during heating and cooling contraction and expansion of lattice parameters caused local strains to occur. Strain maps are not enough for interpretation and quantitative data is also needed for examination of microstructure behavior. Fig. 5.19 shows the strain values for α and β-phase in one-time HT and 5-time HT experiment. Significant difference in between the two plotted graphs is max strain value in cubic Ti, it is 13.65° and 6.45° respectively for 5-time and one-time HT. For

hexagonal Ti there is less strain values in 5-time HT which supports the idea that high number HT derives more ideal microstructure.

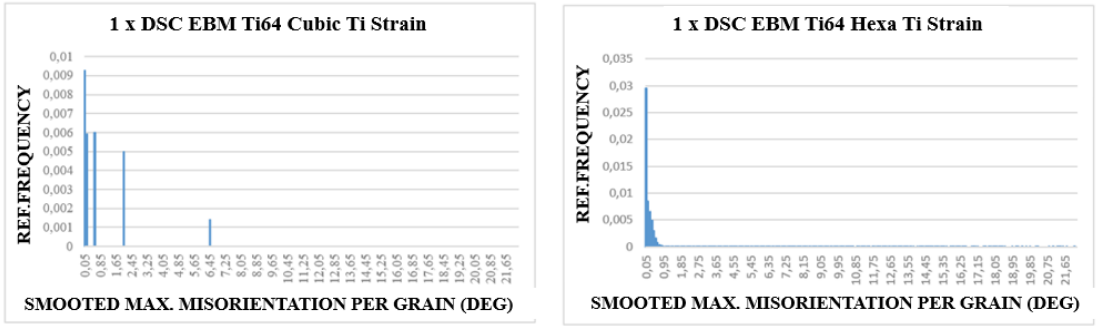

(a)

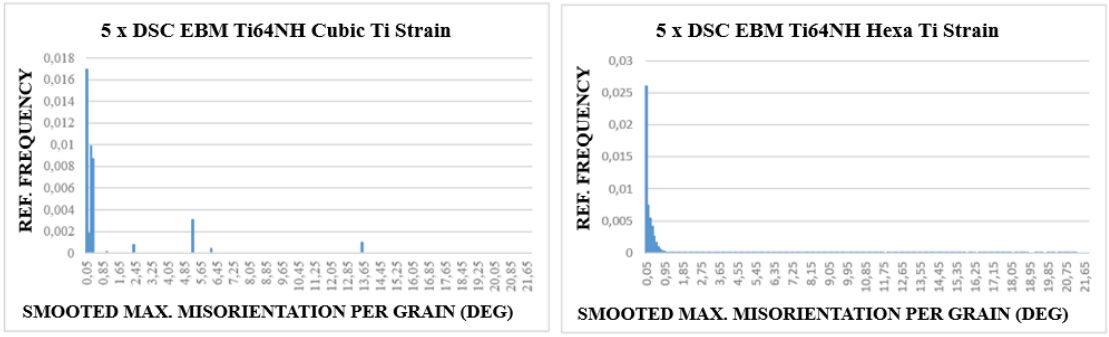

(b)

Fig. 5.19 '(a) Strain contour for 1 x DSC EBM Ti64 α and β phases, (b) Strain contour for 5 x DSC EBM Ti64 NH α and β phases'

Inherited residual stress can be released with greater misorientation of the grains. Grains can be flipped during or after phase transformation and become misoriented grains. In this situation there is misoriented grains, but the stress and strain values decrease which we consider as improvement of microstructure until a certain level of misorientation. The examine the misorientation of each pixel to mean grain orientation, GOS mapping data and images were used, shown in Fig. 5.20

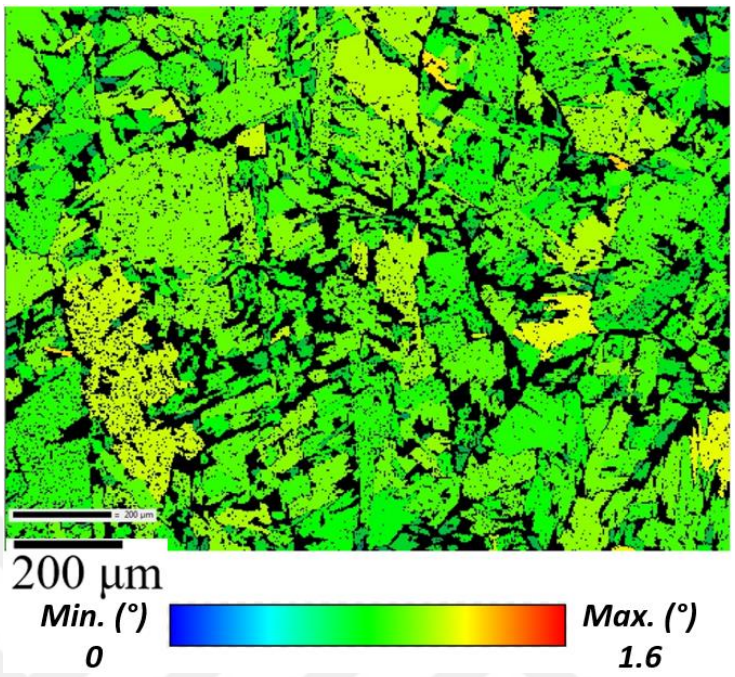

Fig. 5.20 'Grain Orientation Spread map for 5 x DSC EBM Ti64 NH'

Microstructure response in cyclic HT is to release the residual stress and try to become more stable with ideal or preferred phase transformation. In addition, grain size was observed to have lower standard deviation. There is no soaking in 5-time HT, so the phase transformation may not happen 100%.

The third experiment with DSC heat treatment is cyclic heat treatment with soaking. The goal of this experiment is to let the microstructure have enough time for full transformation. 5-time HT in between 1000 – 800 °C was applied with 5 minutes of soaking time at every step of the HT applied. This is shown in the schematic curve shown in Fig. 4.2 (b). The same heating and cooling rate applied with previous experiments, 100 °C/min. this sample labeled as 5 x DSC EBM Ti64 H. Microstructure after HT of this sample is shown in Fig. 5.21. DSC heat input curve is shown in Fig. 5.22

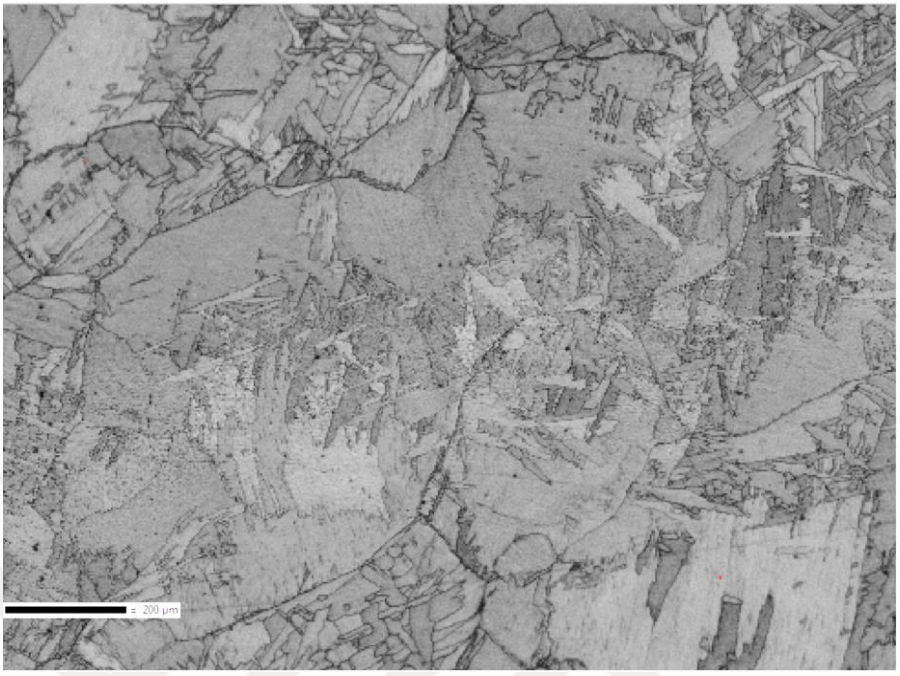

(a) Band Contrast

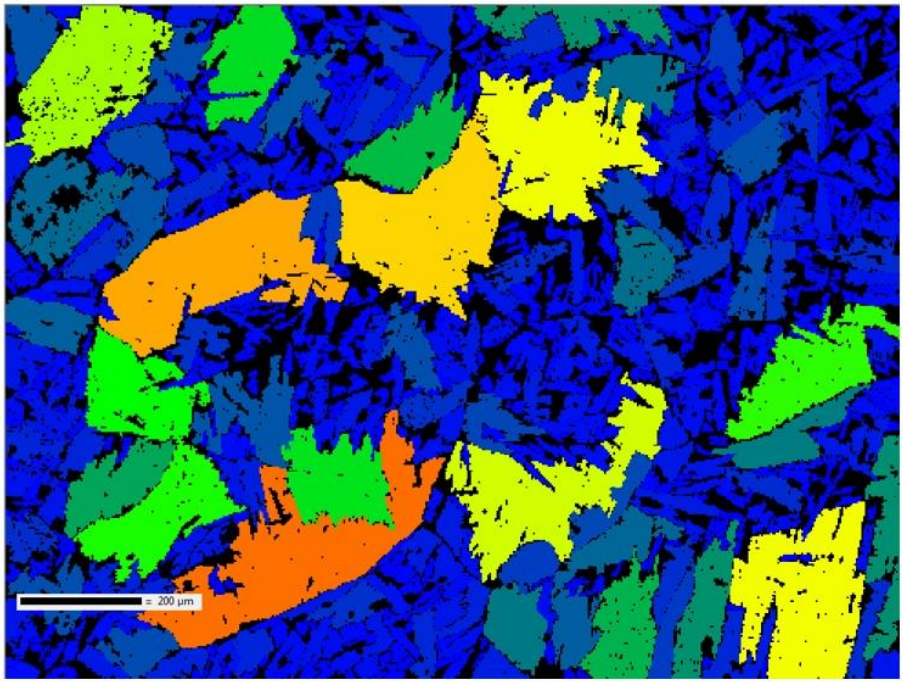

(b)

Fig. 5.21 '5 x DSC EBM Ti64 H sample microstructure'

Since the sample stays longer at above β-transus temperature β grain growth is expected. When we compared the grain size with previous DSC experiments, 5 x DSC EBM Ti64 H sample has the biggest average grain area which is 1576.8 μm^2.

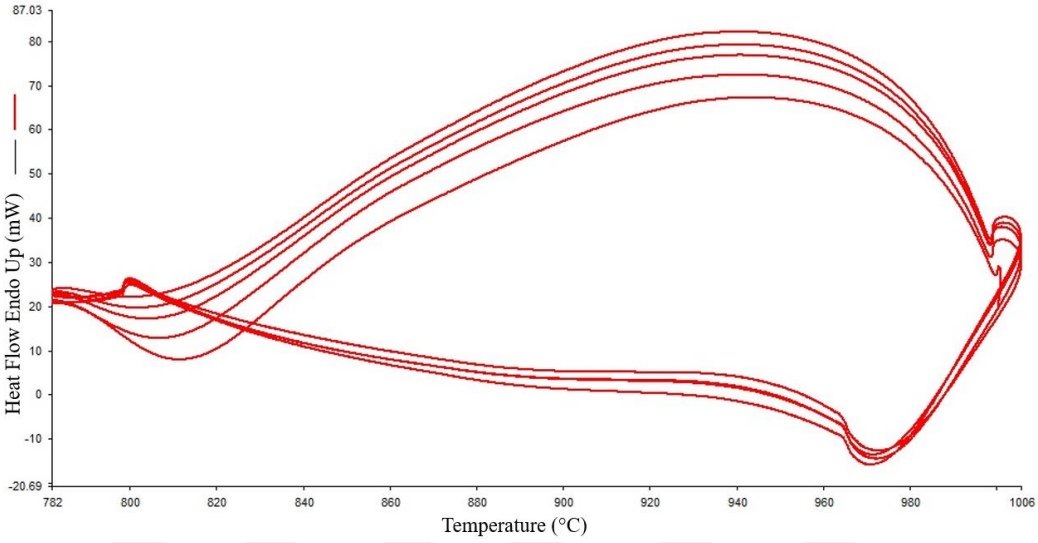

Fig. 5.22 'Heat Flow Curve for 5 x DSC EBM Ti64 H'

Texture component in Fig. 5.23 shows there is a decrease of the number of the grains which have low angle orientation < 45° between basal plane and c-axis of the lattice. Also, the population of the grains with high angle and oriented with other coordinates increased. This is considered as grains that changed their orientation and flipped at high temperature regions with extended soaking time.

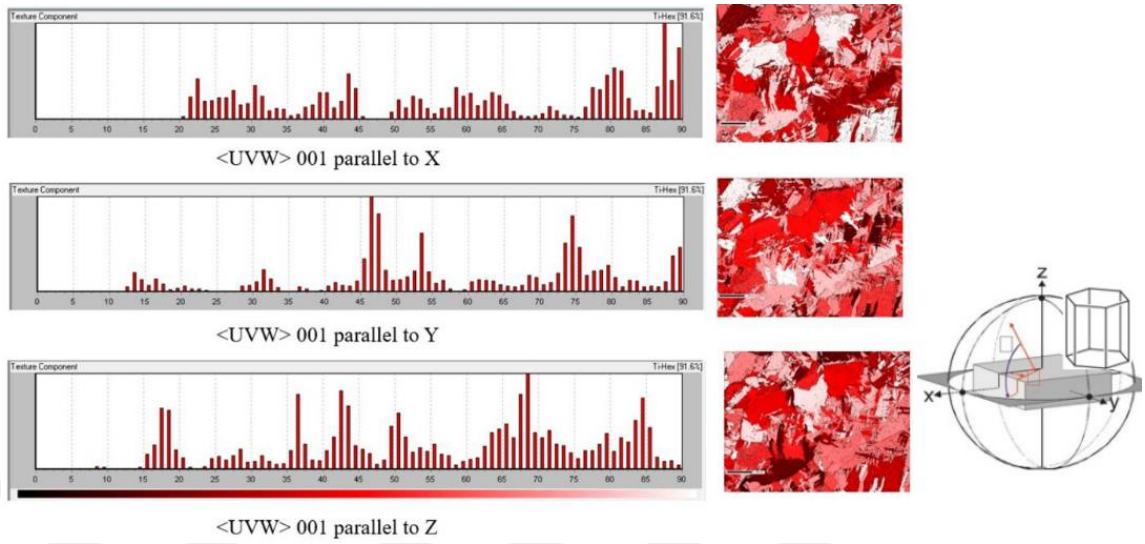

Fig. 5.23 'Texture component of 5 x DSC EBM Ti64 H, (a) X parallel to basal plane, (b) Y parallel to basal plane, (c) Z parallel to basal plane'

It is observed that orientation of the grains is more deviated than HT without soaking, as a result more residual stress released from the microstructure. Stress was released with strains in previous HT since there was not enough heat input to change grain orientation thermodynamically and kinetically. 5 x DSC EBM Ti64 H sample has higher enthalpy for phase transformations and microstructure orientation than previous heat treatments. Strain map in Fig. 5.24 shows 5 x DSC EBM H and quantitative data in the plotted strain values show that this sample has lowest strain values compared to other DSC experiments.

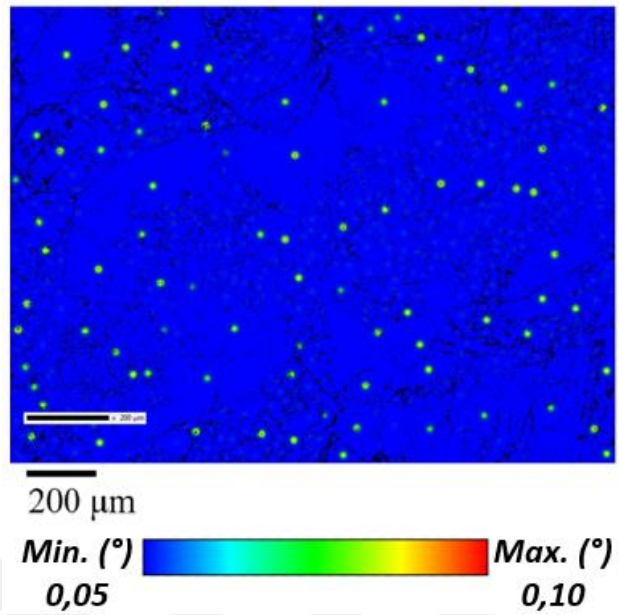

Fig. 5.24 ‘5 x DSC EBM Ti64 H Strain contour map’

It is clear that the number of the strain regions in Fig. 5.24 is lower than previous experiments. (Fig. 5.18) The quantitative data of strain values in 5 x DSC EBM Ti64 H sample plotted in Fig. 5.25 and also observed that it has lowest values compared to previous experiments. (Fig. 5.19)

It can be considered that the microstructure has lower strains because the grains flipped and deviated from the mean grain orientation which GOS map shows. This mechanism lowers the stress and also strains inside the microstructure. Fig. 5.26 shows the grain orientation spread reddish grains are highly misoriented grains which are flipped to release stress.

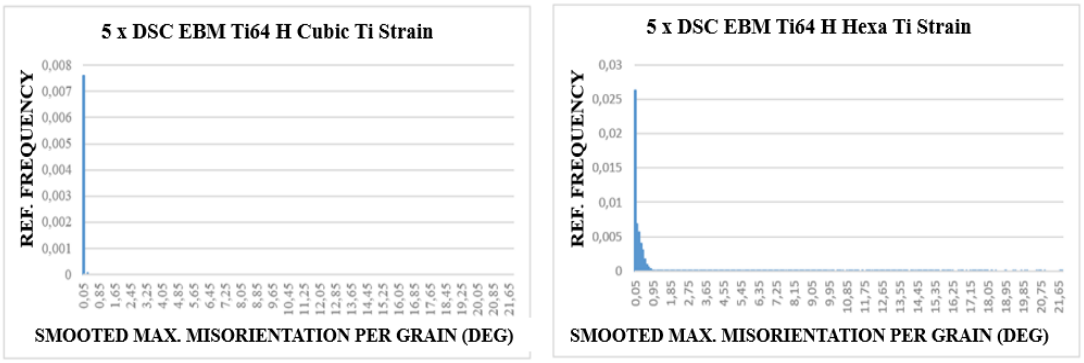

Fig. 5.25 'Strain contour for 5 x DSC EBM Ti64 H α and β phases'

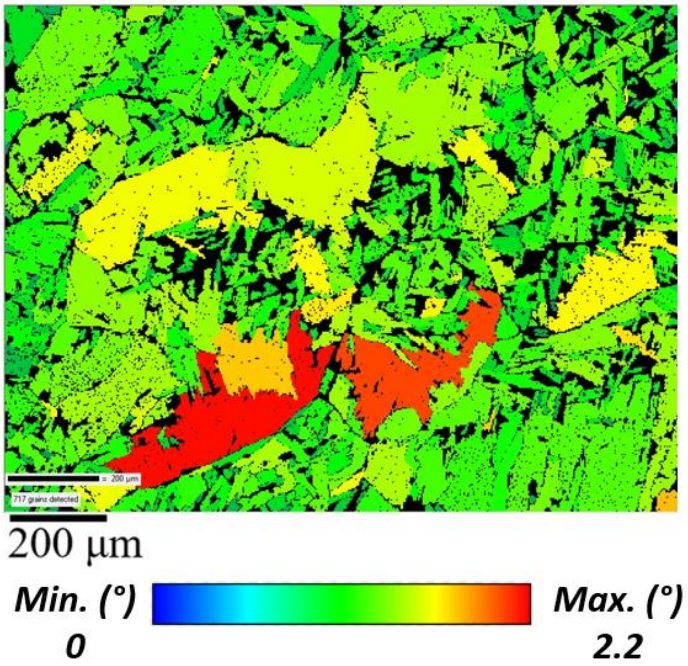

Fig. 5.26 'Grain Orientation Spread map for 5 x DSC EBM Ti64 H'

When we compared the three low rate HT experiments we observed grain size increased with number of heat treatments and with time. The strain trend of three experiments is that the strain value increased until a certain level to release the residual stress inside the microstructure where high strain value regions occurred. When the soaking applied to the HT then the total heat input increased which provides higher enthalpy to

microstructure and the stress released with grain orientation change which also decreased the strain value.

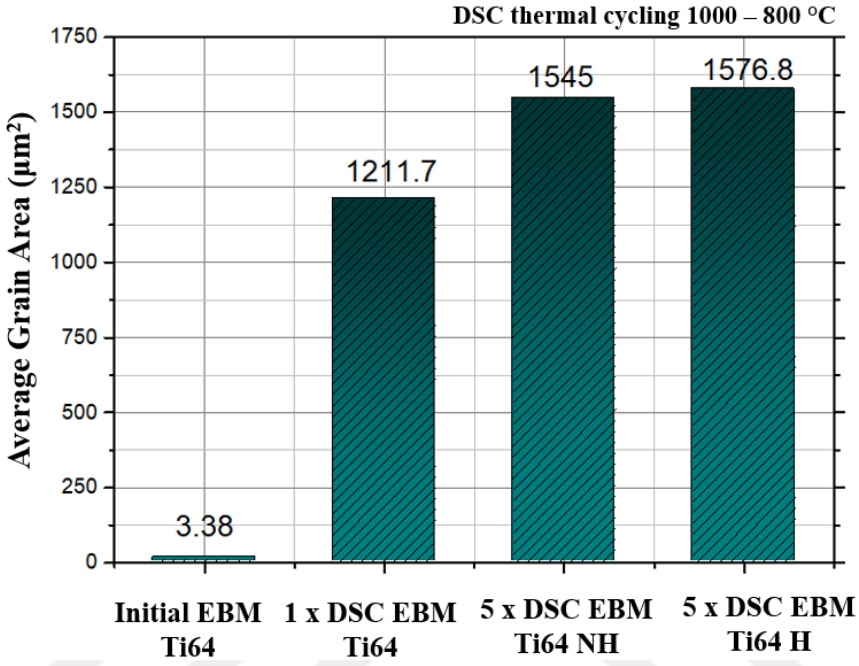

Fig. 5.27 'Grain size comparison of DSC HT experiments'

Recrystallized fraction map provides the information of the grains which are deformed, substructure, or recrystallized based on crystal structure misorientation. Deformed grains: highly misoriented grains which are deviated from the mean orientation higher than 7.5°. Recrystallized grains: the grains deviated from the mean orientation less than 1°. Substructure grains: the grains deviated from the mean orientation in between 1 – 7.5°. Fig. 5.28 shows recrystallized fraction map for initial and three DSC experiment. Blue regions label the recrystallized grains, yellow regions label the sub-structured grains and the red regions labels the deformed grains. The population of recrystallized grains decreased with increase of HT cycles however it is increased with increase of time. Figure

5.29 shows the ratio of recrystallized, sub-structured, and deformed grains for both DSC and initial EBM samples.

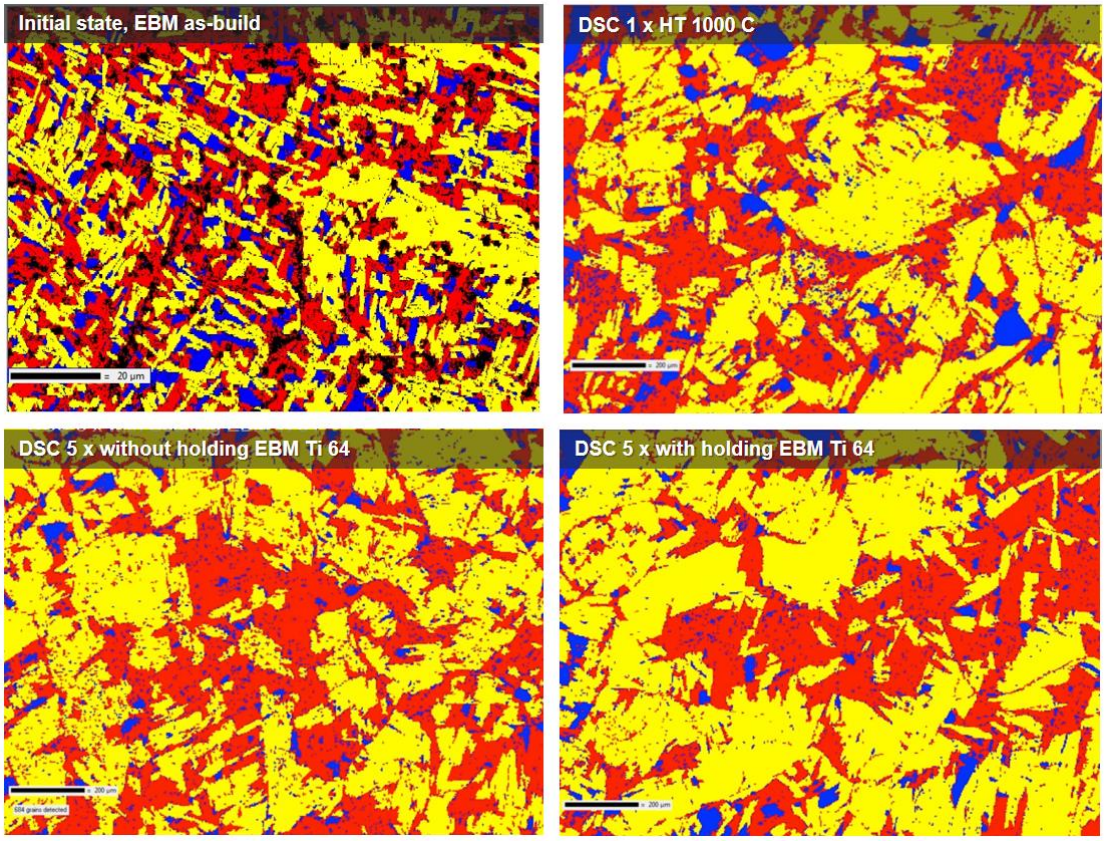

Fig. 5.28 'Recrystallized fraction map of DSC HT experiments and initial condition'

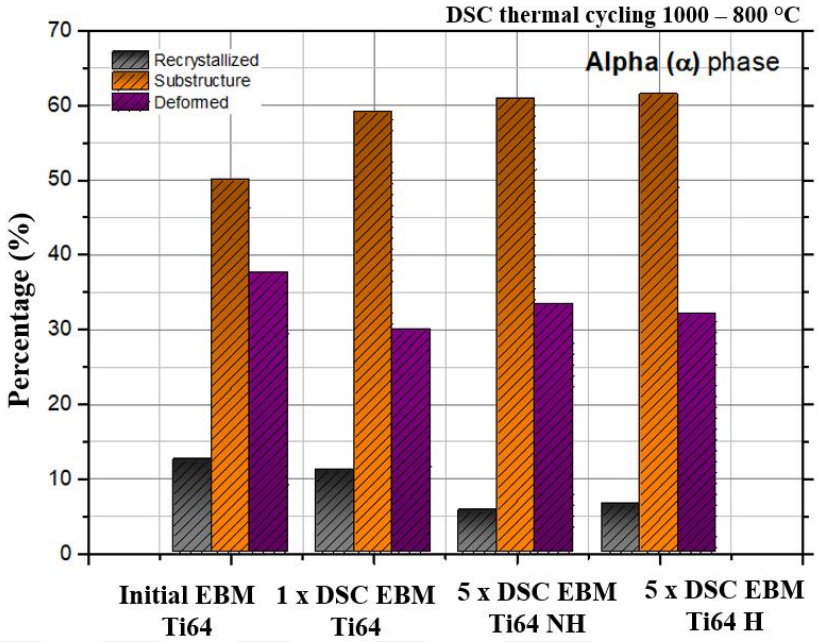

Fig. 5.29 'Recrystallized, sub-structured, and deformed grain fractions for each experiment and initial condition'

5.2.2 EBM Ti6Al4V Microstructure Response and Toughness After Rapid Heat Treatments

We observed the microstructure response to different heat treatments at constant heating and cooling rate (100 °C/min). Further investigation of the current study includes examination of the microstructure response to higher heating and cooling rates and correlation of microstructure with mechanical property, toughness. These experiments are executed by Multi-Scale Joining and Interconnect Technology Group of PSU. Higher heating rates can be achievable with a sophisticated tool like Gleeble®. Heat treatment applied to EBM Ti6Al4V with 50 °C/sec and increased to 1000 °C. Heating rate is 30x faster compared to DSC. This fast heating rate increased the stress and strains related with heating relative to DSC. It is expected that a rapid phase transformation may disturb grains

and affect the orientation of the grains. There is 10 sec soaking time for the sample to let a fully transform microstructure. The heating and cooling curve for this experiment is shown in Fig. 5.30. This sample is labeled as 1 x GL EBM Ti64. The dimensions for the sample shown in Table 4.2, and the Gleeble® jaw span is 20 mm.

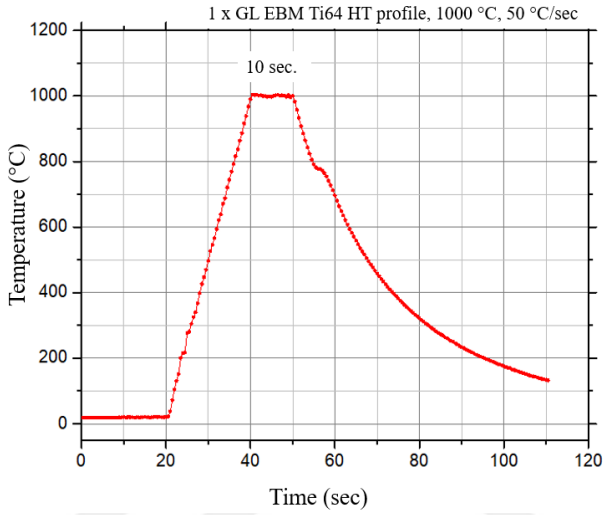

Fig. 5.30 '1 x GL EBM Ti64 HT profile'

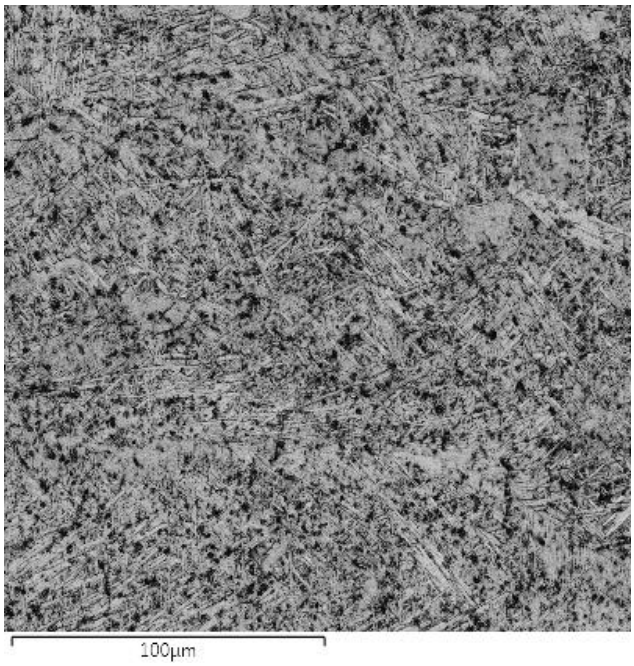

(a) Band Contrast

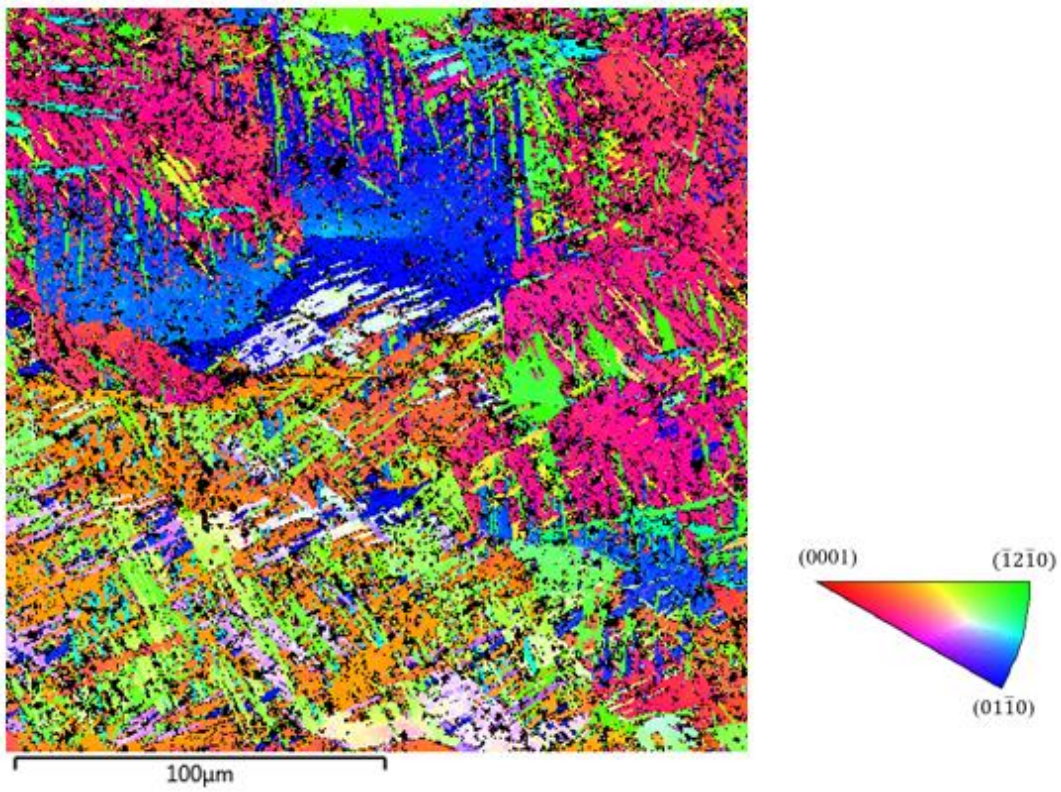

(b) IPF

Fig. 5.31 '1 x GL EBM Ti64 sample microstructure view from HTR after HT'

Gleeble® applied high voltage to the sample and the resistivity of the metal cause sample heating via conductive copper jaws. Because temperature is not evenly distributed, the highest temperature occurs in the center of the sample. This region will be mentioned as both 'Heat Treated Region' (HTR), or 'Heat Affected Zone' (HAZ) schematic view shown in Fig. 5.32.

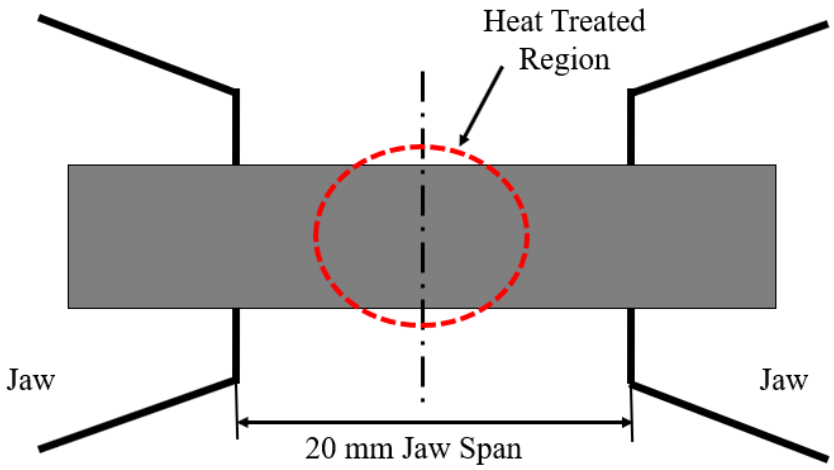

Fig. 5.32 'Schematic view of HTR'

Microstructure analysis was done for both HTR and No HTR. Results are shared from the HTR. Microstructure examination was done in two different locations in HTR and mentioned as HTR1 and HTR2.

The same heat treatment applied to wrought Ti6Al4V by Multi-Scale Joining and Interconnect Technology Group and the results are shared to make a better understanding of the effect of HT to different production methods.

The first significant difference is observed in grain size. As it was expected the grain size decrease with rapid HT on the contrary to slow rate HT experiments. It is a direct result of high cooling rate. DSC HT has lower cooling rate than as build conditions and Gleeble® has higher cooling rate, which provide grain refinement. The grain size distributions for EBM Ti6Al4V and wrought Ti6Al4V are shared in Fig. 5.33. Grain size decreased significantly in the wrought material, around 50% decrease happened. EBM grain size decreased by approximately 10%.

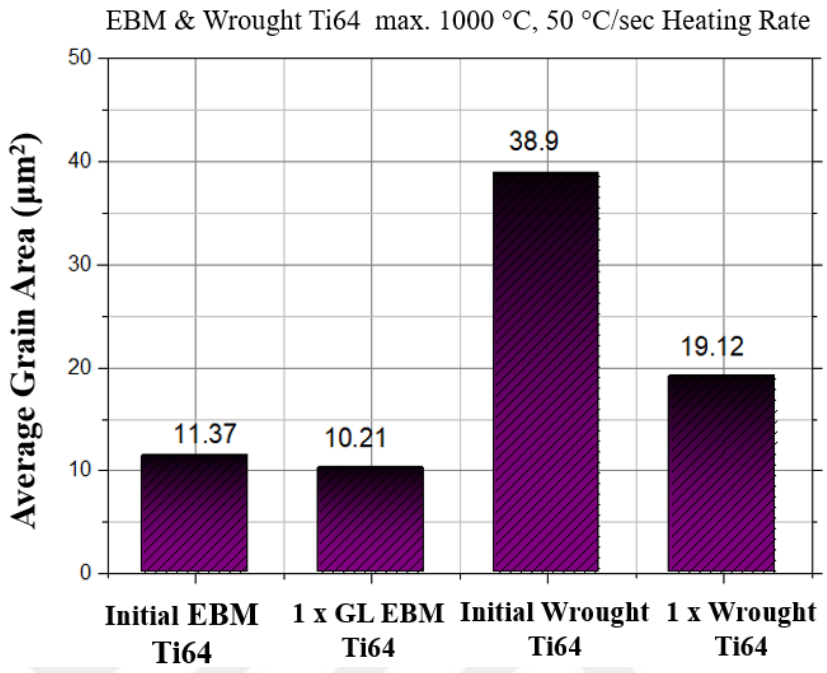

Fig. 5.33 'Grain size comparison of HT and initial conditions for EBM & Wrought Ti6Al4V'

This grain refinement effect is also shown in the recrystallized fraction map. It is observed the sub-structured grains turned to deformed grains after the one-time HT. The grain misorientation increased, however recrystallized grain fraction was not affected in EBM sample. On the other hand; wrought material recrystallized and sub-structured grain population decreased while the number of the deformed grains increased. Fig5.34 shows the percentage of the recrystallized, sub-structured and deformed grains below. Since deformed grain population increased it was expected that the strain value and GOS after HT were affected. But strain value shows that the initial condition has higher strain values.

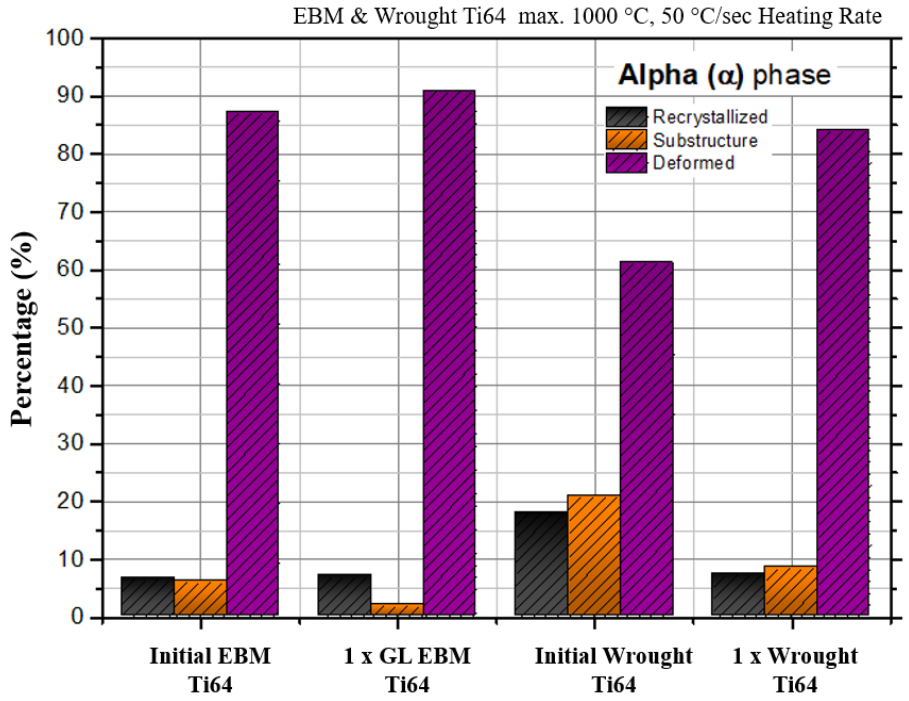

Fig. 5.34 'Recrystallized, sub-structured, and deformed grain fractions for each Rapid HT experiment and initial condition'

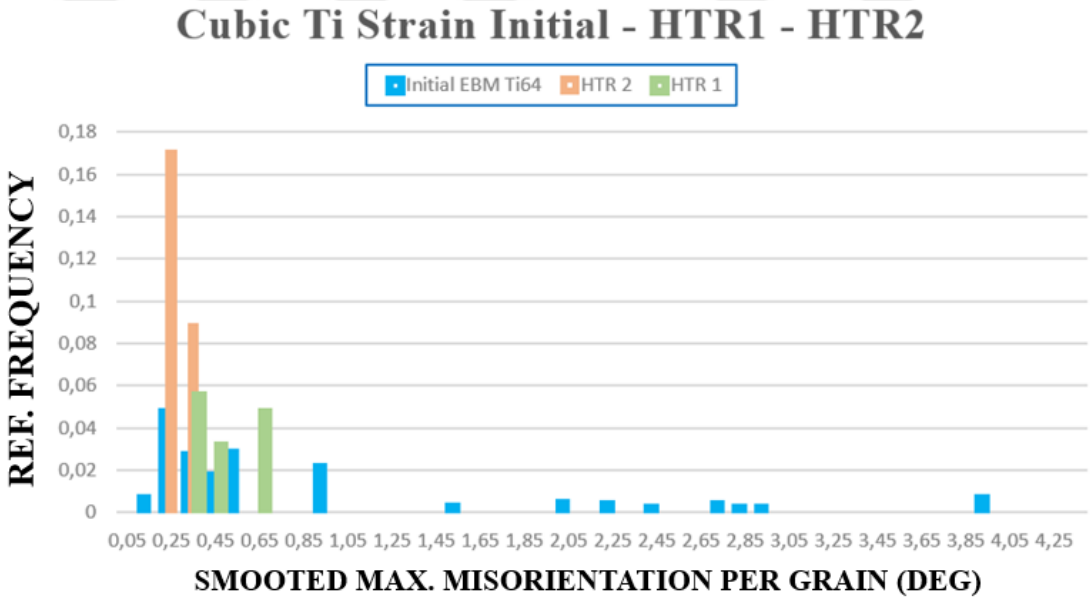

Fig. 5.35 'Strain contour of Rapid HT for β phases'

It is observed form the recrystallized map that the population of the deformed grains were increased but the strain values for both Cubic and Hexagonal titanium did not increase. As a result, it was considered that the grains became more deviated from the mean orientation with rapid HT. The GOS trends showed a tendency to shift on right hand side of the plotted graph. The GOS distribution broaden and shifted which is shown in Fig. 5.37.

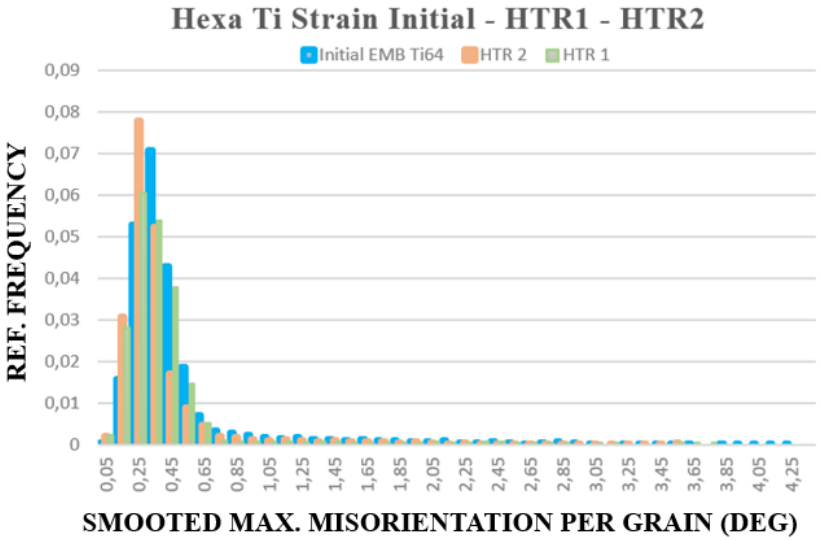

Fig. 5.36 'Strain contour of rapid HT for α phases'

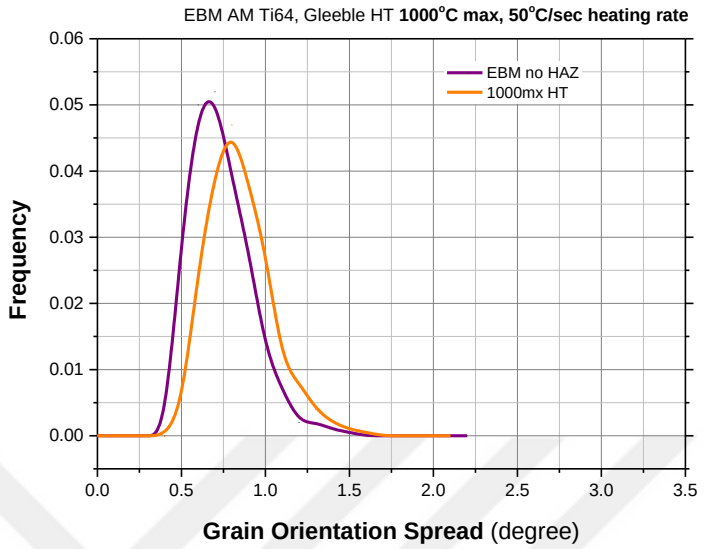

(a) EBM Ti6Al4V

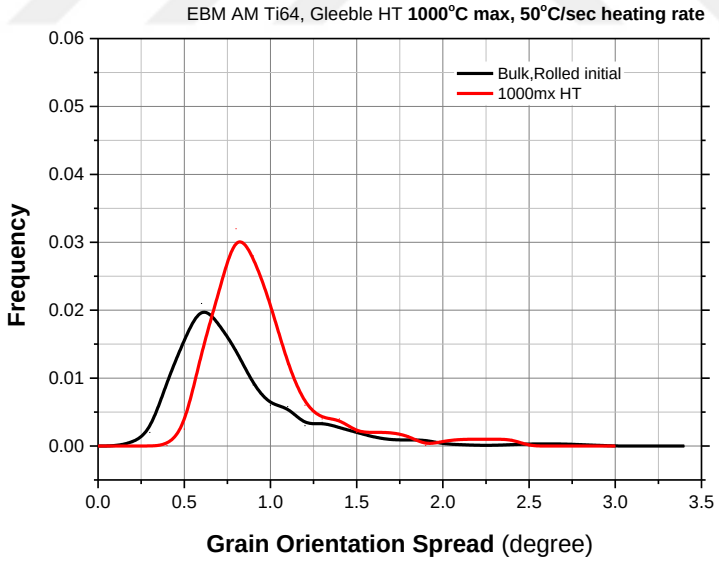

(b) Wrought Ti6Al4V

Fig. 5.37 'Grain orientation trend for wrought Ti6Al4V and EBM Ti6Al4V'

After heat treatment, samples were machined to the dimensions shown in Fig. 4.5 for toughness testing. ASTM standard E23 Impact Testing was executed. The results before and after HT are shown in the Fig.5.38. Wrought titanium has a microstructure texture due to the rolling direction. Texture and pancake shape grains from rolling still exists after annealing. Rapid HT decreased the average grain size and had a recrystallization effect on wrought titanium improving the toughness. In case of EBM microstructure approx. 10% grain refinement was observed after HT. There is a significant improvement observed for toughness after HT. It is considered that only 10% grain refinement should not improve toughness that much: approximately 47% increase. It is considered that the residual stress modification is the major effect on improvement. In addition to that low strain values after HT had substantial effect on toughness improvement. Grains released their stress by changing their orientation which broadens the GOS and this mechanism decrease the strain value of grains. Also, additional small amount of grain refinement improved the toughness of EBM Ti6Al4V. Further examination was done by the Multi-Scale Joining and Interconnect Technology Group at a higher temperature, 1200 °C. Grain growth observed in prior β grains at higher temperature had a negative effect on mechanical properties. Since the microstructure released its residual stress and decreased strain with grain misorientation, 1200 °C HT sample had better toughness property than the initial condition. However; 1200 °C HT sample toughness still lower than 1000 °C HT. Fig. 5.38 shows the impact energy of each 1000 °C and 1200 °C for wrought and EBM built Ti6Al4V.

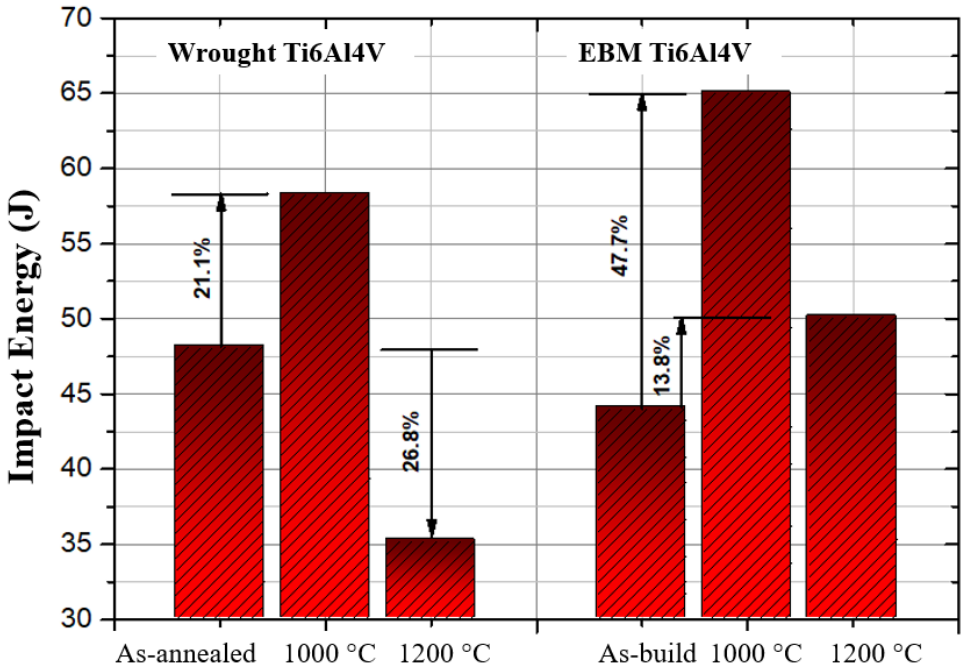

Fig. 5.38 'Toughness for Wrought & EBM Ti6Al4V before and after different temperature HT'

Phase fraction of EBM Ti6Al4V samples for each condition was calculated with Channel 5 software. Phase ratio graph for the various samples is plotted below. The 1-time rapid heat-treated sample had very low amount of alpha phase which is related with the resolution of the image. We can see the amount of the beta phase increased with energy input in between 1-time DSC and 5-time DSC heat treatment.

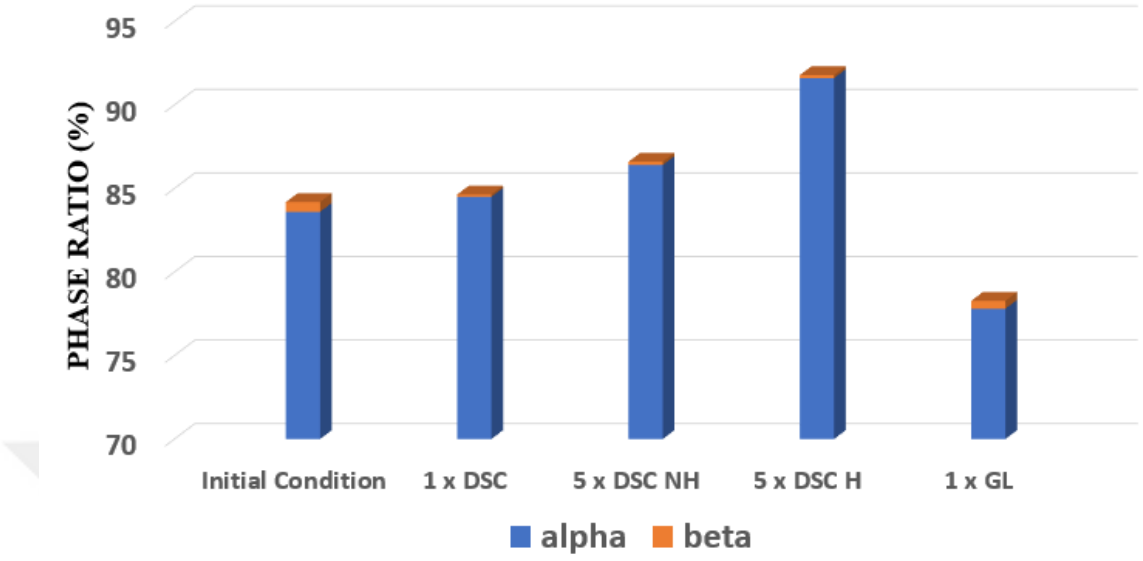

Fig. 5.39 'Phase ratio of EBM Ti6Al4V for each condition'

5.2.3 CMT Ti6Al4V Toughness After Rapid Heat Treatments

Rapid HT increased the toughness of low deposition rate AM method EBM. High deposition rate technique CMT was also investigated with same manner. For CMT two initial conditions were compared at different shielding gas parameters. Thermal convection during build and, cooling rate of post process are directly dependent on gas properties. Two different gas types used in the experiment Ar and Ar+He mix. CMT process has lower cooling rate with Ar gas compared to Ar+He. The same rapid HT was applied to an Ar gas built sample. ASTM E23 impact testing done for three samples to monitor the toughness of each application.

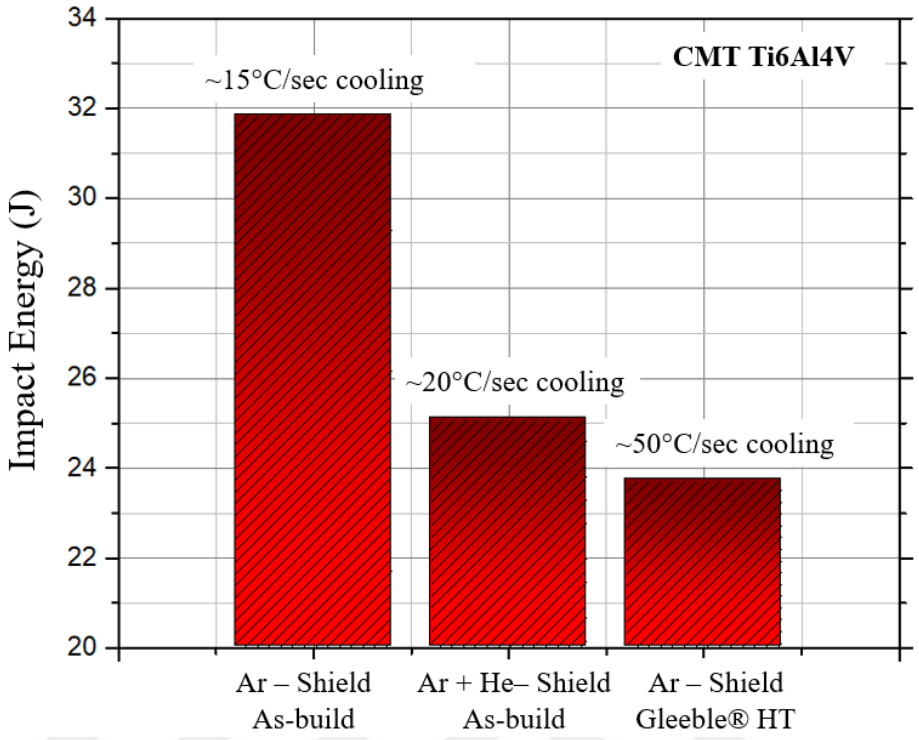

Fig. 5.40 'Toughness for CMT Ar as-build, Ar+He as build, and Ar Rapid HT'

It is observed that toughness values decreased with increasing cooling rate. (Fig. 5.39) The same HT conditions with EBM Ti6Al4V gave different results for high deposition AM technique, CMT. Toughness decreased with heat treatment rather than EBM. Comprehensive microstructure investigation is needed for future study to make correlation with CMT HT microstructure and toughness.

5.2.4 SLM CP:Ti Toughness After Rapid Heat Treatments

Another titanium material subject to the present study is CP:Ti. As it is mentioned in literature review section of the present study, conventionally produced α-titanium alloy mechanical properties cannot be improved with heat treatment. SLM method has very high cooling rates and different microstructure compared to conventionally produced microstructures. SLM has significantly high residual stress in the as-build condition similar to EBM process, however microstructure is different and fully α-phase.

Three different HT were applied with Gleeble® to CP:Ti samples. Maximum temperature for these experiments was 950 °C which is slightly lower compared to previous experiments it is because of the lower β-transus temperature of CP:Ti. Cyclic HT executed in between 950 – 750 °C. Heating and cooling rate applied with the same rates of the previous experiments. First HT: HT1 only one-time max 950 °C with 50 °C/sec heating and cooling rate. Second HT: HT2 three cycles between 950 – 750 °C, 10 sec. soaking time for each temperature and 50 °C/sec. cooling rate. Third HT: HT3 5 cycles between 950 – 750 °C, 10 sec. soaking time for each temperature and 50 °C/sec. cooling rate. Fig. 5.40 shows heating and cooling profile of each HT below.

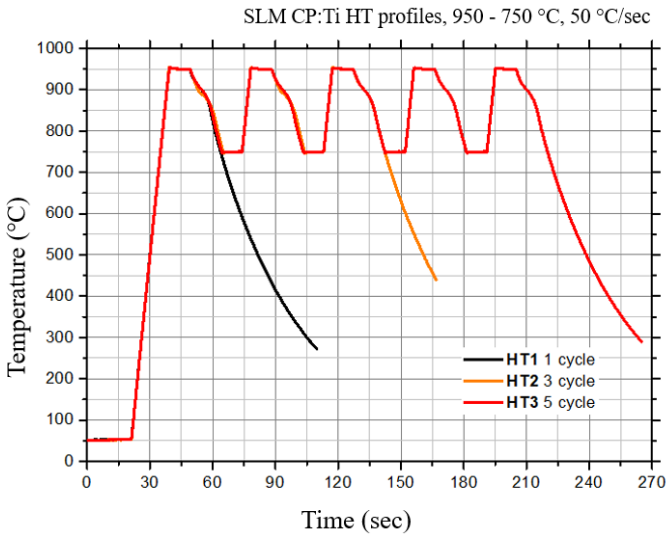

Fig. 5.41 'Applied HT profiles to CP:Ti samples'

After HT, samples were machined to ASTM E23 standard dimensions for Charpy impact testing. The results are shown in Fig.5.41. Toughness was improved with HT until 3 cycles after which toughness decreased but were still higher than the initial condition. Results are similar with EBM Ti6Al4V HT experiments.

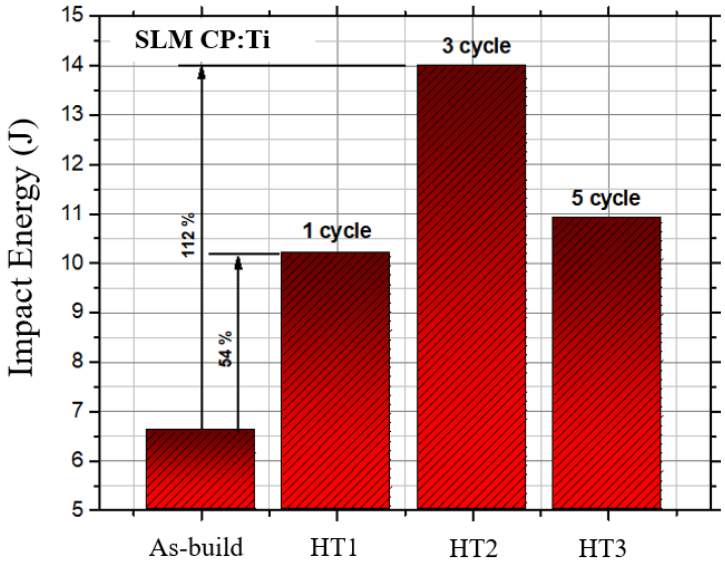

Fig. 5.42 'Toughness for SLM CP:TI, as-build, HT1, HT2, HT3'

Chapter 6 Summary & Conclusion

6.1 Conclusion

EBM, SLM and CMT AM process with two different titanium alloys were investigated. Mechanical property improvement was observed for powder based AM methods; EBM and SLM for the alloys Ti6Al4V and CP:Ti respectively. The mechanism underneath the improvement was stress and strain release within the microstructure and grain orientation change. The mechanism was similar for high heating rate and moderate heating rate applications. The only difference was that rapid change happened with very fast heating rate HT.

High deposition rate AM method CMT had different response to applied HT rather than powder based methods for Ti6Al4V alloy. Toughness values decreased with applied HT. In addition to that, shielding gas effect was observed. Cooling rate and convection depends on gas characteristics especially its thermal diffusivity and conductivity.

- Toughness of EBM Ti6Al4V and SLM CP:Ti can be improved with heat treatment. A 47% improvement of EBM Ti6Al4V and 112% improvement of SLM CP:Ti toughness was observed.
- Cyclic heat treatment provides further improvement on mechanical properties for SLM CP:Ti. Toughness increased with a 3 cycle HT however, a 5 time HT decreased the toughness. Toughness was still higher than initial condition for all HT samples.

- Higher temperature HT application decreased the toughness since beta grain growth occurred at high temperatures. HT of EBM Ti6Al4V with 1200 °C had lower toughness compared to HT 1000 °C with same heating and cooling rate. Still HT 1200°C sample had higher toughness than initial condition.
- High deposition rate AM method CMT Ti6Al4V had different as-build microstructure than EBM it was observed the response of the sample to HT was also different than EBM: toughness decreased after rapid HT.
- Shielding gas composition controls the cooling rate during building in CMT process. Ar gas had a lower cooling rate compared to Ar+He mixed gas. Comparison of as-build condition samples of these two-different shielding gas showed slow cooling rate sample was tougher than mixed gas application.
- The microstructure responded to HT in a sequence of first grain strain then grain re-orientation. This was observed with slow heating rate HT. High residual-stress was inherited inside microstructure from the EBM process. To release this stress grains increased strain values with heat treatment and released some amount of the stress. When high entropy provided with soaking and cyclic HT grains first increased the strain value then release the stress with becoming highly misoriented to mean grain orientation.
- It was observed phase transformation temperature slightly shifted during cyclic DSC HT since the amount of transformed phase changes during heating.
- Strain value decreased with grain misorientation.

- Microstructure response was different in high heating and cooling HT compared to slow heating and cooling rate. Strain value increase was not observed in rapid HT. But strain value increase observed in slow rate HT.

6.2 Summary

Method	Material	Applied HT	HT Type	Observation
EBM	Ti6Al4V	DSC	1-time	Stress release mechanism clarified
			5-time	
			5-time with soaking	
		Gleeble ®	max. 1000°C	Toughness improvement
			max. 1200°C	Toughness deterioration
CMT	Ti6Al4V	Gleeble ®	max. 1000°C	Toughness deterioration
SLM	CP:Ti	Gleeble ®	1-time	Toughness improvement
			3-cycles	Toughness improvement
			5-cycles	Toughness deterioration

Table 6.1 'Table of summary'

AM produced component use has been increased due to their superiorities. However, these products have many advantages compared to conventional methods, their mechanical and microstructural properties should be well known for real engineering applications. In the present study microstructure of three different AM method was investigated with two different titanium alloys. AM methods are rapid production

processes which have high energy input in very confined regions. Very high cooling and heating rate occurs during the process. Before widening the application of these products, we should know very well about their microstructure and their response to different conditions as materials engineers. In the present study microstructures of various AM processes were examined and toughness values examined as mechanical properties of samples.

It was observed that Ti6Al4V produced with EBM has lower toughness when compared to wrought alloy. This is a result of high residual stress and strains which occur due to the high cooling and heating rates inherent in the process. Current study exhibits EBM Ti6Al4V toughness can be improved even more than wrought alloys improvement. HT EBM Ti6Al4V has higher toughness compared to HT wrought Ti6Al4V. The improvement mechanism was explained with slower cooling rate DSC HT. The microstructure released the stress with increasing strain value. Further stress release happened with increased grain misorientation where grains filliped and changed their orientations.

Ar shielding gas in high deposition rate AM, CMT, provides higher toughness compared to Ar+He mixed gas. Ar gas application had lower cooling rate and consequently it had low stress and strain in the as build-condition. Same 1000 °C HT was applied to Ar build CMT sample with Gleeble®. Contrary the response of EBM samples toughness decreased with HT. Future study must investigate the microstructure mechanism in CMT build microstructure.

Since titanium is the best biocompatible metal, it has been used widely in the biomedical industry. Alloying elements such as aluminum and vanadium are known as harmful metals for internal body implant applications. Because of this, companies in biomedical industry investigate if CP:Ti can be used as internal implants. Even though CP:Ti mechanical properties are not suitable for service requirements. The current study investigates mechanical property improvement for SLM CP:Ti. One-time and multiple time HT applied to SLM processed CP:Ti led to toughness improvement. Cyclic HT made further improvement until 3 cycles of HT. More than 3 cycles showed decrease in toughness.

References

1. G. Lutjering, J.C. Williams, Titanium, Engineering Materials and Processes, 2nd Edition, Berlin: Springer, 2007

2. S.K KIM, J.K. PARK, In-situ Measurement of Continuous Cooling $\beta \rightarrow \alpha$ Transformation Behavior of CP-Ti, , Metallurgical and Materials Transactions A, Vol: 33A, April 2002-1051

3. T.R. Bieler, R.M. Trevino, L.Zeng, Alloys: Titanium, Elsevier, 2005

4. Banerjee D, Williams J.C., Perspectives on Titanium Science and Technology, Acta Materialia 2013;61:844

5. R. Gilbert, C.R. Shannon, Heat Treating, ASM Metals Handbook, Vol. 4. 914-917. Metals Park, OH: ASM International, 1991

6. S.S. Muthu, M.M. Savalani, Handbook of Sustainability in Additive Manufacturing, Vol. 1, Singapore: Springer, 2016

7. Additive Manufacturing website, Amazing AM, LLC (http://additivemanufacturing.com/basics/)

8. S. Hällgren, L. Pejryd, J. Ekengren, Additive Manufacturing and High Speed Machining -Cost comparison of short lead time manufacturing methods, Procedia CIRP 50, 384-389,2016

9. D.S. Thomas, Economics of U.S. Additive Manufacturing Industry, NIST Special Publication 1163. Gaithersburg, MD: U.S. Dept. Of Commerce, 2013

10. Wohlers Report, Additive Manufacturing and 3D printing state of industry annual worldwide progress report, 2013.

11. D.S. Thomas, S.W. Gilbert, Costs and Cost Effectiveness of Additive Manufacturing: A Literature Review and Discussion, NIST Special Publication 1176, U.S. Dept. Of Commerce, 2014

12. P. Shah, R. Racasan, P. Bills, Comparison of different additive manufacturing methods using computed tomography, Case Studies in Nondestructive Testing and Evaluation, 6, 69-78, 2016

13. J. Hiemenz, Electron Beam Melting, Advanced Materials & Process, Minnesota, 2007

14. P. K. Gokuldoss, S. Kolla, J. Eckert, Additive Manufacturing Processes: Selective Laser Melting, Electron Beam Melting, and Binder Jetting – Selection Guidlines, Materials, 10, 672, 2017

15. T. G. Spears, S. A. Gold, In-process sensing in selective laser melting (SLM) additive manufacturing, Spears and Gold Integrating Materials and Manufacturing Inovation, 5-2, Springer, 2016

16. G. Vastola, G. Zhang, Q. X. Pei, Y.-W. Zhang, Modeling the Microstructure Evolution Duting Additive Manufacturing of Ti6Al4V: A Comparison Between Electron Beam Melting and Selective Laser Melting, JOM, Vol. 68,No.5, The Minerals, Metals & Materials Society. 2016

17. M. Schorghuber Inventor Cold Metal Transfer welding process and welding installation patent US20090026188 A1. 2009. 18 May 2006.

18. Fronius^{TM}, CMT: Cold Metal Transfer, MIG/MAG dip-transfer arc process

19. C.G. Pickin, S.W. Williams, M. Lunt, Characterization of the cold metal transfer (CMT) process and its application for low dilution cladding, Journal of Materials Processing Technology, 2011, Vol. 211, Issue 3, pp 496-502

20. R. Fokens, Cold Metal Transfer – CMT – A Revolution in Mechanized Root Pass Pipleine Welding, 4th Pipeline Technology Conference, 2009

21. C.G. Pickin, K. Young, Evaluation of cold metal transfer (CMT) process for wlding aluminium alloy, Science and Technology of Welding and Joining, 2006 Sep., Vol.11(5), pp.583-585

22. J. Shang, K.Wang, Q. Zhou, D. Zhang, J.Huang, G.Li, Microstructure characteristics and mechanical properties of cold metal transfer welding MG/Al dissimilar metals, Materials and Design, 2012, 34, pp.559-565

23. P.M. Sequeira Almeida, S. Williams, Innovative Process Model of Ti-6Al-4V Additive Layer Manufacturing Using Cold Metal Transfer (CMT), In: Proceedings of the 21st annual international solid freeform fabrication symposium;2010

24. A.S. Azar, A heat source model for cold metal transfer (CMT) welding, J Therm anal Calorim 122, 2015, pp.741-746

25. M.J. Donachie,Jr, Titanium A Technical Guide, Second Edition, ASM International, Materials Park, Ohio. 2000

26. R.R. Boyer, R.D. Briggs, The Use of β Titanium Alloys in the Aerospace Industry, Journal of Materials Engineering and Performances, 2005, 14(6), pp681-685
27. S. Ramakrishna, M. Ramalingam, T.S. S. Kumar, W. O. Soboyejo, Biomaterials, A Nano Approach, Boca Raton, FL: CRC Press, 2010

28. M.R. Dharme, A.M. Kuthe, S.W. Dahake, Comparison of Fatigue Analysis of Hip Joint Implant for Stainless Steel, Cobalt Chrome Alloys and Titanium Alloys, Trends Biomater. Artif. Organs, 27(2), 58-61,2013

29. Lide, D.R., ed (2005). CRCHandbook of Chemistry and Physics (86^{th} ed.) Boca Raton (FL): CRC Press

30. Titanium, Encyclopedia Britannica. 2006

31. Barksdale, Jelks (1968). "Titanium". In Clifford A. Hampel. The Encyclopedia of the Chemical Elements. New York: Reinhold Book Corporation. pp. 732–738.

32. Stwerka, Albert, Titanium, Guide to the Elements, Oxford University Press. pp81-82, 1998

33. F.P. Beer, E. R. Johnston, Jr, Mechanics of Materials (2ed.) McGraw-Hill, Inc.p.51, 1992

34. Burgers WG. On the process of transition of the cubic-body-centered modification into the hexagonal-close-packed modification of zirconium. Physica 1934;1:561.

35. Rongpei Shi, Variant Selection during Alpha Precipitation in Titanium Alloys A Simulation Study, The Ohio State University, Graduate Program in Materials Science and Engineering, Dissertation, 2014

36. T. Karthikeyan, S. Saroja, M. Vijayalakshmi, Evaluation of misorientation angle-axis set between variants during transformation of bcc to hcp phase obeying Burgers orientation relation, Scripta Materialia, 55 (2006) 771-774

37. Yina Gua, Literature review of titanium alloys and linear friction welding, Linkedin Slide Share, Dec. 2016

38. S. Banerjee, P. Mukhopadhyay, Phase Transformations Examples from Titanium and Zirconium Alloys, Pergamon materials series, Elsevier Science, Burlington, 2010

39. I. Polmear, Light Alloys, 4th edition, Butterworth-Heinemann, Oxford,2006

40. M. Niinomi, Mechanical biocompatibilities of titanium alloys for biomedical applications, Journal of the mechanical behavior of biomedical materials, (2008), 30-42

41. E.W. Collings, The Physical Metallurgy of Titanium Alloys, American Society for Metals, 1984, Metals Park, OH

42. M.J. Donachie, Jr, American Society for Metals, Metals Park, OH, 1982, pp.392
43. T. Ahmed, H.J. Rack, Materials Science and Engineering A, 243(1998), 206-211

44. J.C. Williams, in: R.I. Jaffee, H.M. Burte (Eds.), Titanium Science and Technology, Plenum Press, New York-London, California, 1973

45. R. Boyer, G. Welsch, E.W. Collings, Materials Properties Handbook – Titanium Alloys, ASM International, 1994

46. A.R.G. Brown, D. Clark, J. Eastabrook, K.S. Jepson, Nature, 201, (1964) 914-915

47. M. Grujicic, C.P. Narayan, Materials Science and Engineering: A 151 (1992) 217-226

48. F. Zimmerman, M. Humbert, Determination of the habit plane characteristics in the β- α' phase transformation induced by stress in Ti-5Al-2Sn-4Zr-2Cr-1Fe, Acta Materialie, 2002, Vol.50(7), pp.1735-1740

49. D. Pionnier, M. Humbert, M.J. Philippe, Study of the α" phase texture obtained by martensitic β-α" phase transformation induced by tensile test in a sheet of Ti5Al2Sn4Zr4Mo2Cr1Fe, Acta Materialia, 1998, Vol.45(16), pp. 5891-5898

50. R. Davis, H. Flower, D. West, Martensitic transformation in Ti-Mo alloys, Journal of Materials Science, 1979, Vol.14(3), pp.712-722

51. S. Nag. Materials Science and Engineering, The Ohio State University, Ohio, 2008 pp.315

52. T. Inamura, J.I. Kim, H.Y. Kim, H. Hosoda, K. Wakashima, S. Miyazaki, Composition dependent crystallography of α"-martensite in Ti-Nb-based β-titanium alloy, Philosophical Magazine, 2007, Vol.87(23). P. 3325-3350

53. Y.T. Lee, G. Welsch, Youngs Modulus and Damping of Ti-6Al-4V Alloy as A Function of Heat-Treatment and Oxygen Concentration, Materials and Engineering A-Structural Materials Properties Microst, 1990, Vol.128(1), pp.77-89

54. A. Kumar, T. Jayakumar, B. Raj, D. Banerjee, A new methodology for identification of β-transus temperature in α+β and β titanium alloys using ultrasonic velocity measurement, Philosophical Magazine, 2008, Vol.88(3), pp.327-338

55. C. Hammond, J. Notting, Forging and properties of aerospace materials, Metal Science, University of Leeds, 1977, pp. 474-490

56. Y. Ohmori, T. Ogo, K. Nakai, S. Kobayashi, Effects of omega-phase precipitation on beta-> alpha, alpha" transformations in metastable beta titanium alloy, Materials Science and Engineering A-Structural Materials Properties Microst, 2001, Vol. 312(1-2), pp. 182-188

57. W.B. Pearson, B. William, A handbook of lattice spacings and structures of metals and alloys, Vol.2, Pergamon, Oxford, 1967

58. M.P. Ginebra, F.X. Gil, J.M. Manero, J.A. Planell, in:P.A. Blenkinsop, W.J. Evans, H.M. Flower (Eds.) Titanium'95 Science and Technology, the eight world conference on Titanium The Institute of Materials, Birmingham, UK, 1995, pp.2563-2571

59. D.A. Porter, K.E. Easterling, Phase Transformations in Metals and Alloys, Second edition ed, CRC Press Taylor & Francis Group, Boca Raton,2004

60. D. Banerjee, K. Muraleedharan, J.L. Strudel, Substructure in titanium alloy martensite, Taylor & Francis Group, Philosophical Magazine A, 1998, Vol.77(2), pp.299-323

61. S.C. Wang, M. Aindow, Mj. Starnik, Effect of self-accomodation on alpha/alpha boundary populations in pure titanium, Acta Materialia, 2003, Vol. 51(9), pp.2485-2503

62. H. Margolin, J.P. Nielsen, Modern Materials, Advances in Development and Application, 1960, Vol.2 (ed. H.H. Hausner) Academic Press, New York, p.225

63. E.K. Molchanova, Phase Diagrams of Titanium Alloys, 1965, Israel Program for Scientific Translations, Jerusalem

64. I. Katarov, S. Malinov, W. Sha, Finite Element Modeling of the Morphology of α to β Phase Transformation in Ti-6Al-4V Alloy, Metallurgy and materials transaction A 2002, 33A: p.1027-1041

65. Z.B. Zhao, Q.J. Wang, Q.M. Hu, J.R. Liu, B.B. Yu R. Yang, Effect of β (110) texture intensity on α-variant selection and microstructure morphology during β→α phase transformation in near α titanium alloy, Acta Materialia 126, 2017, pp. 372-382

66. I. Lonardelli, N. Gey, H.R. Wenk, M. Humbert, S.C. Vogel, L. Lutterotti, In situ observation of texture evolution during α→β and β→α phase transformations in titanium alloys investigated by neutron diffraction, Acta Materialia 55, 2007, 5718-5727

67. G. Lutjering, Influence of processing on microstructure and mechanical properties of (alpha+beta) titanium alloys, Materials Science and Engineering A-Structural Materials Properties Microst, 1998, Vol.243(1-2), pp. 32-45

68. Dean, John A., The Analytical Chemistry Handbook, New York: McGraw Hill, Inc. 1995, pp 15.1-15.5, ISBN0-07-016197-6

69. Pungor, Erno, A Practical Guide to Instrumental Analysis, Boca Raton, Florida, 1995, pp. 181-191

70. Skoog, Douglas A., F. J. Holler, T. Nieman, Principles of Instrumental Analysis, 5th Ed., New York, 1998, pp. 805-808, ISBN 0-03-002078-6

71. Dynamic Systems Inc., Product Catalog, Poenstenkill, NY, 2017

72. ASTM E23, Standard Test Methods for Notched Bar Impact Testing of Metallic Materials, Book of Standards, Vol:03.01